

# Multimethod characterization of a chlorinated solvents contaminated site and geoelectrical monitoring of in-situ bioremediation

---

ARISTEIDIS NIVORLIS

ENGINEERING GEOLOGY | FACULTY OF ENGINEERING | LUND UNIVERSITY





Division of Engineering Geology  
Faculty of Engineering  
Lund University  
ISBN 978-91-7895-622-7  
ISRN LUTVDG/(TVDG-1044)/(1-99)/(2020)



# Multimethod characterization of a chlorinated solvents contaminated site and geoelectrical monitoring of in-situ bioremediation

Licentiate Thesis

Aristeidis Nivorlis  
Division of Engineering Geology  
Lund University  
Sweden

2020-08-27



**LUND**  
UNIVERSITY

Copyright Aristeidis Nivorlis

Paper 1 © MDPI

Paper 2 © 2020 The authors (Manuscript unpublished)

Faculty of Engineering, Engineering Geology

ISBN (print) 978-91-7895-622-7

ISBN (pdf) 978-91-7895-623-4

ISRN LUTVDG/(TVTG-1044)/(1-99)/(2020)

Printed in Sweden by Media-Tryck, Lund University  
Lund 2020



Media-Tryck is a Nordic Swan Ecolabel  
certified provider of printed material.  
Read more about our environmental  
work at [www.mediatryck.lu.se](http://www.mediatryck.lu.se)

**MADE IN SWEDEN** 

## **Abstract**

Soil contamination is a widespread problem and actions need to be taken in order to prevent damage to the groundwater and the life around the contaminated sites. In Sweden more than 80.000 sites are potentially contaminated, therefore there is a demand for accurate and efficient methods for site characterization and soil remediation. In the past, the preferred methodology for soil remediation involved the excavation of the contaminated mass which was either deposited in landfills (dig and dump) or treated elsewhere (dig and treat). However, these techniques are associated with significant high risk (secondary exposure) and long-term costs. On the other hand, in-situ bioremediation has the potential to address these issues offering a safer, more sustainable and cost-efficient alternative for soil remediation. Unfortunately, monitoring the progress of in-situ treatments requires soil/water sampling and laboratory analysis, which, if done frequently, can increase the cost dramatically. For this reason, there is a demand for new methodologies that can be used to follow the progress of in-situ bioremediation.

The work presented in this thesis involves a former dry-cleaning facility located in Alingsås (Sweden). The site is contaminated with chlorinated solvents and a pilot in-situ bioremediation plan was launched in November 2017. First, we adapted a multimethod approach for site characterization using several methods: Direct Current resistivity and time-domain Induced Polarization (DCIP), Seismic Refraction Tomography (SRT) and the Membrane Interface Probe (MIP). The aim was to build a refined geological conceptual model. Second, we developed an autonomous and fully automated system for geophysical monitoring with the DCIP method that aims to follow the daily changes in the subsurface. We present a complete workflow that includes data acquisition, pre-processing, inversion and visualization of the daily DCIP monitoring data. The proposed scheme is robust and shows that DCIP monitoring has great potential to record the changes due to the bioremediation; however, it needs to be paired with more information (temperature, geochemistry, contaminant concentrations) to better understand the changes that take place in the subsurface.



## Sammanfattning

Förorenad mark är ett utbrett problem och åtgärder måste vidtas för att förhindra skador på grundvattnet och ekosystem runt de förorenade platserna. I Sverige är mer än 80 000 områden förorenade, därför krävs det tillförlitliga och effektiva metoder för platsundersökning och marksanering. Den traditionellt använda metoden för marksanering består av utgrävning av den förorenade massan med påföljande deponering (gräva och deponera) eller behandling någon annanstans (gräva och ex-situ behandla). Dessa tekniker är dock förknippade med betydande risk (sekundär exponering) och kostnader. In-situ sanering genom biologisk nedbrytning har potential att erbjuda ett säkrare, mer hållbart och kostnadseffektivt alternativ för marksanering. Detta kräver dock kontroll av resultatet genom övervakning av effekten av åtgärderna via provtagning och laboratorieanalys, vilket, om det görs ofta, kan öka kostnaderna dramatiskt och endast bidrar med punktformig data. Av denna anledning finns det behov av nya metoder som kan användas för att följa och verifiera effekterna av den initierade biologiska nedbrytningen på plats.

Det arbete som presenteras i denna avhandling omfattar ett pilotförsök för sanering vid en tidigare kemtvättanläggning belägen i Alingsås (Sverige). Platsen är förorenad med klorerade lösningsmedel och pilotförsöket med in-situ sanering initierades i november 2017. Vi utarbetade undersökningar och övervakning med hjälp av flera olika metoder: kombinerad elektrisk resistivitetstomografi och tidsdomän Inducerad Polarisation (DCIP), seismisk refraktionstomografi (SRT) och membraninterfaceprob (MIP). Syftet var att bygga en förfinad geologisk konceptuell modell för att förstå marksystemet. Vidare utvecklade vi ett autonomt och helautomatiserat system för geofysisk övervakning med DCIP-metoden som syftar till att dagligen följa förändringarna i marken. Vi presenterar ett komplett arbetsflöde som inkluderar datainsamling, databehandling, inversion och visualisering av de dagliga DCIP-mätningarna. Det föreslagna arbetsflödet är robust och visar att DCIP-övervakning har stor potential att registrera kemiska förändringarna till följd av biologisk sanering; emellertid måste den kopplas ihop med mer information (t.ex. temperatur, geokemi, koncentration av föroreningar) för att bättre förstå de förändringar som sker i marken.



## **Preface**

The work of this thesis has been carried out at the Division of Engineering Geology, Lund University in Sweden.

I want to thank my main supervisor Torleif Dahlin and my assisting supervisor Matteo Rossi for excellent support, help and guidance throughout my work. I would also like to thank my assisting supervisors Gianluca Fiandaca, Panagiotis Tsourlos and Alfredo Mendoza for providing valuable comments on my work. Furthermore, I would like to thank my colleagues within the MIRACHL group for their fruitful discussions and suggestions during the planning of the fieldwork and the analysis of the results and my colleagues at the Division of Engineering Geology for a friendly and supportive working environment. Finally, I would like to thank my family for their love and support.

This work has been carried out within the MIRACHL project (<http://mirachl.com/>). Funding is provided by the Swedish Research Council Formas—The Swedish Research Council for Environment, Agricultural Sciences and Spatial Planning (ref. 2016-20099), SBUF—The Development Fund of the Swedish Construction Industry (ref. 13336), ÅForsk (ref. 14-332), SGU—Swedish Geological Survey, Sven Tyréns stiftelse, Västra Götalandsregionen and Lund University.

Aristeidis Nivorlis

Lund, August 2020



## **List of appended papers**

The following two papers are appended in the thesis. The thesis author has contributed to the design of the monitoring system, conducted the major part of the fieldwork required to ensure that the installations are functioning correctly and programmed the automation of measurements and data streaming. The thesis author has performed major parts of the data analysis and interpretation for the appended articles. As the main author, he has been the leading writer of the appended articles, with support and input on specific parts from the co-authors. The co-authors have contributed to the design and installation of the monitoring system, and to the interpretation of the results.

### **Paper I**

Nivorlis, A.; Dahlin, T.; Rossi, M.; Höglund, N.; Sparrenbom, C. Multidisciplinary Characterization of Chlorinated Solvents Contamination and In-Situ Remediation with the Use of the Direct Current Resistivity and Time-Domain Induced Polarization Tomography.

Geosciences 2019, 9, 487.

### **Paper II**

Nivorlis, A.; Dahlin, T.; Rossi, M. Temporal filtering and time-lapse inversion of geoelectrical data for monitoring of in-situ bioremediation

Submitted for publication (Geophysical Journal International)



# Table of Contents

<b>Introduction .....</b>	<b>1</b>
Aim, objectives and limitations.....	2
Outline.....	3
<b>Site description.....</b>	<b>5</b>
<b>Methods .....</b>	<b>9</b>
Direct Current resistivity and time-domain IP .....	9
Resistivity method.....	9
Induced Polarization.....	11
Electrical Resistivity Tomography .....	12
Forward Modelling.....	14
Inversion.....	14
Complementary Methods .....	16
Membrane Interface Probe .....	16
Seismic Refraction Tomography.....	16
Temperature monitoring.....	17
<b>DCIP Monitoring.....</b>	<b>19</b>
DCIP monitoring.....	19
Challenges in data processing .....	20
Inversion results and visualization .....	22
<b>Main Results.....</b>	<b>23</b>
Paper I .....	23
Paper II.....	26
<b>Conclusions and future work .....</b>	<b>31</b>
Future work .....	31
<b>References .....</b>	<b>33</b>



# Chapter 1. Introduction

Soil contamination is a widespread problem that has been recognized in the past decades as the governments and global organizations move towards sustainability and green development. The directive of environmental liability (2004/35/CE) established a common framework based on the ‘polluter pays’ principle among the countries that are members of the European Union. On that basis, more than 80.000 potentially contaminated sites (SEPA, 2014) have been identified by the Swedish Environmental Protection Agency (SEPA). Therefore, there is a demand for modern methodologies for site characterization and soil remediation that are more effective, more efficient, minimize the risk for secondary exposure and are potentially cheaper to deploy on a large scale.

In this context, in-situ bioremediation is an attractive alternative to traditional remediation techniques, such as ‘dig and dump’, ‘dig and treat’ or ‘thermal remediation’, especially in cases where the contaminants have migrated deep into the subsurface, are spread over a large area or are located in urban environments and specifically underneath buildings. However, one draw-back of in-situ bioremediation is that there are no efficient methodologies to monitor the changes that take place in the subsurface and to estimate the effectiveness of the treatment. Currently, the most common way to monitor the remediation is done through periodical water samples from pre-installed wells that will only reflect the dissolved contaminants in water, usually a small fraction of the total pollution. Furthermore, it requires qualified staff to interact directly with the contaminant and should be kept to the minimum. Geophysical methods can provide a useful tool to extrapolate the time-step point information acquired from drilling and water sampling to further increase our understanding about the subsurface and the changes that take place during a remediation experiment.

The Electrical Resistivity Tomography (ERT) has been successfully used in a wide range of subsurface investigations (Loke et al., 2013) such as hydrogeological (Chirindja et al., 2017; Fetter, 2001; Giang et al., 2018; Leroux and Dahlin, 2006; Zago et al., 2020), environment (Auken et al., 2014; Fernandez et al., 2019; Forquet and French, 2012), engineering geology (Abdulsamad et al., 2019; Danielsen and Dahlin, 2009; Rossi et al., 2018) and archaeological (Angelis et al., 2018; Argote-Espino et al., 2016; Simyrdanis et al., 2018a). The Direct Current resistivity and time-domain Induced Polarization tomography (DCIP) is an extension to the traditional ERT survey and measures an additional property, the chargeability,

whilst recent developments (Olsson et al., 2016, 2015) make it possible to record the two electrical properties simultaneously and more efficiently. The DCIP has been successfully used to solve more complex problems such as lithology mapping (Kemna et al., 2004; Slater and Lesmes, 2002), landfill characterization (Bernstone et al., 2000; Chambers et al., 2006; Gazoty et al., 2012b; Ntarlagiannis et al., 2016; Power et al., 2018; Ustra et al., 2012; Wemegah et al., 2017) and microbial activity (Atekwana et al., 2005; Atekwana and Atekwana, 2010; Davis and Atekwana, 2006; Slater et al., 2008). Frequency based spectral Induced Polarization has been applied to monitoring of stimulated bioremediation of uranium contamination with promising results (Flores Orozco et al., 2013), while DCIP has been used to monitor groundwater contamination and leakage (Kuras et al., 2016; Leroux et al., 2010; Park et al., 2016) and gas migration within landfills (Rosqvist et al., 2011; Steelman et al., 2017). In sites contaminated with Non-Aqueous Phase Liquids (NAPLs), DCIP has been successfully applied for characterization (Johansson et al., 2017; Maurya et al., 2018; Power et al., 2014; Simyrdanis et al., 2018b) and monitoring of the changes due to remediation (Caterina et al., 2017; Sparrenbom et al., 2017). The successful use of frequency domain IP for monitoring of free-phase hydrocarbon contamination (Cassiani et al., 2009) injection and transport of microscale zerovalent iron (mZVI) particles for groundwater remediation purposes (Flores Orozco et al., 2015) introduce more opportunities for the DCIP method to be used in that field.

Previous work with geophysical monitoring involves several DCIP measurements which are recorded in consecutive time steps. There are systems that can automatically record more frequent measurements (Chambers et al., 2009), the data are usually processed manually and the results include selected time-steps even though several recordings are available. Therefore, it is of paramount importance to develop and propose efficient and robust routines to be able to deploy scalable geophysical systems that autonomously and automatically collect data without running into the problem of being overloaded with manual processing.

## Aim, objectives and limitations

The overall aim of this study is to follow the changes of an in-situ bioremediation experiment with the use of geophysics and namely the DCIP method.

The first objective is to use the information from geophysical methods (DCIP and Seismic Refraction Tomography) and the information from the Membrane Interface Probe method (lithology and contaminant concentration) to improve the geological conceptual model for the contaminated site. The second objective is to develop efficient and robust routines for quality control, pre-processing, inversion, and visualization of the daily DCIP monitoring data.

DCIP provides a detailed description of the subsurface, in both space and time and has great potential when used to extrapolate the time-step point information from traditional sampling techniques. The resulting DCIP monitoring models need to be further calibrated and jointly interpreted with water and soil sampling. The proposed scheme for processing and inversion is developed based on the data from the Alingsås site. It is suggested that this scheme is tested and potentially calibrated before applied to another site.

## Outline

The outline of this Licentiate thesis is as follows: chapter 2 describes the area of investigation where chapter 3 gives a background description of the methods used in this thesis with emphasis on the geoelectrical method DCIP. Chapter 4 presents the geoelectrical monitoring and the challenges that are associated with it. The main results are summarized in chapter 5 and the conclusions as well as an overview of the future work are presented in chapter 6.



# Chapter 2. Site description

In Alingsås (South Central Sweden, see Figure 1), an industrial-scale dry-cleaning facility (Alingsåstväteriet) started operating in 1963, supplying cleaning services for the military. Sometime during the 1960s or 1970s, a single spill of approximately 200 L of PCE leaked into the ground, resulting in the formation of a DNAPL source zone beneath the building with a plume extending out under the parking lot. That is the only documented spill; however, other instances of undocumented spills could have occurred in the past. Today, the use of PCE has ceased, and the facility is operating under the Administrative Region Västra Götaland as a laundry and textile cleaning (water only) unit, taking care of approximately 40 tons of textiles per day for the regional hospitals. Responsibility for the remediation is shared between the Swedish Government, through the Swedish Geological Survey (SGU) and the current owners (Region Västra Götaland). Due to ongoing operations in the building, in-situ remediation is the favored approach for treatment of the contaminated mass.

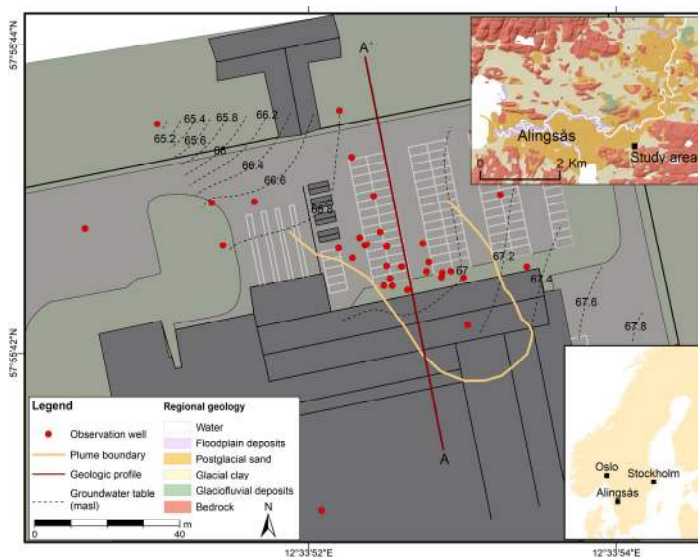


Figure 1. Overview of the Alingsås site where the observation wells (red circles), the groundwater level (black dashed lines), the plume boundaries (orange line) and the regional surface geology (top right, created with data from SGU Jordarter, 1:25,000–1:100,000 © SGU) can be seen. Line A-A' marks the location of geological conceptual model shown in Figure 2.

In the area of investigation, the depth to the crystalline bedrock varies between 2 to 12 m. The sediment overlying the bedrock is deposited in a fining upwards sequence. It consists of a unit of sand with lenses of silt and clay, followed by a layer of clay and on top of the sediment, about 1 m of fill material is present. The geological conceptual model, modified from Branzen (2013), is presented in Figure 2. The sedimentary units show a varying inner heterogeneity with lenses of both finer and coarser material occurring. The bedrock topography slopes gently towards N. The depth to the water table varies between 1.5 to 2 m below the ground surface and the groundwater flows from SE towards NW as can be seen in Figure 1.

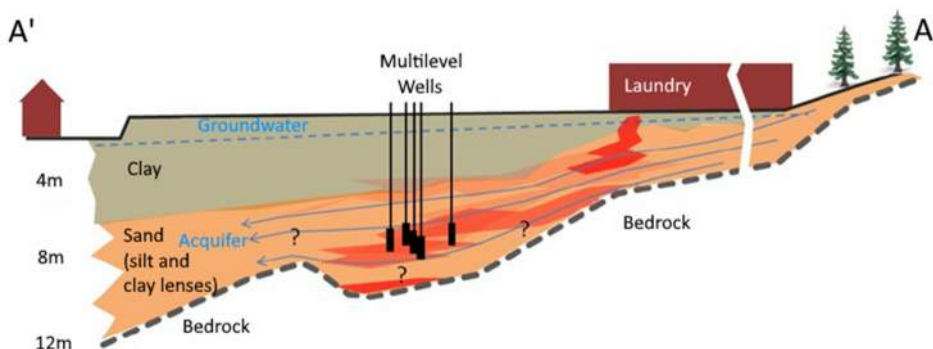


Figure 2. Geological conceptual model (S-N). (Modified from Branzen, 2013).

In order to determine the best approach for treatment of the contamination and to stop further spreading, a pilot in-situ remediation program was launched in November 2017, using a direct push injection method on the north side of the laundry building (Figure 3). In order to evaluate the best approach for a future full-scale remediation scenario, two different remediating agents were injected into the plume at different locations, for comparison. In injection area A (west side, see Figure 3) Provectus ERD-CH4™ substrate containing a carbon source (electron donor) in the form of vegetable oils together with acids and a bacterial consortium (Dehalococcoides mccartyi, Desulfobivrio, Desulfitobacterium and methanogenic archaea bacteria) was injected in two phases between the 7th and the 17th of November 2017, at a total of 32 points. In injection area B (east side, see Figure 3) CAT100™ substrate containing granular activated carbon, zero-valent iron and Trap & Treat® bacteria concentrate were injected, together with a methane inhibitor, between the 28th and the 30th of November 2017, at a total of 37 points. In both cases, the products were injected from a depth of 3 m and downward until reaching the top of the bedrock.

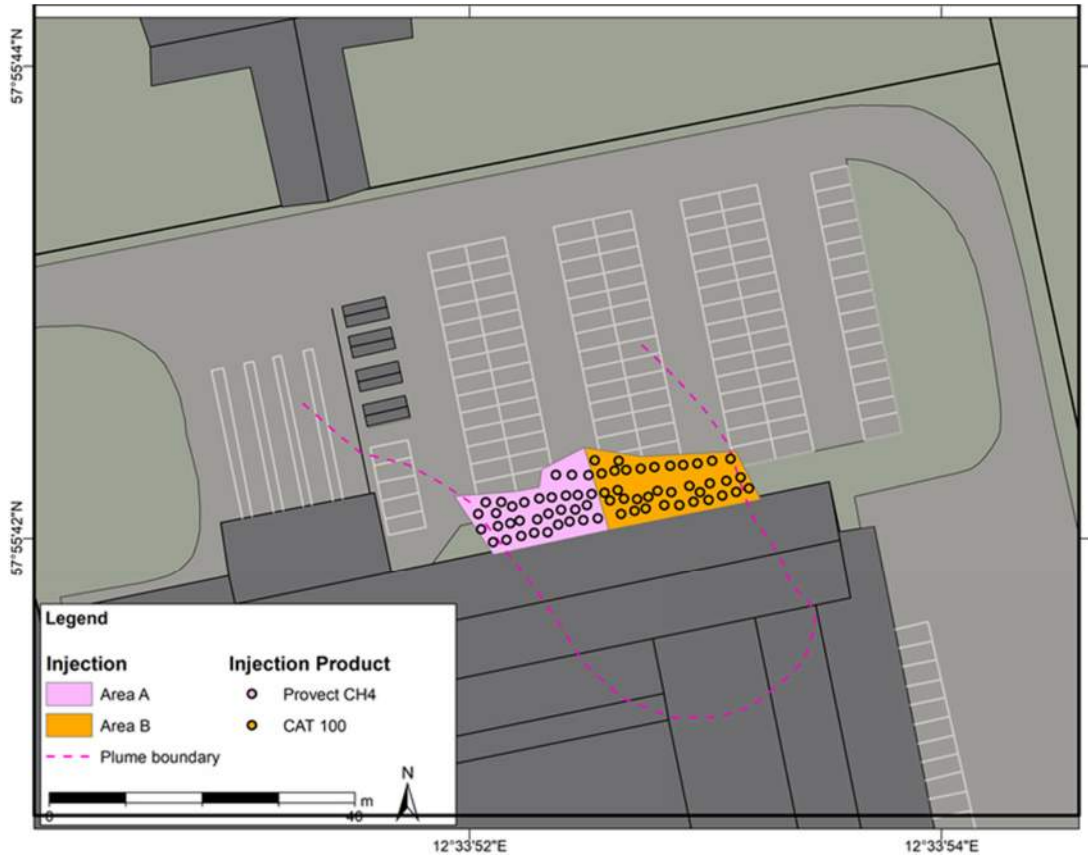


Figure 3. Pilot in-situ bioremediation plan launched during November 2017.



# Chapter 3. Methods

The Direct Current resistivity and time-domain Induced Polarization tomography (DCIP) method was primarily used in this thesis work, therefore this method will be described in some detail. The SRT, MIP and temperature monitoring methods used as complementary methods to the DCIP will be introduced briefly to obtain a clear overview of the overall methodology used in this work.

## Direct Current resistivity and time-domain IP

The Direct Current resistivity and time-domain Induced Polarization (DCIP) method includes the use of the traditional resistivity method and its extension, the induced polarization method. The former measures the distribution of the electrical resistivity where the latter measures the capacity of the ground to store charges. Recent advances in the past years, both in terms of hardware and software, made it possible to measure both quantities simultaneously making the acquisition faster and more accurate therefore increasing the popularity of the method significantly. The essential theory of the DCIP method, which is required to follow the thesis work, is described in this chapter.

### Resistivity method

The electrical resistivity,  $\rho$  ( $\Omega \cdot m$ ) is a fundamental property that quantifies the opposition of a material, the ground in our case, to the flow of electrical currents. For a single resistivity measurement four electrodes are employed, two electrodes are used to inject the current (A and B) and two, usually different, electrodes (M and N) are used to measure the potential difference (Figure 4).

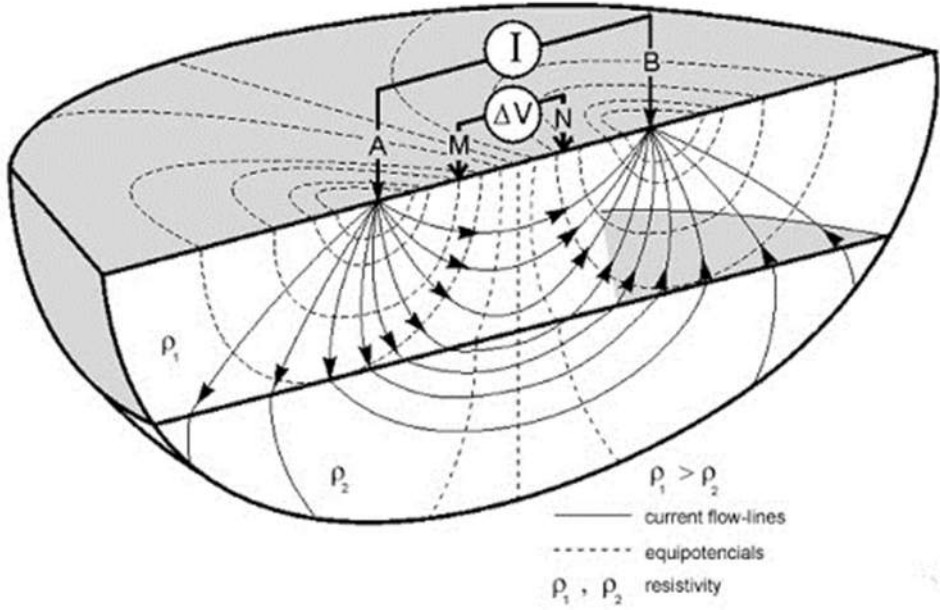


Figure 4. Single resistivity measurement. (Original figure provided by Knödel et al., 2007).

The Ohmic resistance ( $R$ ) of the ground is calculated using the formula:

$$R = \frac{V}{I} \quad (1)$$

where  $V$  is the potential difference and  $I$  is the electrical current injected into the ground. By taking the position of the four electrodes into account, the electrical resistivity can be calculated using the formula:

$$\rho = R \frac{2\pi}{G} \quad (2)$$

where the geometric factor  $G$  can be calculated using the formula:

$$G = \frac{1}{AM} - \frac{1}{BM} - \frac{1}{AN} + \frac{1}{BN} \quad (3)$$

The electrical resistivity calculated from equation (2) corresponds the true electrical resistivity only in cases of a homogeneous and isotropic media. However, the earth is, in most cases, heterogeneous so the previous calculations do not generally yield the true electrical resistivity of the ground. The electrical resistivity calculated by the equation (2) represents a kind of weighted average, although this is not mathematically correct (Cook and Van Nostrand, 1954), of the resistivities of the different subsurface materials and is called the apparent resistivity.

## Induced Polarization

The induced polarization method can be considered as an extension of the resistivity method, as a similar configuration as described in Figure 4 is required. In addition to the electrical resistivity calculation another parameter called apparent chargeability is measured. This parameter measures the ability of the ground to store current in form of electrical energy during the injection of the current, acting very similarly to a capacitor.

In order to measure the energy stored, after each current injection (on time) there is an intermediate pause step where no current is injected (off time). During the off time instead of the voltage being zero, because no current is applied, the stored electrical energy is released and is recorded by the instrument as a gradual drop in the voltage before it drops down to zero (Figure 5).

The apparent chargeability as defined by Siegel (1959) is the ratio between the secondary voltage immediately after the current is turned off ( $V_s$ ) and the primary voltage, while the current is on ( $V_m$ ), as can be seen in Figure 5 left. In reality, the secondary voltage cannot be accurately measured because when the current turns off electromagnetic effects are produced. These electromagnetic effects can be several orders of magnitude higher than the secondary voltage and this makes it very difficult to separate the two signals. For this reason, modern instruments record the chargeability by integrating over the voltage curve several milliseconds after the current is turned off (Figure 5 right and equation (4)).

$$m = \frac{1}{V_m} \int_{t_1}^{t_2} V_s(t) dt = \frac{\sum_{i=1}^n (M_i T M_i)}{\sum_{i=1}^n T M_i} \quad (4)$$

Where  $V(t)$  is the function of voltage over time,  $V_m$  is the voltage before the current cut off,  $M_i$  is the integral chargeability and  $T_i$  is the time window of the  $i_{th}$  gate.

It is obvious that the chargeability is a dimensionless parameter which cannot be larger than 1 because the secondary voltage will always be lower than the primary.

It is possible to encounter negative apparent chargeability values that can be explained in view of negative sensitivity areas (Dahlin and Loke, 2015). This means that the apparent chargeability can range from -1 to 1 V/V or -1000 to 1000 mV/V. The latter form (mV/V) is more commonly encountered.

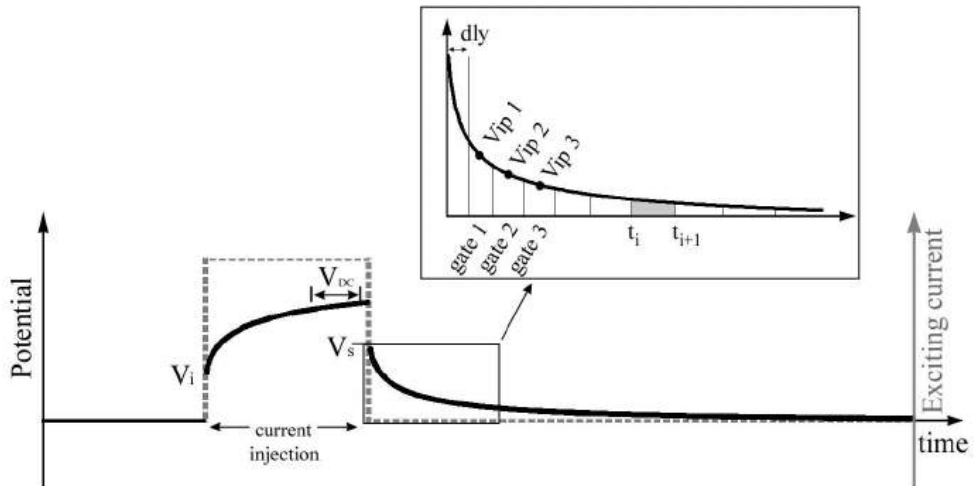


Figure 5. Chargeability as defined by Siegel (main plot) and as measured by modern instruments (small plot) (Gazoty et al., 2012a).

## Electrical Resistivity Tomography

The principles described in the previous sections, describes a single measurement, using four (4) electrodes or a quadrupole, which gives very limited information about the subsurface due to the presence of heterogeneities. For that reason, in a DCIP survey we perform hundreds of single measurements using several combinations of electrodes that are preplaced and connected to the instrument. The instrument performs a series of single measurement with 4 electrodes, based on a given predefined sequence, until all the desired 4-electrode combinations are measured. This type of survey is often called Electrical Resistivity Tomography (ERT) and can be further explained in Figure 6. The total number of possible combinations could be thousands, however several specific configurations, called electrode arrays, are more frequently used. In this thesis work we have mainly used the multiple gradient array (Dahlin and Zhou, 2006) which has high signal to noise (S/N) ratio making it particularly suitable for IP measurements.

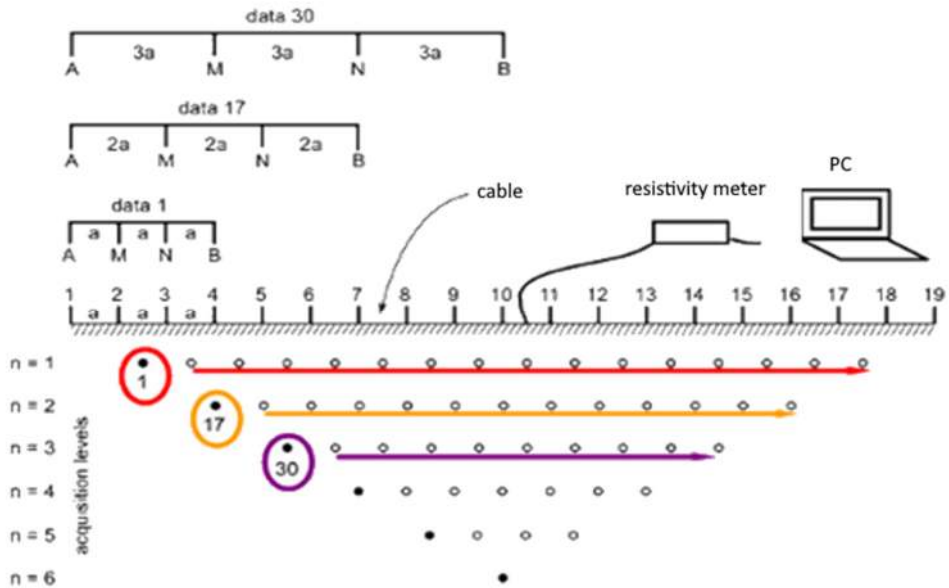


Figure 6. DCIP field survey (modified after Loke and Barker, 1996).

As discussed previously, during a DCIP survey current is injected into the ground and the potential difference is recorded between several receiver pairs. For the 2D case, several arrays offer advantages and within this thesis work the multiple-gradient array (Dahlin and Zhou, 2006) was used. The observations (apparent resistivities) can be plotted in a pseudo-section and illustrate a distorted representation of the distribution (Figure 7) of the electrical properties in the ground.

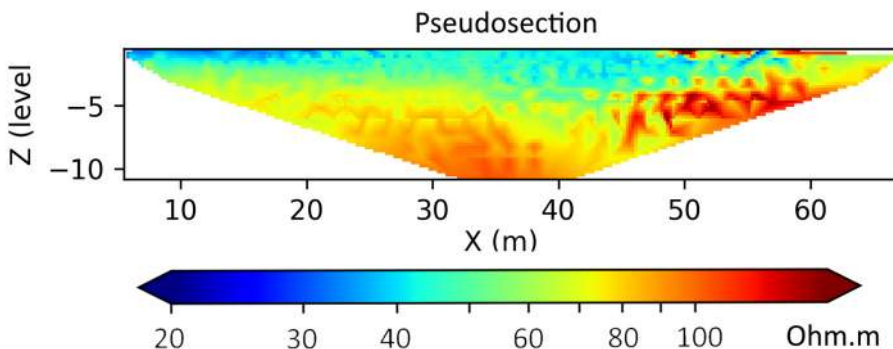


Figure 7. Pseudosection that represents the distribution of apparent resistivities in the ground (observations).

## Forward Modelling

The forward modeling involves the calculation of the response of a model representing the earth's structure for which the electrical resistivity distribution is known. To solve this problem, for given source locations the current flow inside the model needs to be simulated. The equation that governs the current flow in the ground is the Poisson equation:

$$\nabla(-\sigma\nabla V) = \nabla J \quad (5)$$

Where  $V$  is the potential,  $\sigma$  represents the subsurface conductivity and  $J$  describes the current sources.

Although analytical solutions do exist for simple geometries (Cook and Van Nostrand, 1954) for more complex geometries they do not exist. For complex geometries, the eq. 5 is solved using a numerical approach such as the finite element method (FEM) which is used in this work (Loke et al., 2014, 2011). In FEM the earth is divided into a finite number of smaller homogeneous and isotropic cells, called elements. Each element is assigned a value of the electrical properties, as described extensively in (Tsourlos and Ogilvy, 1999) and the solution to eq.(5) is approximated.

## Inversion

As previously described, it is rather straight forward to calculate the response of an array given a known distribution of the electrical properties. However, the distribution of the electrical properties is usually unknown and needs to be determined. That can be achieved through an iterative process called inversion, which tries to find the distribution of parameters that gives theoretical measurements that best fit the real data. The smoothness constrained inversion (Tsourlos and Ogilvy, 1999) is the algorithm that is used in this work to solve the inverse problem and is briefly described in Figure 8.

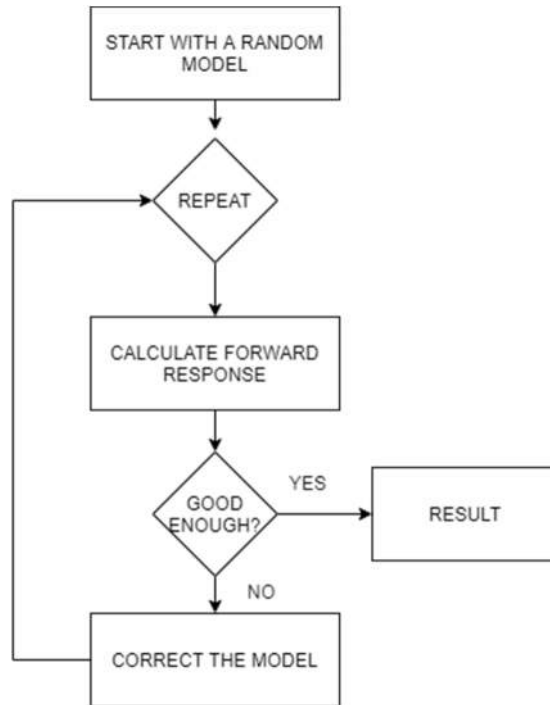


Figure 8. Simplified diagram that describes the general inversion algorithm.

To begin with, a homogeneous earth is most commonly used for the initial model. The model response is calculated (forward solution) then the model is compared with the observed measurements and the misfit is computed. If one of the stopping criteria is met the process terminates, otherwise the model is updated, and the process is repeated. The criteria for terminating the process that are commonly used include a maximum number of iterations, no further improvements in the solution or a solution with an acceptable misfit.

The observations are used by the inversion algorithm to find the distribution of parameters (resistivities) that will generate synthetic measurements (forward response) that are as close as possible.

The distribution of the electrical properties (inverted profile, Figure 9) can be linked with the lithology and with the presence of water or contaminants. The connection however is not trivial and a priori information about the area of investigation is required to interpret the results. Last, it is important to mention that the distribution of the electrical properties can vary through time because of seasonal variations, such as temperature changes and rainfall events, changes in groundwater level and geochemistry. The last is of great importance in this thesis work, because during the in-situ bioremediation the properties of the subsurface are changing, therefore one inverted profile captures a single time-step of the overall changes.

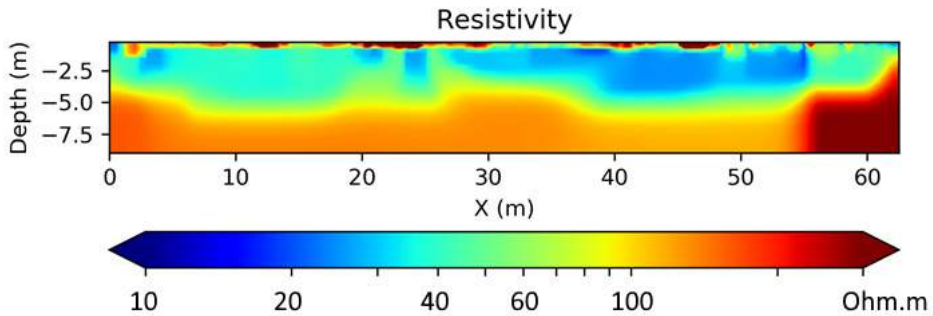


Figure 9. True distribution of resistivities (properties) in the subsurface.

## Complementary Methods

### Membrane Interface Probe

The Membrane Interface Probe (MIP) is a logging method where a probe, equipped with sensors, is directly pushed into the ground in a way similar to a cone penetration test (CPT). First and foremost, the probe is equipped with a detector that can measure the volatile hydrocarbon and solvent contamination at different depths. Moreover, other sensors attached to the probe can estimate the electrical conductivity and hydraulic permeability of the geological units at different depths.

The method is efficient for mapping the contaminants in-situ in the subsurface, while at the same time information that can be used to describe the lithology can be provided. However, the MIP method only provides time specific single point information about the subsurface and additional methods are needed to achieve more continuous spatial coverage.

### Seismic Refraction Tomography

The seismic refraction method estimates the velocity with which a generated elastic wave propagates into the subsurface. A source such as a hammer, explosion or an accelerated weight drop is used to generate, in this case, compressional waves (P-waves), although shear waves (S-waves) could be used as well. The generated waves contain information about the media that they are propagated through and are recorded at several receivers, the geophones, placed at different distances from the

source. The experiment is repeated by moving the source to other positions, thus generating more waves, to obtain further information about the elastic properties of the subsurface (P wave velocity) that can be used to describe the lithology.

In the traditional seismic refraction method, the first arrivals are used to estimate the depth to the refractors, interfaces where the elastic properties (P-wave velocity) change. The groundwater table or the transition from one lithological unit to another are examples of refractors that can be identified by the seismic refraction method.

Seismic Refraction Tomography introduces a more advanced approach where instead of identifying refractors (surfaces) a model of the elastic properties of the subsurface (P-wave velocity) is estimated. That is achieved by an inversion approach, similar to the one described for the DCIP, where a system of non-linear equations are solved to generate a model of the P-wave velocities for the subsurface (White, 1989).

### **Temperature monitoring**

The monitoring of the soil temperature is essential when deploying geoelectrical monitoring systems because the electrical properties are directly affected by the temperature. Even though the electrical properties are affected by temperature, it is not possible to delineate the temperature of the subsurface from the DCIP data, making it paramount to use external probes for that purpose.

The variations of the temperature can be used to understand the changes that take place in the subsurface and understand how the geoelectrical signal can potentially be affected. The effects of seasonal variations can be observed by monitoring the temperature of the soil at different depth intervals. Furthermore, rainfall events can also affect the temperature of the soil, apart from changing the water saturation, and therefore may be identified from the soil temperature data.



# Chapter 4. DCIP Monitoring

## DCIP monitoring

As mentioned previously, the electrical properties of the subsurface often change over time, for example due to variations in the soil temperature, water content or the contamination levels. In these scenarios DCIP measurement can be repeated several times, using exactly the same setup, to make it possible to record the changes in the electrical properties of the subsurface. Then, it becomes possible to produce several inverted profiles that represent the distribution of the electrical properties over time thus revealing how the subsurface is changing over time. This approach is called DCIP monitoring.

The DCIP monitoring is carried out by repeating the geophysical survey consecutive times and often requires several data acquisition campaigns in the area of investigation. The frequency that each individual measurement is recorded and the time-span of the monitoring survey depends on the overall scope. Frequent measurements are needed to capture and understand the more rapid changes, for example due to rainfall events, and longer survey experiments are required to make it possible to identify changes that are usually slower, such as remediation experiments. Furthermore, the seasonal variations (yearly) due to temperature are usually dominant in the shallow layers, introducing the challenge of identifying changes that relate to environmental (gas migration, leachates, contaminations etc.) or engineering geology (soil stabilization, internal erosion in dams) problems.

To address these problem, it is important to have a system that can acquire frequent data for long periods which would require the DCIP equipment (cables, electrodes and instrumentation) to be deployed in the field introducing several risks (damage to the equipment, public safety and theft). This can be solved by deploying a permanent installation (Figure 10), where the cables and the sensors are buried under the ground and the instrument is stored safely in a nearby building (if possible).

To achieve frequent measurements, for example daily, robust routines for data collection need to be developed to make it possible to automatically collect DCIP without the need of an on-site team. In addition, schemes for managing the collected data should be present, so that data are safely archived and backed up after the

collection. Lastly, tools for quality control of the entire procedure are important to be in-place and produce warnings in case of failure.



*Figure 10. Permanent installation of electrodes for a DCIP monitoring experiment. Alingsås, Sweden.*

## Challenges in data processing

The daily collected data from a DCIP monitoring system are often affected by noise. Although it is not common, a system failure might occur therefore gaps in the data are also to be expected. Spatial noise in the data can be observed by analysing the pseudosections that are recorded daily (Figure 11) where temporal noise can be seen by isolating the observed values (apparent resistivities and chargeabilities) of individual quadrupoles (Figure 12) over the entire timespan of a monitoring system. Moreover, frequent daily measurements can quickly accumulate creating large datasets and manual processing is no longer an efficient option for data processing.

There is an inherent need for efficient and robust schemes for filtering large datasets, removing extreme outliers and potentially bad data points that do not appear to be coherent with their neighbouring values (space domain) or their past and future values (time domain).

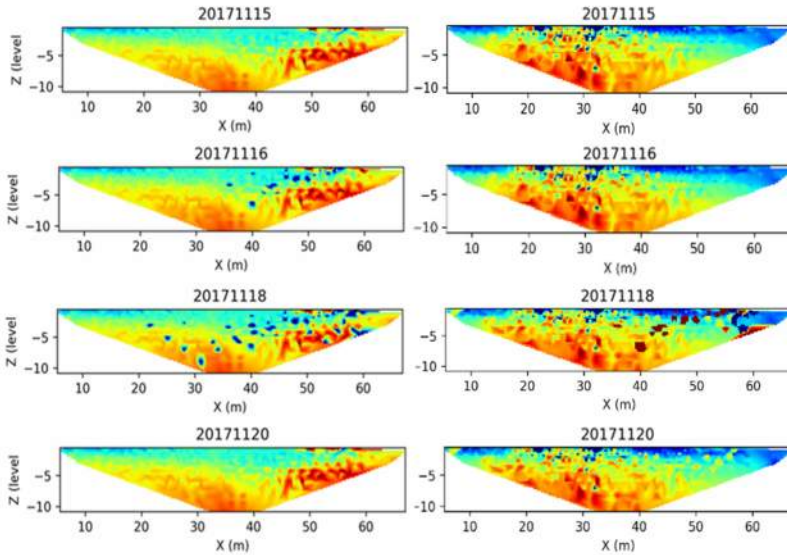


Figure 11. Spatial outliers in the observed apparent resistivity (left) and apparent chargeability (right)) data. Data from individual profiles presented as pseudosections.

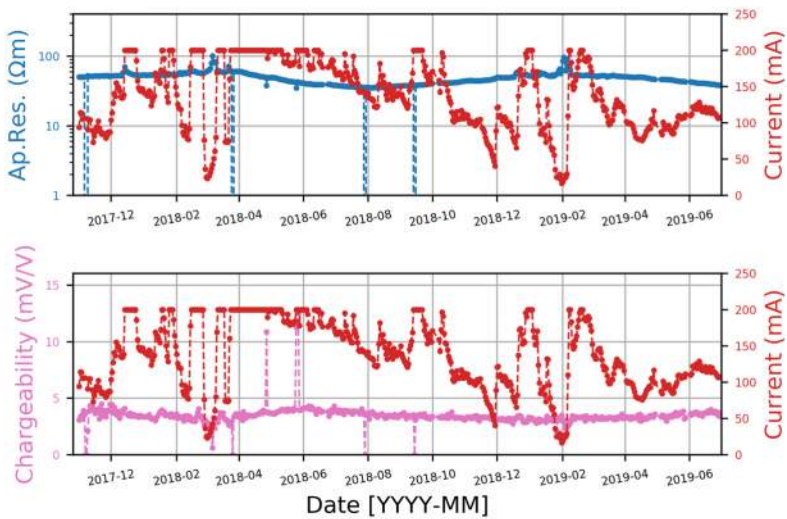


Figure 12. Temporal outliers in the observed apparent resistivity (top) and apparent chargeability (bottom)) data. Data from a single quadrupole presented as time-series.

## Inversion results and visualization

The inversion of monitoring data is an active topic of research. The naïve approach of inverting individual datasets separately is not effective (Kim et al., 2013) as the resulting models could potentially introduce artificial changes (artefacts). Advanced algorithms and efficient routines are needed to estimate models that better describe the subsurface.

In this context, two algorithms are of significant importance and should be mentioned. The time-lapse inversion algorithm (Loke et al., 2014) introduces an additional time constraint in the traditional smoothness constrain inversion. The algorithm solves the inverse geoelectrical problem for two datasets simultaneously and estimates two models of the subsurface while preserving spatial continuity of the electrical properties between the models. The 4D inversion algorithm (Kim et al., 2013; Loke et al., 2014) further expands that idea by simultaneously estimating several geoelectrical models instead of two.

In the 4D algorithm the data space is increased exponentially therefore rapidly making inversions computationally expensive and making it inefficient to invert many datasets at once. Furthermore, in cases where a new dataset is recorded daily it might be inefficient to invert all the previous steps again, since the solution for the previous data are already computed. For that reason, an optimal solution needs to be identified that produces good quality results and which can be efficiently executed multiple times.

# Chapter 5. Main Results

## Paper I

Paper I adopts a multimethod approach for site characterization by using the MIP, SRT and DCIP method.

First, the MIP soundings were used to create the geological profiles (Figure 13) and describe the geology in the study area. The concentrations of the contaminants measured by the MIP soundings, show that the highest concentrations of contaminants are found in the clay layer. Also, the presence of a thin sandy layer above the bedrock acts as a porous media that flushes the contaminant downstream.

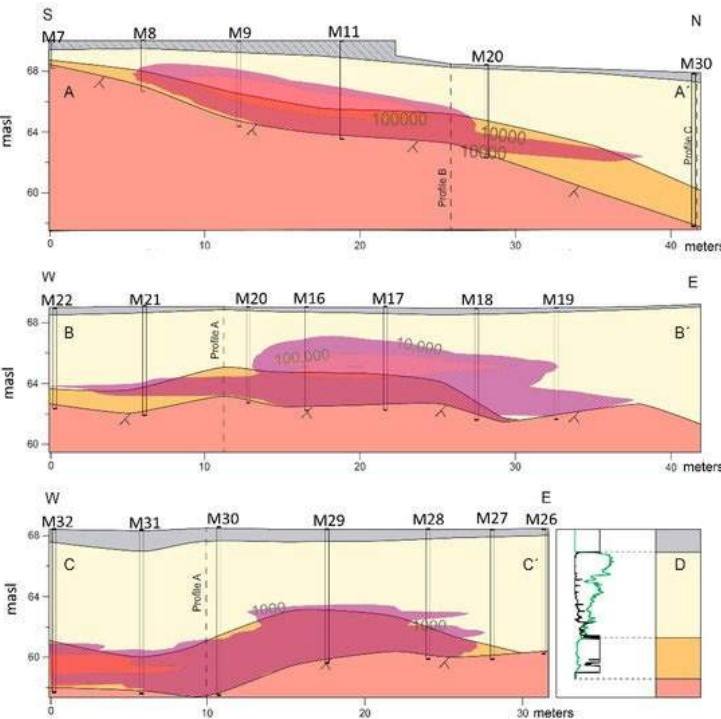


Figure 13. Geological profiles created from MIP data. Filling material (grey), fine material (yellow), coarse material (orange) and bedrock (red). The contamination is indicated by the purple contour map.

The contaminants sink into the sediments, since they are heavier than water, until they reach an impermeable layer, and then they can continue to migrate along its slope. In Alingsås, the crystalline bedrock is expected to act as an impermeable layer, although there are no drillings to verify that the contaminants haven't spread in there. For that reason, the SRT was used to estimate the bedrock topography for a larger area covering the parking lot. The bedrock topography from the SRT was used together with the MIP to create the final map. The results (Figure 14) show that the bedrock slopes downwards towards NNW, and this, together with the NW groundwater flow, can explain the extension of the plume.

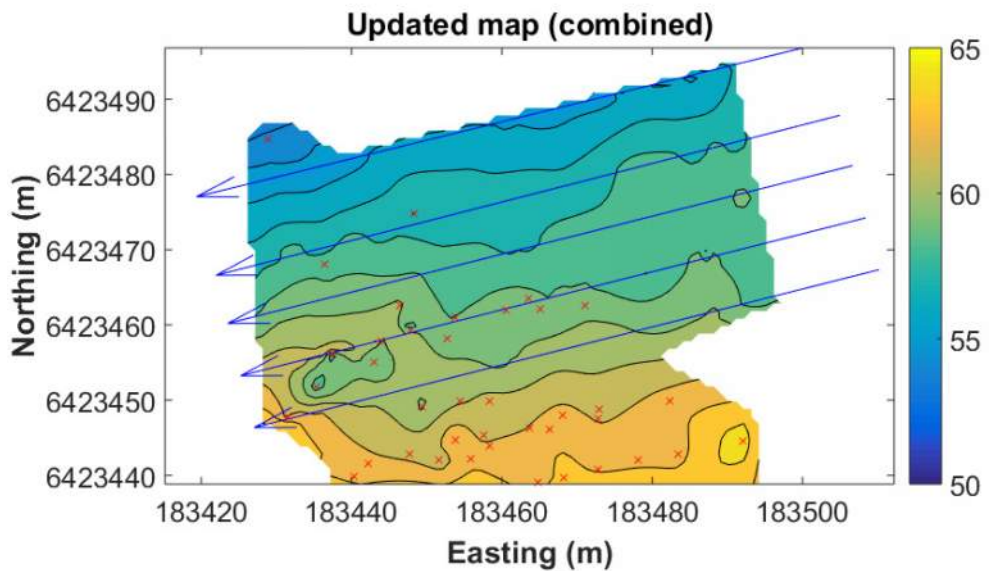


Figure 14. Final bedrock topography estimated by combining the results from the MIP and SRT methods.

Last, the DCIP monitoring system data collected before the bioremediation was initiated, has been used to map the geology in the area. The results are in good correlation with the geological profiles (Figure 13), although the lithology seems more heterogeneous than was previously thought. Furthermore, there is a strong increase in the electrical resistivity observed in Line 3 and Line 4 that can be correlated with high concentrations of contaminants in those areas (Figure 15). The correlation between the geoelectrical measurements and the contaminants, as well as the heterogeneity of the soil, is evident in the inverted result of the cross-hole tomography (Figure 16).

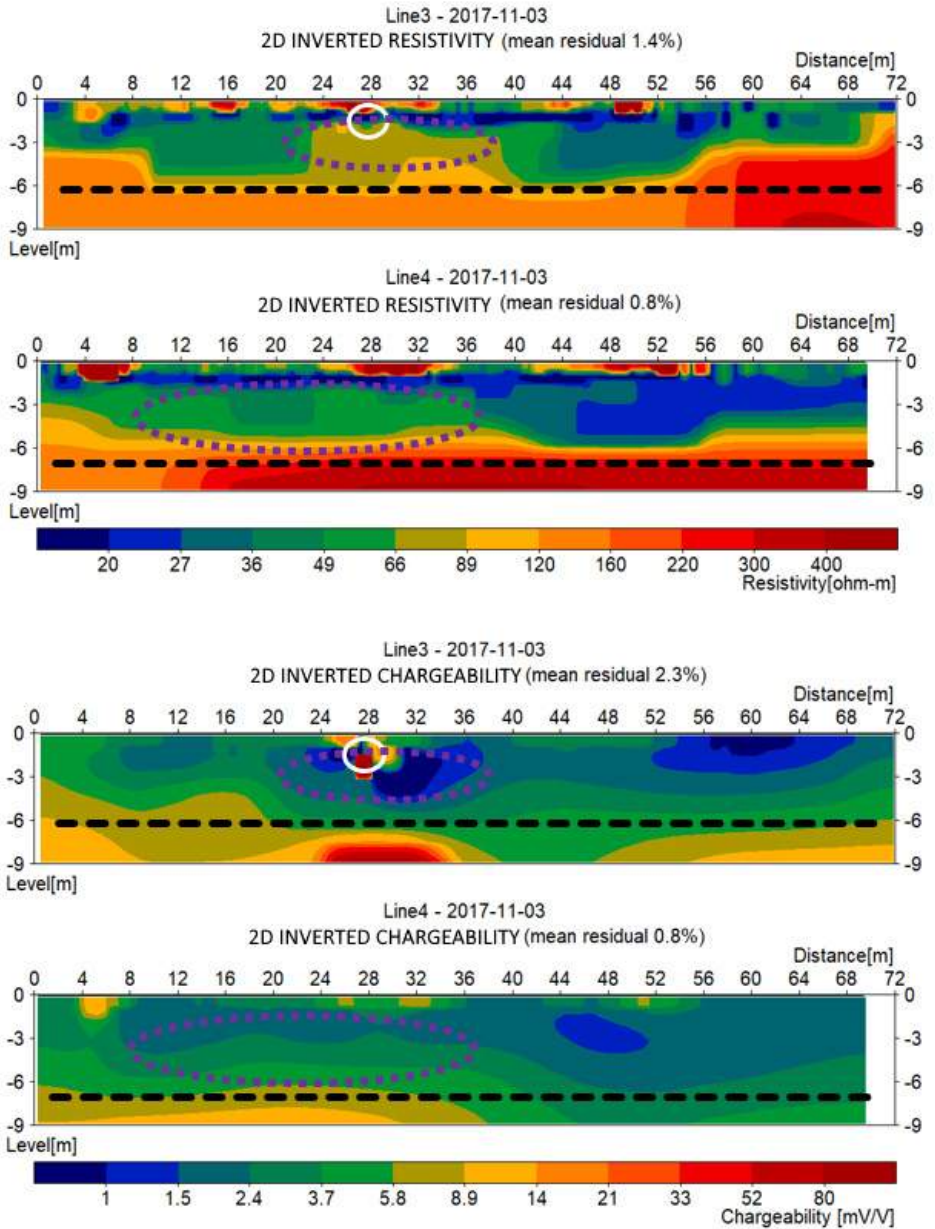


Figure 15. DCIP results from the baseline survey, November 2017 showing the interpreted bedrock (black dashed line), the interpreted contamination (purple dashed circle) and the location of buried metal infrastructure (white circle)

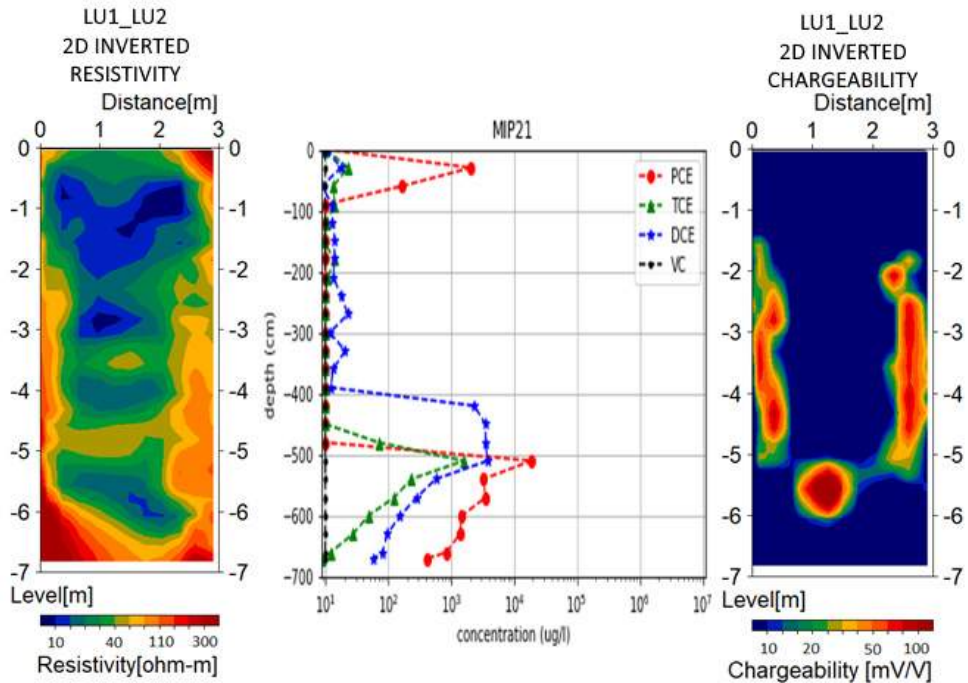


Figure 16. Inverted cross-hole tomography results for LU1-LU2. Resistivity (left), chargeability (right) and concentration from MIP sounding (middle).

## Paper II

A robust scheme for pre-processing, inversion and visualization of monitoring data is presented. 20-months of daily data were used in this work.

First, the time-series data from individual quadrupoles were filtered using first a median filter and then a low pass Butterworth filter to remove outliers. The proposed approach is very fast and can be used to effectively remove outliers from the data before the inversion.

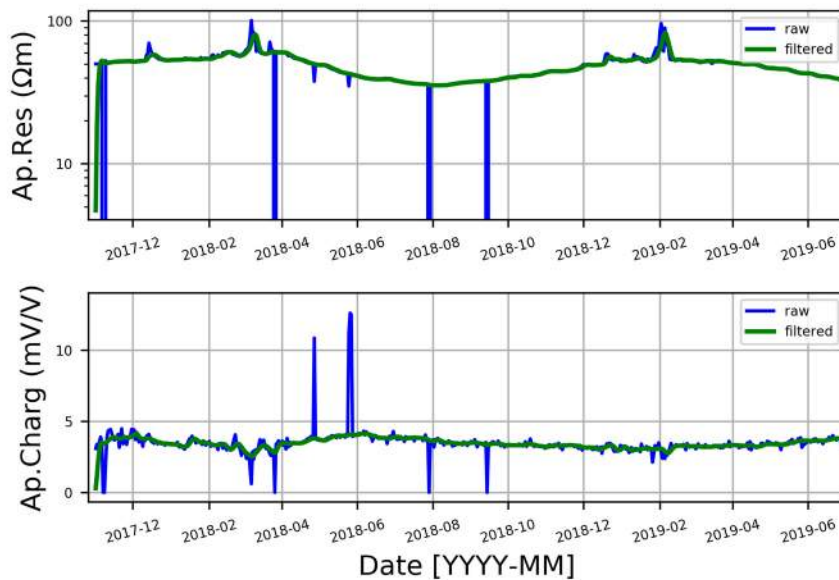


Figure 17. Example of filtering of raw data for quadrupole 34 of Line 3. The example refers to the data point involving electrodes distance 7-16-13-14 meters (A-B-M-N).

The data were inverted using the time-lapse algorithm. First, using the data from the baseline a reference profile was calculated and then weekly (median) profiles were computed for the entire dataset (20 months). The weekly profiles were finally inverted against the reference baseline profile.

The inverted results (Figure 18) show that the two treated areas behave differently during the 20-month period after the remediation program was launched. The area treated with the iron particles (Line 3) shows a general decrease in the electrical resistivity that dominates the entire time period. On the other hand, the area treated with the mixture of bacteria (Line 3) appears more resistive as the time progress.

Figure 19 illustrate the change in resistivity and chargeability for three areas of interest, the two treated areas and a reference area that no treatment took place. A block of 10x2 meter was selected for each area and the average value for the % change in resistivity and the change in chargeability is presented. It is evident that the resistivity values in the area where they injected the iron particles (Figure 19b, east area) are reduced significantly when compared with the baseline. On the other hand, the area where they injected the bacteria (Figure 19a, west area) and the untreated area (Figure 19c, end of Line 3) appear to change in a very similar way. That could mean that either the method fails to identify changes due to the effects of remediation or the experiment was unsuccessful.

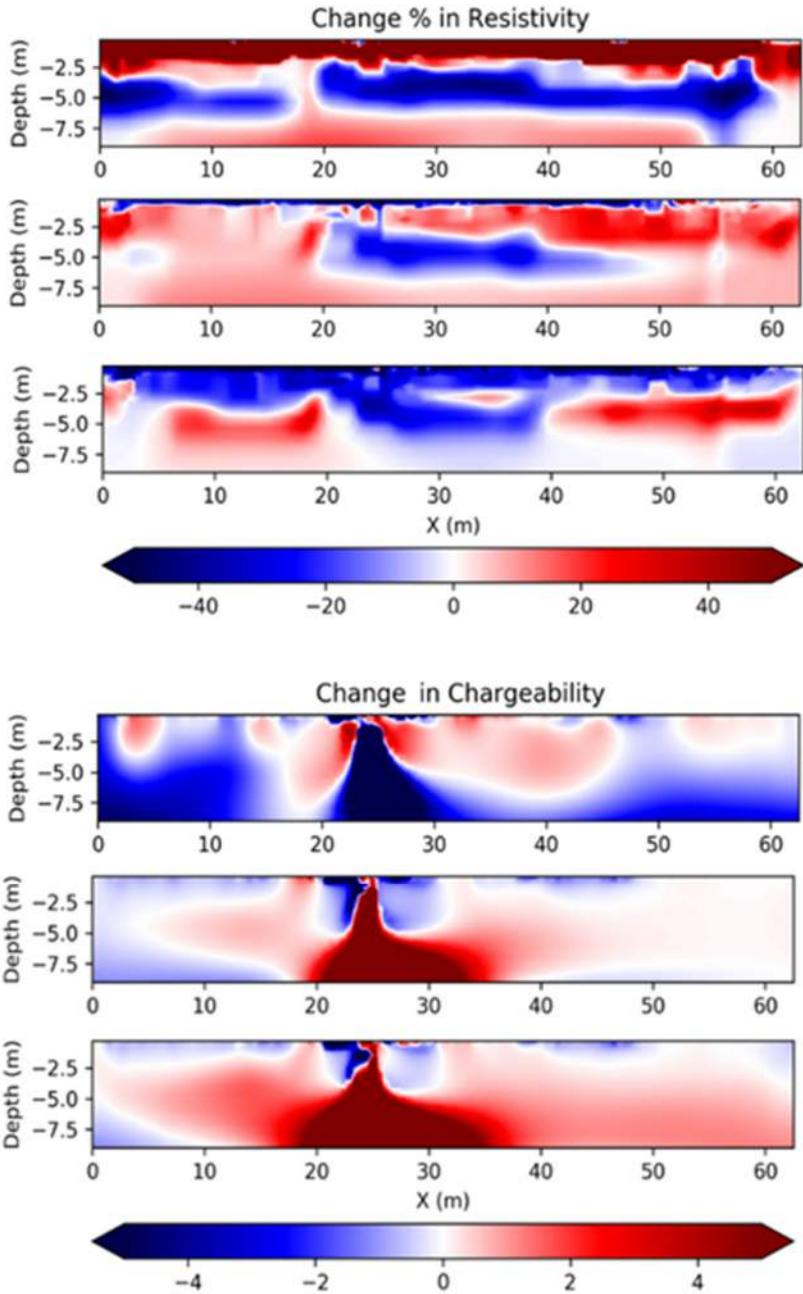


Figure 18. Examples of time-lapse inversions of Line3: from dates 2018-03-08 (top row), 2018-10-21 (middle row) and 2019-02-27 (bottom row). Percentage change in resistivity (top three) and absolute change in chargeability (bottom three) compared to baseline dataset.

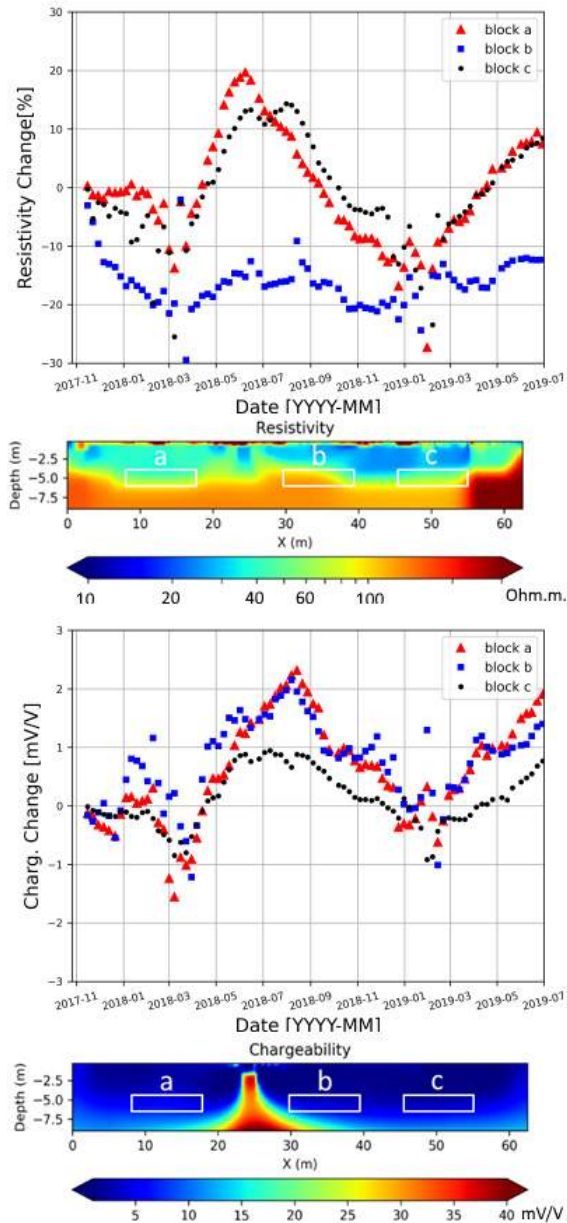


Figure 19. Analysis of the time dependent variations of resistivity (top) and chargeability (bottom) for Line 3. Resistivity is represented as percentage changes of inverted data respect to background, while chargeability is the absolute variation of inverted integral chargeability respect to background values. The values of the plots are calculated averaging inside the three areas (a, b, c) highlighted in the inverted results from the baseline below the respective time dependent variations.



# Chapter 6. Conclusions and future work

The work presented in this thesis demonstrates the effectiveness of geophysical methods for site characterization and mapping of the contamination. The use of point specific information, such as drillings or wells, is very important to make an accurate interpretation of the geophysical data. Furthermore, the geophysical data can be used to extrapolate the point specific information and create models that have greater spatial coverage.

The DCIP method has several advantages in monitoring of in-situ bioremediation. A permanent installation of the system along with several automation routines in terms of data acquisition and pre-processing, significantly reduces the cost of geophysical site investigation. The proposed data workflow can establish a robust framework that may be used as a base for a fully autonomous system, that could generate a result as soon as a new time step is recorded, bringing geoelectrical monitoring one step closer to real-time monitoring.

## **Future work**

The inverted profiles are strongly affected by seasonal variations due to temperature among other factors, so the inverted results need to be corrected for the temperature. Removing the effect of the temperature from the inverted profiles will highlight the changes that take place due to the injection of the products and the bioremediation.

Information from hydrogeochemical sampling should be used to verify the geophysical results, especially the results from Paper II. It is a relevant fact that the geoelectrical signature of the treated area (west) follows the same pattern as the untreated area which may mean that the treatment applied in the western treated area is not effective in reducing contamination as desired.

The spectral information contained in the DCIP data was not used in this work. It remains a challenge to propose robust routines that can be universally applied to large datasets, which would remove outliers and prepare the data for the inversion.

The use of neural networks could possibly be a solution to that problem. The spectral content can be further analysed for variations in time due to the remediation.

Hydrogeological models can be used to estimate the flow of the fluids in the subsurface. The hydrogeological models can be used to understand how the subsurface behaves and what to expect in the future. The geoelectrical monitoring can be used for example, to calibrate the hydrogeological models. Hydrogeophysics for in-situ bioremediation is indeed a very challenging field that can provide valuable tools for planning and monitoring of a bioremediation plan.

# Chapter 7. References

- Abdulsamad, F., Revil, A., Soueid Ahmed, A., Coperey, A., Karaoulis, M., Nicaise, S., Peyras, L., 2019. Induced polarization tomography applied to the detection and the monitoring of leaks in embankments. *Engineering Geology* 254, 89–101. <https://doi.org/10.1016/j.enggeo.2019.04.001>
- Angelis, D., Tsourlos, P., Tsokas, G., Vargemezis, G., Zacharopoulou, G., Power, C., 2018. Combined application of GPR and ERT for the assessment of a wall structure at the Heptapyrgion fortress (Thessaloniki, Greece). *Journal of Applied Geophysics* 152, 208–220. <https://doi.org/10.1016/j.jappgeo.2018.04.003>
- Argote-Espino, D.L., López-García, P.A., Tejero-Andrade, A., 2016. 3D-ERT geophysical prospecting for the investigation of two terraces of an archaeological site northeast of Tlaxcala state, Mexico. *Journal of Archaeological Science: Reports* 8, 406–415. <https://doi.org/10.1016/j.jasrep.2016.06.047>
- Atekwana, E.A., Atekwana, E., Legall, F.D., Krishnamurthy, R.V., 2005. Biodegradation and mineral weathering controls on bulk electrical conductivity in a shallow hydrocarbon contaminated aquifer. *Journal of Contaminant Hydrology* 80, 149–167. <https://doi.org/10.1016/j.jconhyd.2005.06.009>
- Atekwana, E.A., Atekwana, E.A., 2010. Geophysical signatures of microbial activity at hydrocarbon contaminated sites: A review. *Surveys in Geophysics* 31, 247–283. <https://doi.org/10.1007/s10712-009-9089-8>
- Auken, E., Doetsch, J., Fiandaca, G., Christiansen, A.V., Gazoty, A., Cahill, A.G., Jakobsen, R., 2014. Imaging subsurface migration of dissolved CO<sub>2</sub> in a shallow aquifer using 3-D time-lapse electrical resistivity tomography. *Journal of Applied Geophysics* 101, 31–41. <https://doi.org/10.1016/j.jappgeo.2013.11.011>
- Bernstone, C., Dahlin, T., Ohlsson, T., Hogland, W., 2000. DC-resistivity mapping of internal landfill structures: Two pre-excavation surveys. *Environmental Geology* 39, 360–371. <https://doi.org/10.1007/s002540050015>
- Branzen, H., 2013. Förstärkt självrening av grundvatten förorenat med klokerade etener.
- Cassiani, G., Kemna, A., Villa, A., Zimmermann, E., 2009. Spectral induced polarization for the characterization of free-phase hydrocarbon contamination of sediments with low clay content. *Near Surface Geophysics* 7, 547–562.
- Caterina, D., Flores Orozco, A., Nguyen, F., 2017. Long-term ERT monitoring of biogeochemical changes of an aged hydrocarbon contamination. *Journal of Contaminant Hydrology* 201, 19–29. <https://doi.org/10.1016/j.jconhyd.2017.04.003>

- Chambers, J.E., Kuras, O., Meldrum, P.I., Ogilvy, R.D., Hollands, J., 2006. Electrical resistivity tomography applied to geologic, hydrogeologic, and engineering investigations at a former waste-disposal site. *GEOPHYSICS* 71, B231–B239. <https://doi.org/10.1190/1.2360184>
- Chambers, J.E., Meldrum, P.I., Gunn, D.A., Wilkinson, P.B., Kuras, O., Weller, A.L., Ogilvy, R.D., 2009. Hydrogeophysical monitoring of landslide processes using automated time-lapse electrical resistivity tomography (ALERT). Presented at the Near Surface 2009 - 15th European Meeting of Environmental and Engineering Geophysics. <https://doi.org/10.3997/2214-4609.20147066>
- Chirindja, F.J., Dahlin, T., Juizo, D., 2017. Improving the groundwater-well siting approach in consolidated rock in Nampula Province, Mozambique. *Hydrogeology Journal* 25, 1423–1435. <https://doi.org/10.1007/s10040-017-1540-1>
- Cook, K.L., Van Nostrand, R.G., 1954. Interpretation of Resistivity Data Over Filled Sinks. *Geophysics* 19, 761–790.
- Dahlin, T., Loke, M.H., 2015. Negative apparent chargeability in time-domain induced polarisation data. *Journal of Applied Geophysics* 123, 322–332. <https://doi.org/10.1016/j.jappgeo.2015.08.012>
- Dahlin, T., Zhou, B., 2006. Multiple-gradient array measurements for multichannel 2D resistivity imaging. *Near Surface Geophysics* 4, 113–123.
- Danielsen, B.E., Dahlin, T., 2009. Comparison of geoelectrical imaging and tunnel documentation at the Hallandsås Tunnel, Sweden. *Engineering Geology* 107, 118–129. <https://doi.org/10.1016/j.enggeo.2009.05.005>
- Davis, C.A., Atekwana, E., 2006. Potential application of biogeophysics to EOR and remediation investigations. *SEG Technical Program Expanded Abstracts* 25, 1471–1474. <https://doi.org/10.1190/1.2369798>
- Fernandez, P.M., Bloem, E., Binley, A., Philippe, R.S.B.A., French, H.K., 2019. Monitoring redox sensitive conditions at the groundwater interface using electrical resistivity and self-potential. *Journal of Contaminant Hydrology* 226. <https://doi.org/10.1016/j.jconhyd.2019.103517>
- Fetter, C.W., 2001. *Applied Hydrogeology*, 4th ed. Prentice Hall.
- Flores Orozco, A., Velimirovic, M., Tosco, T., Kemna, A., Sapion, H., Klaas, N., Sethi, R., Bastiaens, L., 2015. Monitoring the injection of microscale zerovalent iron particles for groundwater remediation by means of complex electrical conductivity imaging. *Environmental Science and Technology* 49, 5593–5600. <https://doi.org/10.1021/acs.est.5b00208>
- Flores Orozco, A., Williams, K.H., Kemna, A., 2013. Time-lapse spectral induced polarization imaging of stimulated uranium bioremediation. *Near Surface Geophysics* 11, 531–544. <https://doi.org/10.3997/1873-0604.2013020>
- Forquet, N., French, H.K., 2012. Application of 2D surface ERT to on-site wastewater treatment survey. *Journal of Applied Geophysics* 80, 144–150. <https://doi.org/10.1016/j.jappgeo.2012.02.002>

- Gazoty, A., Fiandaca, G., Pedersen, J., Auken, E., Christiansen, A., Pedersen, J., 2012a. Application of time domain induced polarization to the mapping of lithotypes in a landfill site. *Hydrology and Earth System Sciences* 16, 1793–1804. <https://doi.org/10.5194/hess-16-1793-2012>
- Gazoty, A., Fiandaca, G., Pedersen, J., Auken, E., Christiansen, A.V., 2012b. Mapping of landfills using time-domain spectral induced polarization data: the Eskelund case study. *Near Surface Geophysics* 10, 575–586. <https://doi.org/10.3997/1873-0604.2012046>
- Giang, N.V., Kochanek, K., Vu, N.T., Duan, N.B., 2018. Landfill leachate assessment by hydrological and geophysical data: case study NamSon, Hanoi, Vietnam. *Journal of Material Cycles and Waste Management* 20, 1648–1662. <https://doi.org/10.1007/s10163-018-0732-7>
- Johansson, S., Sparrenbom, C., Fiandaca, G., Lindskog, A., Olsson, P.-I., Dahlin, T., Rosqvist, H., 2017. Investigations of a Cretaceous limestone with spectral induced polarization and scanning electron microscopy. *Geophysical Journal International* 208, 954–972. <https://doi.org/10.1093/gji/ggw432>
- Kemna, A., Binley, A., Slater, L., 2004. Crosshole IP imaging for engineering and environmental applications. *Geophysics* 69, 97–107. <https://doi.org/10.1190/1.1649379>
- Kim, J.-H., Supper, R., Tsourlos, P.I., Yi, M.-J., 2013. 4D Inversion of Resistivity Monitoring Data through Lp Norm Minimizations. *Geophysical Journal International* 195, 1640–1656. <https://doi.org/10.1093/gji/ggt324>
- Knödel, K., Lange, G., Voigt, H.-J., 2007. *Environmental Geology: Handbook of Field Methods and Case Studies*. Springer-Verlag, Berlin Heidelberg. <https://doi.org/10.1007/978-3-540-74671-3>
- Kuras, O., Wilkinson, P.B., Meldrum, P.I., Oxby, L.S., Uhlemann, S., Chambers, J.E., Binley, A., Graham, J., Smith, N.T., Atherton, N., 2016. Geoelectrical monitoring of simulated subsurface leakage to support high-hazard nuclear decommissioning at the Sellafield Site, UK. *Science of The Total Environment* 566–567, 350–359. <https://doi.org/10.1016/j.scitotenv.2016.04.212>
- Leroux, V., Dahlin, T., 2006. Time-lapse resistivity investigations for imaging saltwater transport in glaciofluvial deposits. *Environmental Geology* 49, 347–358. <https://doi.org/10.1007/s00254-005-0070-7>
- Leroux, V., Dahlin, T., Rosqvist, H., 2010. Time-domain IP and resistivity sections measured at four landfills with different contents. Presented at the Near Surface 2010 - 16th European Meeting of Environmental and Engineering Geophysics. <https://doi.org/10.3997/2214-4609.20144851>
- Loke, M., Barker, R.D., 1996. Rapid Least-Squares Inversion of Apparent Resistivity Pseudosections Using a Quasi-Newton Method. *Geophysical Prospecting* 44, 131–152. <https://doi.org/10.1111/j.1365-2478.1996.tb00142.x>
- Loke, M.H., Chambers, J.E., Rucker, D.F., Kuras, O., Wilkinson, P.B., 2013. Recent developments in the direct-current geoelectrical imaging method. *Journal of Applied Geophysics* 95, 135–156. <https://doi.org/10.1016/j.jappgeo.2013.02.017>

- Loke, M.H., Dahlin, T., Leroux, V., 2011. Constrained time-lapse inversion of 3-D resistivity surveys data. Presented at the Near Surface 2011 - 17th European Meeting of Environmental and Engineering Geophysics.
- Loke, M.H., Dahlin, T., Rucker, D.F., 2014. Smoothness-constrained time-lapse inversion of data from 3D resistivity surveys. *Near Surface Geophysics* 12, 5–24. <https://doi.org/10.3997/1873-0604.2013025>
- Maurya, P.K., Balbarini, N., Møller, I., Rønne, V., Christiansen, A.V., Bjerg, P.L., Auken, E., Fiandaca, G., 2018. Subsurface imaging of water electrical conductivity, hydraulic permeability and lithology at contaminated sites by induced polarization. *Geophysical Journal International* 213, 770–785. <https://doi.org/10.1093/gji/ggy018>
- Ntarlagiannis, D., Robinson, J., Soupios, P., Slater, L., 2016. Field-scale electrical geophysics over an olive oil mill waste deposition site: Evaluating the information content of resistivity versus induced polarization (IP) images for delineating the spatial extent of organic contamination. *Journal of Applied Geophysics* 135, 418–426. <https://doi.org/10.1016/j.jappgeo.2016.01.017>
- Olsson, P.-I., Dahlin, T., Fiandaca, G., Auken, E., 2015. Measuring time-domain spectral induced polarization in the on-time: Decreasing acquisition time and increasing signal-to-noise ratio. *Journal of Applied Geophysics* 123, 316–321. <https://doi.org/10.1016/j.jappgeo.2015.08.009>
- Olsson, P.-I., Fiandaca, G., Larsen, J.J., Dahlin, T., Auken, E., 2016. Doubling the spectrum of time-domain induced polarization by harmonic de-noising, drift correction, spike removal, tapered gating and data uncertainty estimation. *Geophysical Journal International* 207, 774–784. <https://doi.org/10.1093/gji/ggw260>
- Park, S., Yi, M.-J., Kim, J.-H., Shin, S.W., 2016. Electrical resistivity imaging (ERI) monitoring for groundwater contamination in an uncontrolled landfill, South Korea. *Journal of Applied Geophysics, New trends in Induced Polarization* 135, 1–7. <https://doi.org/10.1016/j.jappgeo.2016.07.004>
- Power, C., Gerhard, J.I., Karaoulis, M., Tsourlos, P., Giannopoulos, A., 2014. Evaluating four-dimensional time-lapse electrical resistivity tomography for monitoring DNAPL source zone remediation. *Journal of Contaminant Hydrology* 162–163, 27–46. <https://doi.org/10.1016/j.jconhyd.2014.04.004>
- Power, C., Tsourlos, P., Ramasamy, M., Nivorlis, A., Mkandawire, M., 2018. Combined DC resistivity and induced polarization (DC-IP) for mapping the internal composition of a mine waste rock pile in Nova Scotia, Canada. *Journal of Applied Geophysics* 150, 40–51. <https://doi.org/10.1016/j.jappgeo.2018.01.009>
- Rosqvist, H., Leroux, V., Dahlin, T., Svensson, M., Lindsjö, M., Månsson, C.-H., Johansson, S., 2011. Mapping landfill gas migration using resistivity monitoring. *Proceedings of the Institution of Civil Engineers - Waste and Resource Management* 164, 3–15. <https://doi.org/10.1680/warm.2011.164.1.3>
- Rossi, M., Dahlin, T., Olsson, P.-I., Günther, T., 2018. Data acquisition, processing and filtering for reliable 3D resistivity and time-domain induced polarisation tomography in an urban area: Field example of Vinsta, Stockholm. *Near Surface Geophysics* 16, 220–229. <https://doi.org/10.3997/1873-0604.2018014>

- SEPA, 2014. Nationell Plan för Fördelning av Statliga Bidrag för Efterbehandling; Report 6617. Swedish Environmental Protection Agency: Stockholm, Sweden Volume 30.
- Simyrdanis, K., Moffat, I., Papadopoulos, N., Kowlessar, J., Bailey, M., 2018a. 3D Mapping of the Submerged Crowie Barge Using Electrical Resistivity Tomography. *International Journal of Geophysics* 2018. <https://doi.org/10.1155/2018/6480565>
- Simyrdanis, K., Papadopoulos, N., Souprios, P., Kirkou, S., Tsourlos, P., 2018b. Characterization and monitoring of subsurface contamination from Olive Oil Mills' waste waters using Electrical Resistivity Tomography. *Science of the Total Environment* 637–638, 991–1003. <https://doi.org/10.1016/j.scitotenv.2018.04.348>
- Slater, L., Ntarlagiannis, D., Yee, N., O'Brien, M., Zhang, C., Williams, K.H., 2008. Electrode voltages in the presence of dissolved sulfide: Implications for monitoring natural microbial activity. *Geophysics* 73, F65–F70. <https://doi.org/10.1190/1.2828977>
- Slater, L.D., Lesmes, D., 2002. IP interpretation in environmental investigations. *Geophysics* 67, 77–88. <https://doi.org/10.1190/1.1451353>
- Sparrenbom, C.J., Åkesson, S., Johansson, S., Hagerberg, D., Dahlin, T., 2017. Investigation of chlorinated solvent pollution with resistivity and induced polarization. *Science of The Total Environment* 575, 767–778. <https://doi.org/10.1016/j.scitotenv.2016.09.117>
- Steelman, C.M., Klazinga, D.R., Cahill, A.G., Endres, A.L., Parker, B.L., 2017. Monitoring the evolution and migration of a methane gas plume in an unconfined sandy aquifer using time-lapse GPR and ERT. *Journal of Contaminant Hydrology* 205, 12–24. <https://doi.org/10.1016/j.jconhyd.2017.08.011>
- Tsourlos, P.I., Ogilvy, R.D., 1999. An algorithm for the 3-D inversion of tomographic resistivity and induced polarisation data: Preliminary results. *Journal of the Balkan Geophysical Society* 2, 30–45.
- Ustra, A.T., Elis, V.R., Mondelli, G., Zuquette, L.V., Giacheti, H.L., 2012. Case study: A 3D resistivity and induced polarization imaging from downstream a waste disposal site in Brazil. *Environmental Earth Sciences* 66, 763–772. <https://doi.org/10.1007/s12665-011-1284-5>
- Wemegah, D.D., Fiandaca, G., Auken, E., Menyeh, A., Danuor, S.K., 2017. Spectral time-domain induced polarisation and magnetic surveying - An efficient tool for characterisation of solid waste deposits in developing countries. *Near Surface Geophysics* 15, 75–84. <https://doi.org/10.3997/1873-0604.2016048>
- White, D.J., 1989. Two-Dimensional Seismic Refraction Tomography. *Geophys J Int* 97, 223–245. <https://doi.org/10.1111/j.1365-246X.1989.tb00498.x>
- Zago, M.M., Fries, M., Ramires, J.E.F., 2020. Groundwater infiltration in a gold mine—A geoelectrical investigation model as an aid to dewatering process determination. *Journal of Applied Geophysics* 172. <https://doi.org/10.1016/j.jappgeo.2019.103909>



Paper I





Article

# Multidisciplinary Characterization of Chlorinated Solvents Contamination and In-Situ Remediation with the Use of the Direct Current Resistivity and Time-Domain Induced Polarization Tomography

Aristeidis Nivorlis <sup>1,\*</sup>, Torleif Dahlin <sup>1</sup>, Matteo Rossi <sup>1</sup>, Nikolas Höglund <sup>2</sup> and Charlotte Sparrenbom <sup>2</sup>

<sup>1</sup> Engineering Geology, Lund University, Box 118, SE-22100 Lund, Sweden; torleif.dahlin@tg.lth.se (T.D.); matteo.rossi@tg.lth.se (M.R.)

<sup>2</sup> Department of Geology, Lund University, Sölvegatan 12, SE-22362 Lund, Sweden; nikolas.hoglund@geol.lu.se (N.H.); charlotte.sparrenbom@geol.lu.se (C.S.)

\* Correspondence: anivorlis@gmail.com

Received: 14 October 2019; Accepted: 19 November 2019; Published: 20 November 2019



**Abstract:** Soil contamination is a widespread problem and action needs to be taken in order to prevent damage to the groundwater and the life around the contaminated sites. In Sweden, it is estimated that more than 80,000 sites are potentially contaminated, and therefore, there is a demand for investigations and further treatment of the soil. In this paper, we present the results from a methodology applied in a site contaminated with chlorinated solvents, for characterization of the contamination in order to plan the remediation and to follow-up the initial step of in-situ remediation in an efficient way. We utilized the results from three different methods; membrane interface probe for direct measurement of the contaminant concentrations; seismic refraction tomography for investigating the depth to the bedrock interface; and direct current resistivity and time-domain induced polarization tomography to acquire a high-resolution imaging of the electrical properties of the subsurface. The results indicate that our methodology is very promising in terms of site characterization, and furthermore, has great potential for real-time geophysical monitoring of contaminated sites in the future.

**Keywords:** geophysics; contamination; characterization; monitoring; remediation

## 1. Introduction

Soil contamination is a widespread problem in most developed countries due to the increased use of hazardous substances in the industry. In the European Union, a common framework based on the ‘polluter pays principle’ was established through the directive of environmental liability (2004/35/CE), to be applied in cases of environmental damage.

On basis of that framework, the Swedish Environmental Protection Agency (SEPA) has identified more than 80,000 potentially contaminated sites in Sweden [1]. Expansion of the cities pushes new construction towards many contaminated sites, which need to be treated urgently. The contaminated materials are often treated via transportation to landfills with (“dig and treat”) or without any treatment (“dig and dump”), introducing the risk of secondary exposure and/or movement of the problem. Because these techniques are associated with significant risk and long-term costs, SEPA (2014) recommends the use of alternative methods.

In this context, one method of particular interest is in-situ remediation of the contaminated mass. In-situ remediation is very favorable in cases where the contaminated mass has great volume, is located deep and/or the traditional approach would require the demolition of buildings, because it can provide

a much cheaper and safer alternative. A major concern in cases of in-situ remediation, however, is the effectiveness of the treatment and reliability of the monitored changes that take place in the subsurface.

For effective characterization of the contaminated mass, the use of geochemical analyses of groundwater and soil samples [2] is necessary, where the Membrane Interface Probe (MIP) method is considered an industry ‘standard’ and a compliment to the sampling [3]. Although these methods produce reliable results, they offer poor spatial coverage of the contaminated mass. Geophysical methods can provide a valuable tool to extrapolate the localized information acquired from sampling and MIP soundings for effective characterization of the contaminated mass.

Direct Current resistivity time-domain Induced Polarization tomography (DCIP) is a non-invasive geoelectric method that has the potential to provide an indirect indication of the contaminant [4]. Frequency based spectral Induced Polarization has been applied to monitoring of stimulated bioremediation of uranium contamination with promising results [5]. The method has been used in landfill characterization [6–12], spatial and temporal distribution of leachates [13–15], and gas migration within landfills [16,17]. Furthermore, the method has been used in sites contaminated with Non-Aqueous Phase Liquids (NAPLs) for characterization [18–22] and monitoring of the changes due to remediation [23,24]. DCIP has also been applied successfully to monitoring of injection and transport of microscale zerovalent iron (mZVI) particles for groundwater remediation purposes [25].

The excessive and careless use of chlorinated solvents in, for instance, dry-cleaning facilities has created a significant demand for more effective, safer and cost-efficient tools for characterization, monitoring and scientific research on in-situ bioremediation.

In this study, we have investigated an industrial (former dry-cleaning) area contaminated with tetrachloroethylene (PCE) and its degradation products trichloroethene (TCE), dichloroethane (DCE) and vinyl chloride (VC). To follow SEPA recommendations, a pilot in-situ remediation test was conducted by the injection of two commercially available products, applying stimulated reductive dechlorination of the contaminant.

The aim of this study is to improve our understanding about the underground hydrogeological system, investigate the distribution of the contaminant and its effect on the geophysical response and identify temporal changes in the geophysical signal shortly after the initiated remediation.

## 2. Area of Investigation

In Alingsås (South Central Sweden, see Figure 1), an industrial-scale dry-cleaning facility (Alingsås tvätteriet) started operating in 1963, supplying cleaning services for the military. Sometime during the 1960s or 1970s, a single spill of approximately 200 L of PCE leaked into the ground, resulting in the formation of a DNAPL source zone beneath the building with a plume extending out under the parking lot. That is the only documented spill; however, other instances of undocumented spills could have occurred in the past. Today, the use of PCE has ceased, and the facility is operating under the Administrative Region Västra Götaland as a laundry and textile cleaning (water only) unit, taking care of approximately 40 tons of textiles per day for the regional hospitals. Responsibility for the remediation is shared between the Swedish Government, through the Swedish Geological Survey (SGU) and the current owners (Region Västra Götaland). Due to ongoing operations in the building, in-situ remediation is the favored approach for treatment of the contaminated masses.

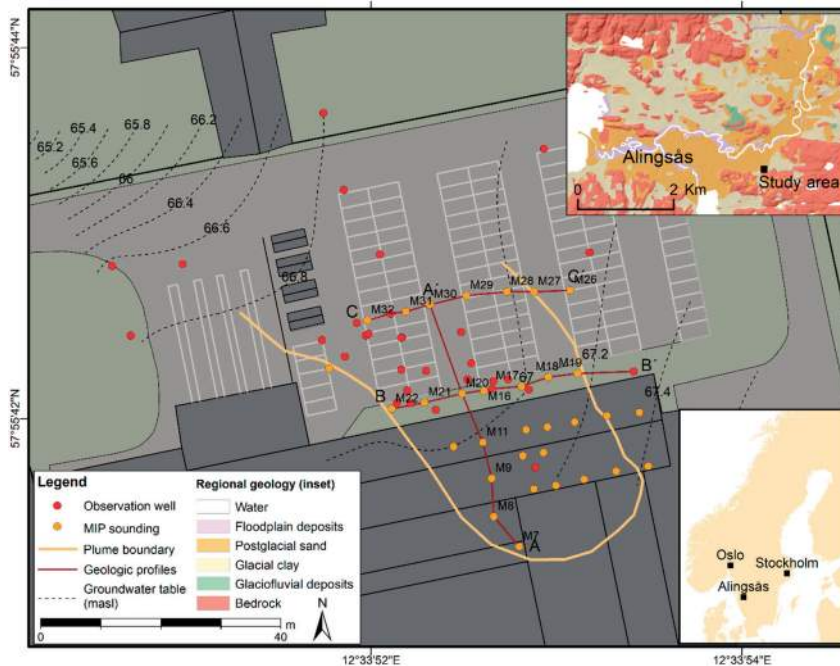


**Figure 1.** Overview of the Alingsås site where the observation wells (red circles), the Membrane Interface Probe (MIP) soundings (orange circles), the groundwater level (black dashed lines), the plume boundaries (orange line) and the regional surface geology (top right, created with data from SGU Jordarter, 1:25,000–1:100,000 © SGU) can be seen. Line A-A', B-B' and C-C' marks the location of geological profiles shown in Figure 2.

Alingsås is located on the eastern segment of the Swedish Southwestern Gneiss Region, characterized by gneissic granite and veiny granitic gneiss [26]. The segment is demarcated to the northwest by the Mylonite Zone, a tectonic zone several kilometers wide extending through southwestern Sweden [26]. The study area, east of central Alingsås, is located on the southern slope of Sävåån valley, a typical feature of the Swedish joint valley landscape (see regional map in Figure 1). The bedrock, which is exposed in several outcrops just south of the facility, slopes in a NNW direction towards Sävåån River. On top of the bedrock are quaternary deposits varying from 0 to 1 m in thickness in the upper slopes to more than 20 m in thickness towards the valley floor.

In the area of investigation, the depth to the bedrock varies between 2 to 10 m. The sediment overlying the bedrock is deposited in a fining upwards sequence. It consists of a meter of sand and gravel at the bottom, followed by clayey sandy silt, with sandy silty clay on top. On top of the sediment, about 1 m of fill material is present. Profiles describing the conceptual geology (Figure 2, conceptual models, A–C) are elaborated based on interpretation of MIP results (Figure 2, conceptual model, D) and borehole records. The interpreted results suggest, from the bedrock and up, a three-layer structure consisting of a coarse bottom unit, a “mixed fines” unit and a coarse gravel filling. The sedimentary units show a varying inner heterogeneity with lenses of both finer and coarser material occurring. The topography slopes gently towards NNW. The depth to the water table varies between 1.5 to 2 m below the ground surface and the groundwater flows from SE towards NW.

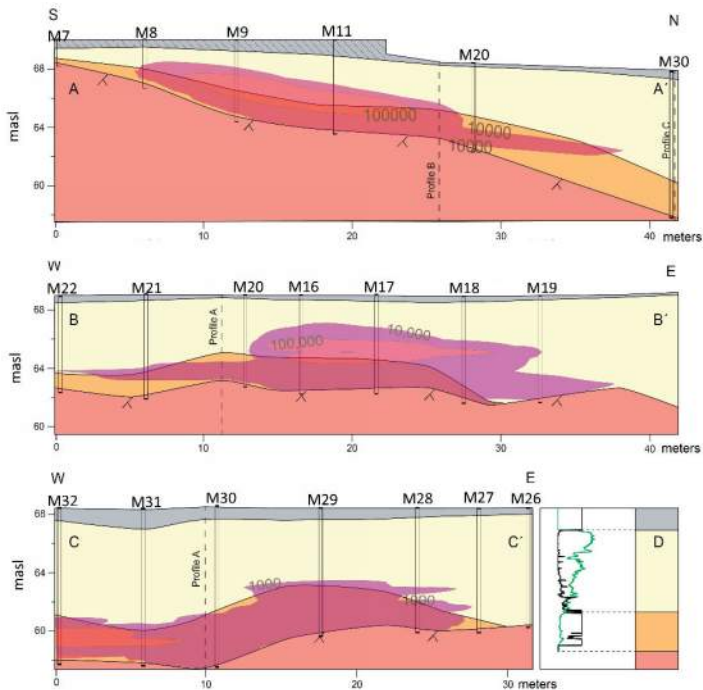


**Figure 2.** Geological and contaminant sections interpolated from MIP sounding data. The information about the geology (electrical conductivity (green mS/m) and estimated hydraulic conductivity (black, m/day)) is sampled every 1.5 cm and the information about the contamination (purple shows total concentration of PCE, TCE, DCE and VC in  $\mu\text{g/l}$ ) is sampled every 30 cm. The bedrock (red), bottom coarse unit (orange), mixed fine unit (light yellow) and coarse filling unit (grey) are interpreted based on the information about the geology based on the drill log (D). Profile locations are shown in Figure 1. The figure was generated by processing of the raw data from [27] through [28].

Between February 2nd and February 10th, 2017, the site was investigated using the MIP method [27] and the raw data [28] were further processed in this work. The plume was delineated to an area beneath the building and it extended outward beneath parts of the parking lot. The plume migrates towards NNW (Figure 1), following the dip of the bedrock. In order to determine the best approach for treatment of the contamination and stop further spreading, a pilot in-situ remediation program was launched in November 2017, using a direct push injection method on the north side of the laundry building (Figure 3). In order to evaluate the best approach for a future full-scale remediation scenario, two different remediating agents were injected into the plume at different locations, for comparison.

In injection area A (west side, see Figure 3) Provectus ERD-CH<sub>4</sub><sup>TM</sup> substrate containing carbon source (electron donor) in the form of vegetable oils together with acids and a bacterial consortium (*Dehalococcoides mccartyi*, *Desulfovibrio*, *Desulfitobacterium* and methanogenic archaea bacteria) was injected in two phases between the 7th and the 17th of November 2017, with a total of 32 points. In injection area B (east side, see Figure 3) CAT100<sup>TM</sup>-substrate containing granular activated carbon, zero-valent iron and Trap & Treat<sup>®</sup> bacteria concentrate were injected, together with a methane inhibitor, between the 28<sup>th</sup> and the 30<sup>th</sup> of November 2017, in a total of 37 points. In both cases, the products were injected from a depth of 3 m and downward until reaching the top of the bedrock.

### 3. Method Description

#### 3.1. Direct Current Resistivity and Time-Domain Induced Polarization

The DCIP method estimates the electrical resistivity and chargeability distribution in the subsurface [29]. For the DCIP measurements, an ABEM Terrameter LS2 was used in the 100% duty-cycle mode [30] and the full waveforms were recorded and processed to enhance the data quality [31]. A pulse-length of 4 seconds was used averaging over four current pulses with alternate polarity to enhance the signal to noise ratio.

The measurements were focused on the contaminant source and plume area outside of the buildings where the pilot injection was planned to take place. Four DCIP surface lines (Figure 3) with electrodes buried 40 cm into the ground were established to provide a permanent installation with a total of 64 stainless steel metal plate electrodes (10 × 10 cm) for each line in the DCIP monitoring system. The spacing between the electrodes is 1 m; however, the first four electrodes (except Line 4) and the last nine electrodes (all lines) are separated by 2 m to increase the depth of investigation. A multiple gradient array measurement sequence was used for the measurements [32].

The processed data were inverted for the resistivity and integral chargeability of the ground using Res2dinvx64 (Geotomo Software, version 4.08). The grid refinement (horizontal model cell size of half the electrode spacing) and L1-norm (robust) inversion options were used, where the latter is better at handling strong contrast as well as noise in the data compared to least-squares (L2 norm) inversion. For the time-lapse inversion the smoothness constrained time-lapse inversion was used [33] and the data sets shortly after the injection period were inverted against the baseline which was measured one week prior to the injection.

Furthermore, four boreholes with stainless steel ring electrodes were deployed, two in each injection area, to be used as pairs for cross-hole tomography. The separation of the wells was 2.7 m in injection area A, 2.5 m in injection area B and the electrodes were installed every 0.25 cm in each well up to the maximum depth. For the measurement sequence, the dipole-dipole array, containing a mixed set of inline and cross-borehole measurements, was used. The data were inverted using the DC2DPRO [34,35] software (version 1.01) using the least-squares inversion and the L1-norm error minimization option.

#### 3.2. Seismic Refraction

Seismic refraction was used as a help to delineate depth to bedrock, as it provides continuous data over the area as opposed to borehole and MIP data, which offer only low spatial coverage. The seismic refraction method estimates the velocity with which the generated elastic wave (P-wave) propagates in the subsurface [36]. The data were collected with a Geometrics StrataVisor paired with a Geometrics Geode recorder to increase the number of channels. Vertical component 4.5 kHz geophones, where used, were attached to a land streamer cable. An accelerated weight drop, mounted on a car, was used as a source. In total six parallel two-dimensional (2D) lines with 70 receivers were collected covering the parking lot area (Figure 3). The spacing between the geophones was 1.25 m and the shots were fired between every 7,8 geophones. An offset shot was fired where sufficient space was available.

The first arrival events were picked for every line and then a 2D tomography was performed to obtain the distribution of P-wave velocities in the subsurface. The data was processed and inverted using the software Reflexw (Sandmeier Geophysical Research, version 8.5) with a curved ray-tracing model in a finite difference approximation.

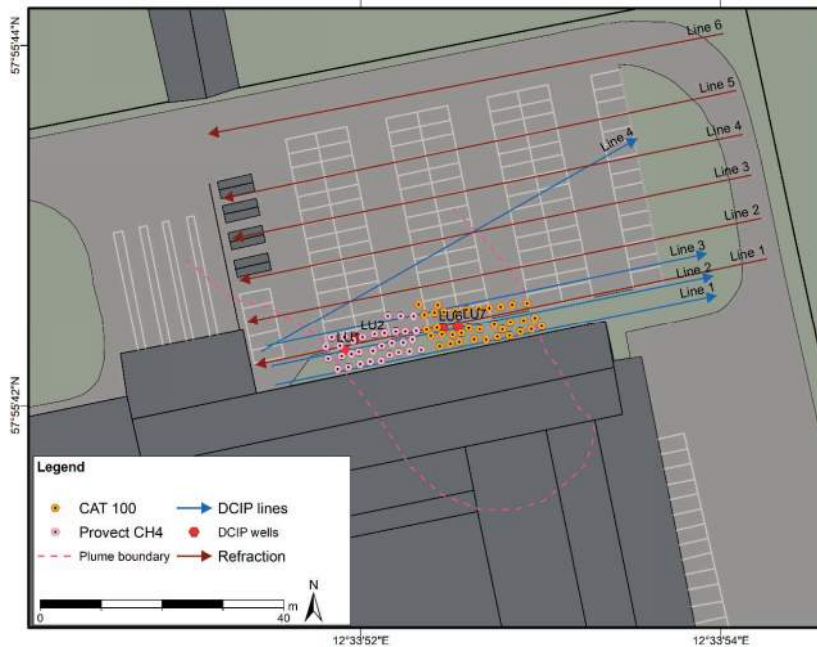


**Figure 3.** Overview of the geophysical survey and initiated pilot in-situ bioremediation. Seismic refraction tomography (brown lines) electrical resistivity tomography (blue lines), injection area A where the Provectus ERD-CH<sub>4</sub><sup>TM</sup> was injected (purple points) and injection area B where the CAT100<sup>TM</sup> was injected (orange points). The four boreholes used for cross-hole tomography are marked as red dots (LU1, LU2, LU6 and LU7). The boundaries of the plume are marked with purple dashed line.

## 4. Baseline Survey Results

### 4.1. Seismic Refraction Survey

Seismic refraction was used to investigate the depth to bedrock in the area around the parking lot, which is a downgradient of the contaminated source zone. The first seismic refraction line is not included in the results because the first arrivals were inconsistent due to the close proximity to the building. This could be due to reflected waves from the building's foundations that reach the receivers faster than the refracted wave from the bedrock, providing a false image of the subsurface.

The interface between the sediments and the bedrock was expected to be identified by a sharp contrast in the inverted model. Furthermore, since we have information about the depth to bedrock from a different method, the direct push drilling, which was done in conjunction with the MIP soundings, we used the result from the SeismicLine3 (Figure 4) to identify a velocity which represents the interface between the soft-sediments (low velocities) and the bedrock (higher velocities). The SeismicLine3 was chosen because it overlaps with more drill points in compared to the other lines. Based on the above, the velocity of 3500 m/s was chosen to represent the interface between the bedrock and the sediments.

The results for all seismic refractions were plotted in a three-dimensional (3D) 'fence' diagram (Figure 5). We used the of 3500 m/s velocity to fit a surface within the different tomography lines to acquire pseudo-3D representation of the bedrock surface, using linear interpolation.

Finally, we exported the 3D surface acquired with the methodology described above and we used it to 'expand' the previously known depth to bedrock, based on the limited point information from the drillings and the MIP soundings (Figure 1). Figure 6 illustrates the depth to bedrock results that we acquired using the above methodology.

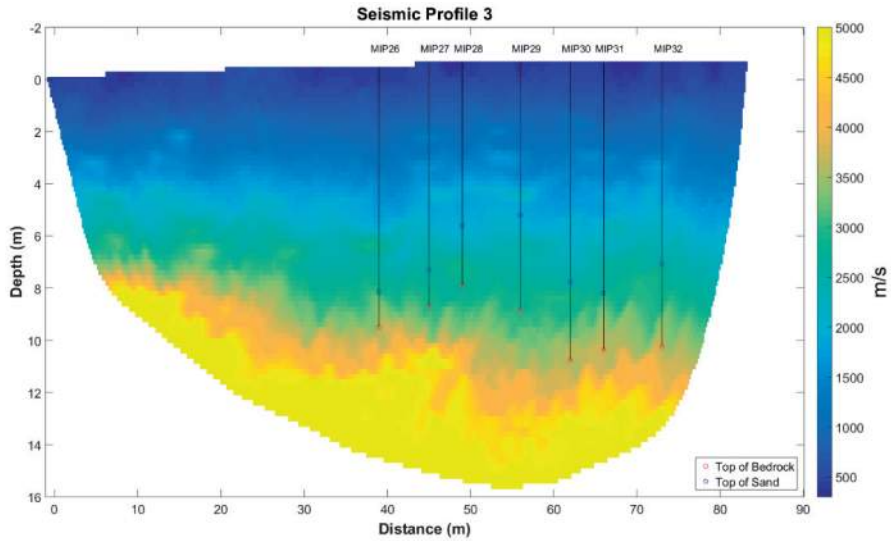


**Figure 4.** Inverted result from seismic refraction tomography from SeismicLine3. The interpreted MIP sounding [27,28] are plotted on top of the tomogram to be used for calibrating the seismic result.

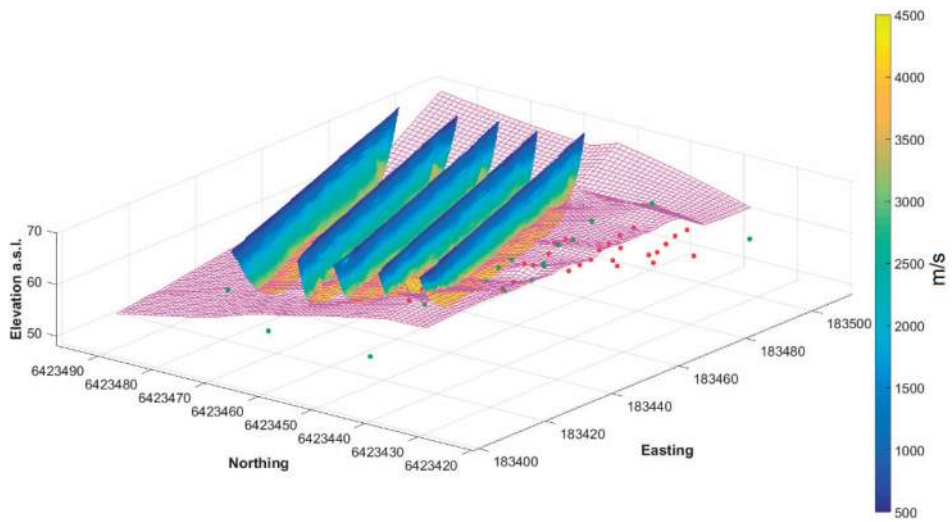


**Figure 5.** Fence diagram with the results from the Seismic Refraction Topographies. The sediment-bedrock interface is fitted through the tomographies and is shown as a pink mesh. Coordinates are in SWEREF99 TM12.

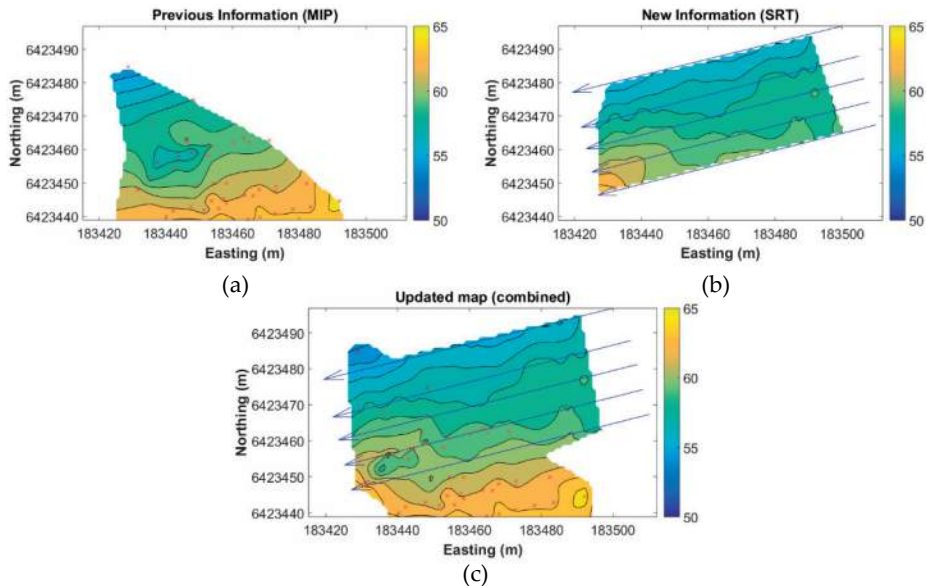


**Figure 6.** Interpolated surface map of depth to bedrock from the (a) MIP soundings [27,28] (b) Seismic Refraction tomography (SRT) (c) combined. The bedrock surface is plotted with absolute elevation (meters above sea level). Coordinates are in SWEREF99 TM12.

#### 4.2. Direct Current Resistivity and Time-Domain Induced Polarization

The baseline resistivity and induced polarization data were collected using the autonomous system before any injections were performed. The data were collected to understand the geophysical signature of the geology and the contaminant prior to the injection of the fluids. Furthermore, the baseline data was also to estimate the signal to noise ratio and to identify buried infrastructure that could cause issues in the interpretation of the results.

The data quality was very good, for both resistivity and chargeability data, based on the repeatability of the measurements (stacking), the low number of outliers (measurements that differ from their neighboring) and the regular shape of the IP decay curves. Furthermore, the residuals acquired from the inversions were similarly low (Figure 7), as they were expected to be.

Firstly, the results appear to show a strong ‘3D-effect’ that affects the lines closer to the building, mainly the first line, which is judged to be caused by the foundations of the building (see Figure 7). For the first three lines that run parallel to the building for most part, the edge of the building is marked. Furthermore, low resistivity and high chargeability responses (Figure 8) can be seen in the first three lines and they coincide with known buried infrastructure objects such as groundwater/stormwater pipes and power cables, which most likely cause the anomalies (Figure 7).

The resistivity results from Line 4 (Figure 7) illustrate a layered stratigraphy where a high resistivity layer appears at the depth of 7 m and below, and this is interpreted as the granite bedrock. On top of that, there is a layer with significantly lower resistivities, which is interpreted as the quaternary sediments on top of the bedrock. There is a thin top layer of higher resistivity that corresponds to fill material that forms the base of the parking lot, underlain by a thin, low resistive layer that might be caused by a higher content of fines in the sediments. Below that, the resistivity of the sediments does not change so much with depth until the bedrock is reached, but it changes laterally. This can be seen at a distance interval of 23 to 38 m from the beginning of Line 3 (WSW), where the resistivity is significantly higher from around 2 m depth to the bedrock level, namely around 80  $\Omega\text{m}$  instead of below 50  $\Omega\text{m}$  as in the surrounding parts. Similarly, for Line 4, the resistivity changes from around

50  $\Omega\text{m}$  to below 30  $\Omega\text{m}$  at the distance of 35 m from the beginning of the line. A similar pattern can be observed to some extent from Line 2; however, the pattern becomes less visible the closer to the building the line is situated, making it very difficult to be distinguished in the first line.

The chargeability results from Line 4 (Figure 7) illustrate a rise in the signal at a depth of 6–8 m which can partly be observed in Line 3 and Line 2, and maybe at an even higher magnitude. The response appears to be linked with the sand layer, where most of the contaminant degradation has been observed via the MIP soundings. Unfortunately, the signal is masked in the lines closer to the building due to the very strong shallow anomalies (Figure 7) coming from the buried infrastructure and building foundation. The first line suffers the most, making it very hard to distinguish the same pattern due to the high magnitude of the shallow anomalies.

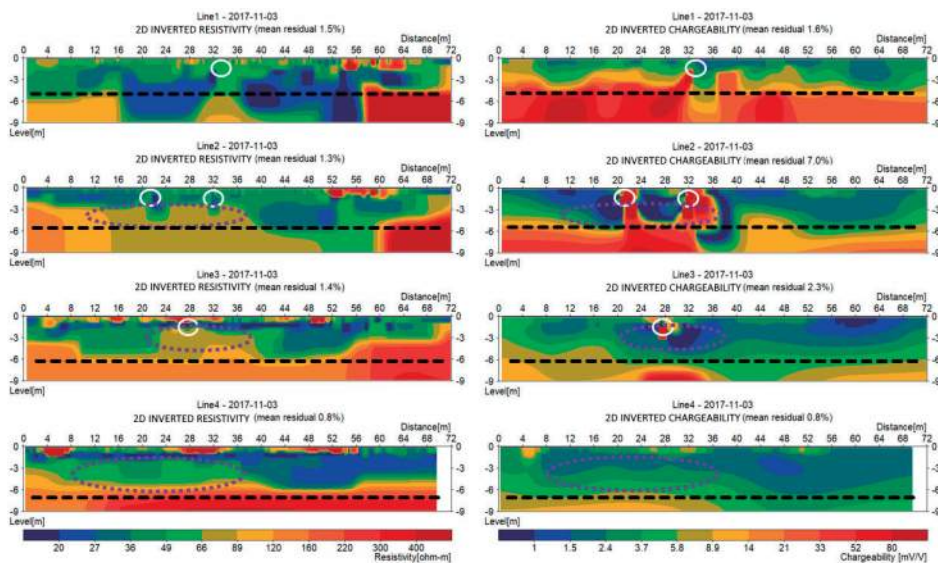


**Figure 7.** Direct Current resistivity (left) and time-domain Induced Polarization (right) results for Line 1 (top) to Line 4 (bottom) measured 3rd of November 2017 before the injections took place. For profile location, see Figure 3. The purple dashed line indicates the contamination plume, the white circles indicate the position of known metal pipes and the black dashed line indicates the sediment to bedrock interface based on the joint interpretation of the conceptual model and the geophysical results.

#### 4.3. Cross-Hole Electrical Tomography

The resistivity results from the two cross-hole tomographies (Figure 8) show a high resistivity response (300  $\Omega\text{m}$ ) in close proximity to the well pipe, where the same resistive response appears to have high chargeability values (>100 mV/V) in the chargeability sections.

The area between the two wells appears with a low resistivity response ( $\sim 10 \Omega\text{m}$ ) down to the depth of about 2 m with very low chargeabilities. Below a depth of 2 m, the resistivity shows a significant range (10–100  $\Omega\text{m}$ ) where the chargeability is very low (<10 mV/V). At a depth of about 6 m at the area between the wells, there is an anomaly in the chargeability response in the range of 80–120 mV/V.

The MIP soundings 21 and 16 (Figure 1) are in very close proximity of the cross-hole tomographies LU1\_LU2 and LU6\_LU7 (Figure 3), respectively. The MIP soundings show a strong increase in the concentrations of the contaminant (PCE) and its degradations products (TCE, DCE and VC) (Figure 8) from the depth of approximately 5 m and below.

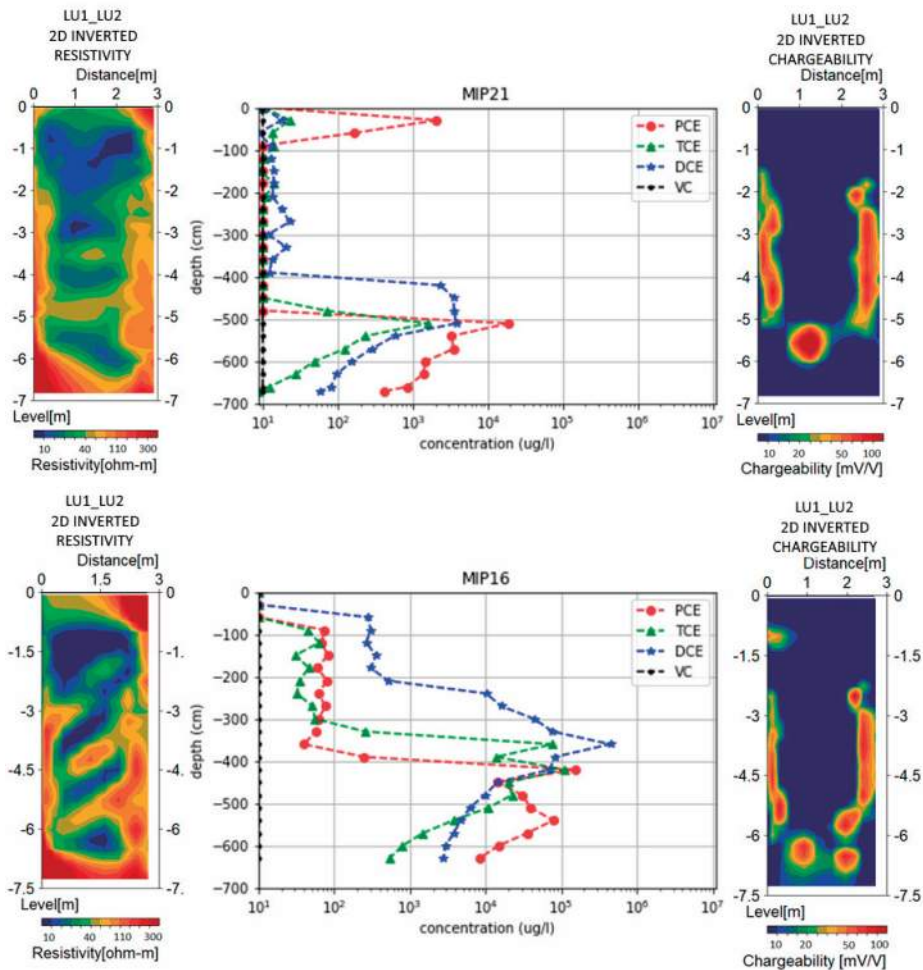


**Figure 8.** Cross-hole tomography results for resistivity (left) and time-domain chargeability (right) in comparison with the respective concentrations from the MIP sounding (middle [28]) for LU1-LU2 (top) and LU6-LU7 (bottom). The locations of the boreholes can be seen in Figure 3.

### 5. Short-Term Monitoring Time-Lapse Results

The resistivity and chargeability data collected during the month the injections took place and short after were inverted and analyzed to identify spatial and temporal changes in the subsurface. Those changes should, at least partly, correspond to the effects of the injections in the ground and are expected to be rapid due to the nature of the direct push injection method used.

The results from the time-lapse inversion of Line 3, which crosses the area where the fluids were injected (Figure 9), identify changes within the area of the injected products with an increased resistivity at the boundaries of the injection area. The changes in the resistivity following the injection of CAT100™ (East, see Figure 3) shows zones of increase as well as decrease in resistivity over the area during the injection of the product (Figure 9 middle-left) where two weeks after the injection the same area appears with a decrease in the resistivity (Figure 9 bottom-left) in comparison with the baseline survey. On the other hand, the area where the Provectus ERD-CH4™ was injected (West, see Figure 3) shows an increase in resistivity with distinct boundaries which corresponds to the injected volume

(Figure 9 bottom-left). The temporal changes in chargeability (Figure 9 right) are rather small and are mainly around the pipe buried at 20 m from the start of the DCIP-line, either due to the more permeable area surrounding the pipe being filled up with injection liquids or due to artifacts introduced by the time-lapse inversion algorithm.

The temporal changes seen from Line 4, which is located outside the injection area (Figure 3) show an increase in resistivity at the depth of 6–7 m (Figure 10 middle-left), which coincides with the coarse (sand and gravel) layer that appears to be present in the area at that depth. The hydraulic conductivity of the coarse layer should be higher than the upper (clay) and lower (bedrock) geological units; therefore, one possible interpretation is that the injection fluids, most likely the CAT100™, show up due to flushing through the coarse-grained unit and into this down gradient area. The temporal changes in the chargeability are very low, meaning that there is no direct effect in the chargeability signature of the subsurface due to the injection, at least not in the time-step following the injections. The very small changes also strengthen the previous observation that the changes in the chargeability in Line 3 could be due to artifacts of the time-lapse inversion caused by the strong responses from the buried infrastructure.

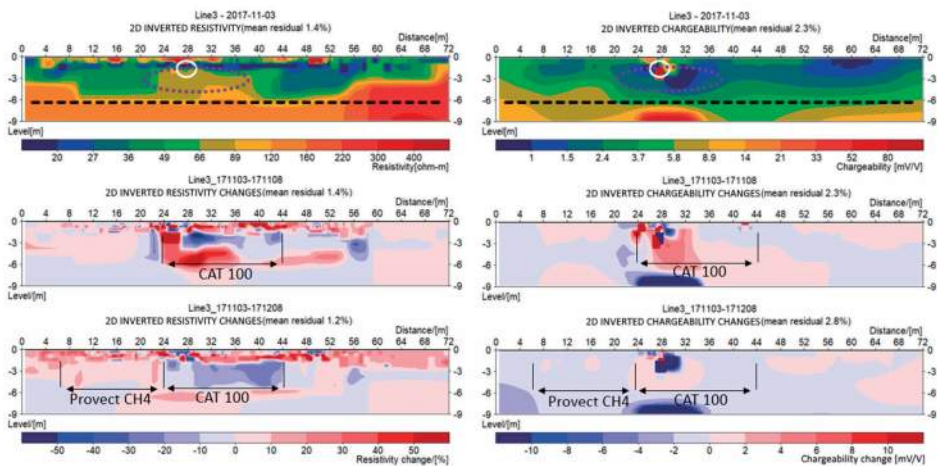


**Figure 9.** DCIP results from Line 3 baseline measurements 3rd of November 2017 (top) and time lapse changes between (left) the baseline and during the first injection 8th of November 2017 (middle) (right) the baseline and after second injection 8th of December 2017 (bottom). Resistivity results are shown on the left and chargeability on the right. The purple dashed line indicates the contamination plume based on the joint interpretation of the conceptual model and the geophysical result.

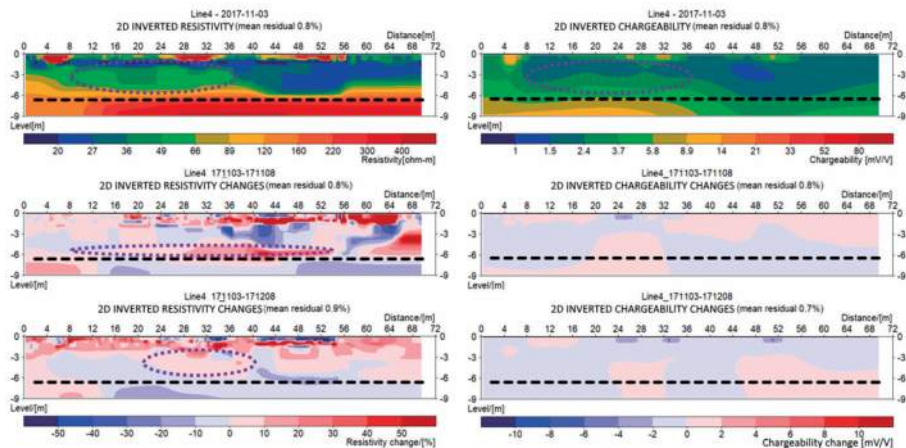


**Figure 10.** DCIP results from Line 4 (down gradient the injection area) baseline measurements 3rd of November 2017 (top) and time lapse changes between (left) the baseline and during the first injection 8th of November 2017 (middle) (right) the baseline and after second injection 8th of December 2017 (bottom). Resistivity results are shown on the left and chargeability on the right. The purple dashed line indicates the contamination plume based on the joint interpretation of the conceptual model and the geophysical result.

## 6. Discussion

The contaminant is heavier than water and would, therefore, gravitationally sink in the ground, until it reaches an impermeable layer, which, in our study area, is probably the crystalline bedrock. Thus, it is imperative to know the boundaries of the bedrock interface. The results from the seismic refraction tomography indicate that the bedrock is dipping towards north-northwest, which, in combination with the groundwater flow, explains the migration of the PCE that led to the formation of the plume as showed from the MIP-soundings (Figure 2). Furthermore, we utilize the seismic results to extrapolate the previous knowledge about the sediment-bedrock interface to investigate the possibility of the PCE to migrate in different directions. Based on our conceptual model for the area and the results from the geophysics, a scenario with spreading in other directions is highly unlikely, because neither the bedrock interface slope nor the groundwater flow would contribute to that. On the other hand, if the bedrock is fractured, it could be possible for the contaminant to migrate deeper into the bedrock; however, there is no such indication of that from the data collected in this work. This scenario needs to be carefully re-evaluated in the future.

The rather limited depression in the bedrock (Figure 6a), which was identified by the MIP soundings MIP31, MIP32, MIP33 [28] is not visible in the seismic refraction tomography. This is due to a limitation of the refraction seismic method, which, in this case, is unable to resolve small scale variations in the bedrock interface, because the first arrivals are not coming from the vertical direction but from the sides of the narrow depression. Therefore, the updated map for the depth to bedrock combines the information from the drillings (ground-truth) with the information from the geophysics. This is done to generate the depth to bedrock map (Figure 6c) that better represents the area of investigation.

The results from the resistivity Line 4 are in good agreement with the conceptual model and the seismic survey, where the MIP soundings also indicate an interesting anomaly in the area where the contaminant has higher concentrations. The contaminant appears in the geophysical section as an increase in the resistivity, which is supported by previous studies of DNAPL contaminated sites [4]. The results from the resistivity Line 3 shows some influence from the infrastructure, mainly the buried objects (power cables, water pipes etc.) and the foundation of the building. However, the increase of the resistivity response is in good correlation with the information from the MIP soundings and the

conceptual model. The pattern is similar with the one observed in Line 4, which is interpreted as the geophysical signal from the contaminant.

The model that was proposed by Johansson [4] describes a rise in the chargeability due to the degradation products of PCE (TCE, DCE, VC and Cl<sup>-</sup>). We can identify an increase in the chargeability in the surface layouts that are not affected by the infrastructure (Line 3 and Line 4). Unfortunately, the infrastructure increases the complexity in the chargeability signal close to the building because the buried objects (mainly metal pipes) have high responses, which masks the expected lower responses coming from the degradation products of the contaminant.

The results from the cross-borehole tomography (Figure 8) are very important in order to extract more detailed information about the subsurface over a smaller area. The electrodes are placed in the ground through drilling; therefore, the resolution is not reduced with depth as is the case with the surface layouts. The resistivity results (Figure 7) indicate that the subsurface is not as homogeneous as previously described by the resistivity results of Line 3 and Line 4. The resistivity in the upper clay layer varies significantly, which could be explained by the presence of several silt and/or sand lenses in the clay, which is also verified by the drilling and MIP soundings. The results from the chargeability illustrate a strong borehole effect from the filling material around the well, which is bentonite pellets down to approximately the last meter and a half where it is sand (well filter). Of great importance is the clear anomaly of a high chargeability response at the bottom levels of the boreholes, which is depth-wise in excellent correlation with the contaminant and its degradation products measured with the MIP method (Figure 8).

The temporal changes observed in Line 4 show no direct effect of the injection products on the chargeability signature of the subsurface, at least for the period right after the injections took place. The temperature of the injection fluids can partly explain the increase in the resistivity because the fluids are expected to be colder than the groundwater, since they were stored in the parking lot area during the cold winter where the temperature was close to 0 °C. The resistivity changes in Line 3 are very promising for using the method in order to identify injection fluids; however, more precise work needs to be done in order to extract quantitative results of the fluid distribution in the subsurface. The temporal resistivity changes, which correspond to the coarse layer present at Line 4, suggest that the injection fluids may have been flushed through the high hydraulic permeability media, the sand and gravel, in the direction down gradient of the injection area. The value of the injection fluids can be questioned if injected directly into high hydraulic permeability media, and this should be carefully considered, to avoid that the fluids flushes away from the area of interest.

The composition of the two consortiums differs significantly; the CAT100™ (east) contains iron particles to enhance the degradation process, while the Provectus™ (west) is essentially a cocktail of microbes that will actively feed from the contaminant reducing its concentration. Therefore, it is expected that the geophysical response from the two consortiums will be different as we can observe looking at the time-lapse results from Line 3 (Figure 9) and Line 4 (Figure 10).

## 7. Conclusions/Future Work

In this work, we have used seismic refraction, direct current and time-domain induced polarization tomography to investigate a site contaminated by chlorinated hydrocarbons. Geophysical data were used to expand previous knowledge of the area based on direct push drillings, with the membrane interface probe (MIP) sounding method.

The results from the MIP method were analyzed to create a simplified conceptual model for the area of interest and the geophysical data were used to expand that model. The formation of the DNAPL plume can be explained by the dipping of the bedrock (impermeable layer) and the ground water flow. Based on the bedrock topography and the groundwater flow direction we do not expect that the contaminant would have migrated in different paths, apart from possibly into bedrock fractures beneath the bedrock surface.

The resistivity results can identify the plume boundaries due to the increase in resistivity, whereas results from the chargeability can verify the presence of degradation products. A challenge arises in the interpretation of the results, especially the chargeability, in areas where the buried infrastructure generates strong responses, masking the much lower responses coming from the contamination. In such cases, it is important to have good quality borehole data, and to acquire data that would be less influenced by the infrastructure.

The time-domain resistivity and induced polarization results from Line 3, Line 4 and the cross-hole tomography appear to be very promising for the monitoring of the pilot test launched in late 2017. The method can provide qualitative information about the contaminant and the degradation products since the contaminant can be identified in the baseline survey. Therefore, the monitoring is expected to show promising results, since we can already observe changes, for the understanding of the impacts of in-situ remediation of chlorinated solvents as well as to pinpoint where actual samples need to be taken to verify changes in the underground.

**Author Contributions:** Conceptualization, A.N.; Data curation, A.N.; Formal analysis, A.N., T.D. and M.R.; Funding acquisition, T.D. and C.S.; Investigation, A.N., T.D. and M.R.; Methodology, A.N., T.D. and M.R.; Project administration, T.D. and C.S.; Visualization, A.N., M.R. and N.H.; Writing—original draft, A.N.; Writing—review and editing, A.N., T.D., M.R., N.H. and C.S.

**Funding:** This work has been carried out within the MIRACHL project (<http://mirachl.com/>). Funding is provided by the Swedish Research Council Formas—The Swedish Research Council for Environment, Agricultural Sciences and Spatial Planning (ref. 2016-20099), SBUF—The Development Fund of the Swedish Construction Industry (ref. 13336), ÅForsk (ref. 14-332), SGU—Swedish Geological Survey, Sven Tyréns stiftelse, Västra Götalandsregionen and Lund University.

**Acknowledgments:** The authors would also like to acknowledge the valuable contribution of Stefano Fanari for assisting with the processing of the seismic refraction data, Ulf Winnberg for sharing the MIP raw data and Roger Wisén for his input while planning and carrying out the seismic refraction survey.

**Conflicts of Interest:** The authors declare no conflict of interest. The founding sponsors had no role in the design of the study; in the collection, analyses or interpretation of data; in the writing of the manuscript; and in the decision to publish the results.

## Abbreviations

MIP	membrane interface probe
DCIP	direct current time-domain induced polarization tomography
NAPLs	non-aqueous phase liquids
PCE	tetrachloroethylene
TCE	trichloroethene
DCE	dichloroethane
VC	vinyl chloride
DNAPLs	dense non-aqueous phase liquids
SGU	Swedish geological survey
SEPA	Swedish environmental protection agency
SRT	seismic refraction tomography

## References

1. Swedish Environmental Protection Agency. *Nationell Plan för Fördelning av Statliga Bidrag för Efterbehandling*; Report 6617; Swedish Environmental Protection Agency: Stockholm, Sweden, 2014; Volume 30. (In Swedish)
2. Lin, K.S.; Mdlovu, N.V.; Chen, C.Y.; Chiang, C.L.; Dehvari, K. Degradation of TCE, PCE, and 1,2-DCE DNAPLs in contaminated groundwater using polyethylenimine-modified zero-valent iron nanoparticles. *J. Clean. Prod.* **2018**, *175*, 456–466. [[CrossRef](#)]
3. Scheffer, B.; van de Ven, E. Experiences of Perozone and C-Sparge at Two Former Dry Cleaner Sites in the Netherlands. *Ozone Sci. Eng.* **2010**, *32*, 130–136. [[CrossRef](#)]

4. Johansson, S.; Fiandaca, G.; Dahlin, T. Influence of non-aqueous phase liquid configuration on induced polarization parameters: Conceptual models applied to a time-domain field case study. *J. Appl. Geophys.* **2015**, *123*, 295–309. [[CrossRef](#)]
5. Flores Orozco, A.; Williams, K.H.; Kemna, A. Time-lapse spectral induced polarization imaging of stimulated uranium bioremediation. *Surf. Geophys.* **2013**, *11*, 531–544. [[CrossRef](#)]
6. Bernstone, C.; Dahlin, T.; Ohlsson, T.; Hogland, W. DC-resistivity mapping of internal landfill structures: Two pre-excitation surveys. *Environ. Geol.* **2000**, *39*, 360–371. [[CrossRef](#)]
7. Chambers, J.E.; Kuras, O.; Meldrum, P.I.; Ogilvy, R.D.; Hollands, J. Electrical resistivity tomography applied to geologic, hydrogeologic, and engineering investigations at a former waste-disposal site. *Geophysics* **2006**, *71*, B231–B239. [[CrossRef](#)]
8. Gazoty, A.; Fiandaca, G.; Pedersen, J.; Auken, E.; Christiansen, A.V. Mapping of landfills using time-domain spectral induced polarization data: The Eskelund case study. *Surf. Geophys.* **2012**, *10*, 575–586. [[CrossRef](#)]
9. Ustra, A.T.; Elis, V.R.; Mondelli, G.; Zuquette, L.V.; Giacheti, H.L. Case study: A 3D resistivity and induced polarization imaging from downstream a waste disposal site in Brazil. *Environ. Earth Sci.* **2012**, *66*, 763–772. [[CrossRef](#)]
10. Power, C.; Tsourlos, P.; Ramasamy, M.; Nivorlis, A.; Mkandawire, M. Combined DC resistivity and induced polarization (DC-IP) for mapping the internal composition of a mine waste rock pile in Nova Scotia, Canada. *J. Appl. Geophys.* **2018**, *150*, 40–51. [[CrossRef](#)]
11. Ntarlagiannis, D.; Robinson, J.; Soupios, P.; Slater, L. Field-scale electrical geophysics over an olive oil mill waste deposition site: Evaluating the information content of resistivity versus induced polarization (IP) images for delineating the spatial extent of organic contamination. *J. Appl. Geophys.* **2016**, *135*, 418–426. [[CrossRef](#)]
12. Wemegah, D.D.; Fiandaca, G.; Auken, E.; Menyeh, A.; Danuor, S.K. Spectral time-domain induced polarisation and magnetic surveying—An efficient tool for characterisation of solid waste deposits in developing countries. *Surf. Geophys.* **2017**, *15*, 75–84. [[CrossRef](#)]
13. Park, S.; Yi, M.-J.; Kim, J.-H.; Shin, S.W. Electrical resistivity imaging (ERI) monitoring for groundwater contamination in an uncontrolled landfill, South Korea. *J. Appl. Geophys.* **2016**, *135*, 1–7. [[CrossRef](#)]
14. Leroux, V.; Dahlin, T.; Rosqvist, H. Time-domain IP and Resistivity Sections Measured at Four Landfills with Different Contents. In Proceedings of the Near Surface 2010—16th Europe Meeting of Environment and Engineering Geophysics (EAGE), Zurich, Switzerland, 6–8 September 2010.
15. Kuras, O.; Wilkinson, P.B.; Meldrum, P.I.; Oxy, L.S.; Uhlemann, S.; Chambers, J.E.; Binley, A.; Graham, J.; Smith, N.T.; Atherton, N. Geoelectrical monitoring of simulated subsurface leakage to support high-hazard nuclear decommissioning at the Sellafield Site, UK. *Sci. Total Environ.* **2016**, *566*–567, 350–359. [[CrossRef](#)] [[PubMed](#)]
16. Rosqvist, H.; Leroux, V.; Dahlin, T.; Svensson, M.; Lindsjö, M.; Månsson, C.-H.; Johansson, S. Mapping landfill gas migration using resistivity monitoring. *Proc. Inst. Civ. Eng.—Waste Resour. Manag.* **2011**, *164*, 3–15. [[CrossRef](#)]
17. Steelman, C.M.; Klazinga, D.R.; Cahill, A.G.; Endres, A.L.; Parker, B.L. Monitoring the evolution and migration of a methane gas plume in an unconfined sandy aquifer using time-lapse GPR and ERT. *J. Contam. Hydrol.* **2017**, *205*, 12–24. [[CrossRef](#)]
18. Flores Orozco, A.; Kemna, A.; Oberdörster, C.; Zschornack, L.; Leven, C.; Dietrich, P.; Weiss, H. Delineation of subsurface hydrocarbon contamination at a former hydrogenation plant using spectral induced polarization imaging. *J. Contam. Hydrol.* **2012**, *136*–137, 131–144. [[CrossRef](#)]
19. Power, C.; Gerhard, J.I.; Karaoulis, M.; Tsourlos, P.; Giannopoulos, A. Evaluating four-dimensional time-lapse electrical resistivity tomography for monitoring DNAPL source zone remediation. *J. Contam. Hydrol.* **2014**, *162*–163, 27–46. [[CrossRef](#)]
20. Johansson, S.; Sparrenbom, C.; Fiandaca, G.; Lindskog, A.; Olsson, P.-I.; Dahlin, T.; Rosqvist, H. Investigations of a Cretaceous limestone with spectral induced polarization and scanning electron microscopy. *Geophys. J. Int.* **2017**, *208*, 954–972. [[CrossRef](#)]
21. Simyrdanis, K.; Papadopoulos, N.; Soupios, P.; Kirkou, S.; Tsourlos, P. Characterization and monitoring of subsurface contamination from Olive Oil Mills' waste waters using Electrical Resistivity Tomography. *Sci. Total Environ.* **2018**, *637*–638, 991–1003. [[CrossRef](#)]

22. Maurya, P.K.; Balbarini, N.; Møller, I.; Rønne, V.; Christiansen, A.V.; Bjerg, P.L.; Auken, E.; Fiandaca, G. Subsurface imaging of water electrical conductivity, hydraulic permeability and lithology at contaminated sites by induced polarization. *Geophys. J. Int.* **2018**, *213*, 770–785. [CrossRef]
23. Sparrenbom, C.J.; Åkesson, S.; Johansson, S.; Hagerberg, D.; Dahlin, T. Investigation of chlorinated solvent pollution with resistivity and induced polarization. *Sci. Total Environ.* **2017**, *575*, 767–778. [CrossRef] [PubMed]
24. Caterina, D.; Flores Orozco, A.; Nguyen, F. Long-term ERT monitoring of biogeochemical changes of an aged hydrocarbon contamination. *J. Contam. Hydrol.* **2017**, *201*, 19–29. [CrossRef] [PubMed]
25. Flores Orozco, A.; Velimirovic, M.; Tosco, T.; Kemna, A.; Sapon, H.; Klaas, N.; Sethi, R.; Bastiaens, L. Monitoring the injection of microscale zerovalent iron particles for groundwater remediation by means of complex electrical conductivity imaging. *Environ. Sci. Technol.* **2015**, *49*, 5593–5600. [CrossRef] [PubMed]
26. Göransson, M.; Bergström, U.; Shomali, H. Beskrivning till Bergkvalitetskartan Alingsås Kommun. Sveriges Geologiska Undersökning. 2007. Available online: <http://resource.sgu.se/produkter/k/k68-beskrivning-bergkvalite.pdf> (accessed on 20 February 2018).
27. Balzarini, T.; Van Herreweghe, S. EnISSA campaign, WSP SVERIGE AB, Tvätterigatan 3, Alingsås (SE). Project reference: 17/171. 2017; unpublished work.
28. Winnberg, U.; SGU, Stockholm, Sweden. Personal communication, 2018.
29. Loke, M.H.; Chambers, J.E.; Rucker, D.F.; Kuras, O.; Wilkinson, P.B. Recent developments in the direct-current geoelectrical imaging method. *J. Appl. Geophys.* **2013**, *95*, 135–156. [CrossRef]
30. Olsson, P.-I.; Dahlin, T.; Fiandaca, G.; Auken, E. Measuring time-domain spectral induced polarization in the on-time: Decreasing acquisition time and increasing signal-to-noise ratio. *J. Appl. Geophys.* **2015**, *123*, 316–321. [CrossRef]
31. Olsson, P.-I.; Fiandaca, G.; Larsen, J.J.; Dahlin, T.; Auken, E. Doubling the spectrum of time-domain induced polarization by harmonic de-noising, drift correction, spike removal, tapered gating and data uncertainty estimation. *Geophys. J. Int.* **2016**, *207*, 774–784. [CrossRef]
32. Dahlin, T.; Zhou, B. A numerical comparison of 2D resistivity imaging with 10 electrode arrays. *Geophys. Prospect.* **2004**, *52*, 379–398. [CrossRef]
33. Loke, M.H.; Dahlin, T.; Rucker, D.F. Smoothness-constrained time-lapse inversion of data from 3D resistivity surveys. *Surf. Geophys.* **2014**, *12*, 5–24. [CrossRef]
34. Yi, M.-J.; Kim, J.H.; Chung, S.-H. Enhancing the Resolving Power of Least-Squares Inversion with Active Constraint Balancing. *Geophysics* **2003**, *68*, 931–941. [CrossRef]
35. Kim, J.H.; Supper, R.; Tsourlos, P.; Yi, M.-J. 4D Inversion of Resistivity Monitoring Data through Lp Norm Minimizations. *Geophys. J. Int.* **2013**, *195*, 1640–1656. [CrossRef]
36. Sheehan, J.R.; Doll, W.E.; Mandell, W.A. An evaluation of methods and available software for seismic refraction tomography analysis. *J. Environ. Eng. Geophys.* **2005**, *10*, 21–34. [CrossRef]



Paper II





# Temporal filtering and time-lapse inversion of geoelectrical data for monitoring of in-situ bioremediation

Aristeidis Nivorlis<sup>1,\*</sup>, Matteo Rossi<sup>1</sup>, Torleif Dahlin<sup>1</sup>

<sup>1</sup> Engineering Geology, Lund University, Box 118, SE-22100 Lund, Sweden

\* Correspondence: [aristeidis.nivorlis@tg.lth.se](mailto:aristeidis.nivorlis@tg.lth.se)

## Abstract

We present long-term Direct Current resistivity and time-domain Induced Polarization (DCIP) monitoring of an in-situ remediation of chlorinated hydrocarbons. The system was installed in late October 2017 to collect daily data and monitor the pilot in-situ remediation that started a few days later, in early November 2017. The remediation plan is a pilot study to test the effectiveness of two different fluids injected into the ground by direct push injections. The article describes the fully automated system that is responsible for data acquisition, quality control and transferring. Data from the first 20 months are pre-processed, using digital signal processing algorithms for outlier detection and removal, and inverted using weekly averages against a common reference dataset which was measured before the remediation plan began with the aim of highlighting the changes against the baseline. Based on the time-series analysis of the inverted datasets, we can detect two portions of ground that show different geophysical properties and that coincide with the locations where the different fluids were injected. Our semi-automated methodology has the possibility to be used for real-time geophysical monitoring in the future.

## Introduction

Contaminated soil has been recognized as a widespread problem in the past decades as governments and global organizations are striving more and more towards sustainability and green development. It is now evident that future infrastructure projects, mining exploitation and industrial activities should cause no harm to the environment. Several areas have been polluted in the past. There are cases of landfills affected by leakages with the potential to pollute the groundwater (Apgar and Langmuir, 1971; Cabral et al., 2000; Hopkins and Popalisky, 1970; Kelly, 1966; Röling et al., 2000), or cases of excessive use of fertilizers and pesticides (Garrido et al., 2000; Kolpin et al., 2000; Liapis et al., 2000).

In Sweden, there are strict rules in place to avoid situations of industrial waste causing damage to the environment, but in the past there were cases of reported accidents and cases where the actual waste was not handled properly. These led to the contamination of many sites and in the national ongoing risk assessment more than 80.000 sites have been identified as potentially contaminated (SEPA, 2014). Former dry-cleaning facilities in Sweden used Tetrachloroethylene (PCE) extensively with little or no control of environmental impact until the 1980's. Several spills of the chemical occurred during the operation of these facilities that has led to chlorinated hydrocarbon (PCE) contamination of approximately 18.000 sites in the country.

The expansion of cities has created a need for more space, and former industrial areas, once located in the suburbs of the cities, are strong candidates to provide expansion space. Furthermore, if the contamination migrates deeper into the subsurface there is a high risk that it will contaminate the aquifer systems which might have dramatic implication on the groundwater resources. There is a demand for efficient characterization and design of modern remediation plans to be applied in the aforementioned areas to reduce the risk of further spread of the problem and to make it possible to use the ground for expanding the current infrastructure network of the cities.

In this context, in-situ remediation provides a modern cost-efficient and effective solution that can be applied to reduce the concentration of the contaminant in the ground and prevent it from spreading any further. In contrast with traditional methods (i.e. dig and treat), it does not require the removal of the entire mass, which can lead to direct exposure to the contaminants and associated health concerns. Furthermore, in cases where the contaminant mass has large volume or is deeply buried, in-situ remediation may be the only option or it is preferable because it can drastically reduce the overall cost.

The development of tools for efficient monitoring of the on-going in-situ remediation is an essential aspect of the process.

Analysis of groundwater and soil samples, while the remediation is on-going, provide necessary quantification and can be used to monitor changes in the subsurface accurately. The information provided is however localized at a point and often quite limited due to the cost related to the collection and analysis of the samples. Furthermore, it requires qualified staff to interact directly with the contaminant and therefore should be kept to the minimum. Geophysical monitoring can provide a valuable tool to interpolate the sparse and point information from the groundwater and soil samples and monitor more effectively the changes in the subsurface, both in space and time. Geophysical methods can also be used as a base for designing a drilling and sampling program so that it becomes as representative as possible, or to identify spots where an existing sampling program needs to be augmented.

The direct current (DC) resistivity method has been successfully used in a broad spectrum of subsurface investigations (Loke et al., 2013) such as environmental (Auken et al., 2014; Fernandez et al., 2019; Forquet and French, 2012), engineering geology (Abdulsamad et al., 2019; Danielsen and Dahlin, 2009; Rossi et al., 2018) and hydrogeological (Chirindja et al., 2017; Fetter, 2001; Leroux and Dahlin, 2006; Zago et al., 2020). The DC resistivity method was successfully applied for landfill characterization (Bernstone et al., 2000; Chambers et al., 2006), where the Induced Polarization method (DCIP), an extension of the traditional DC resistivity method, has also been used (Gazoty et al., 2012; Ntarlagiannis et al., 2016; Power et al., 2018; Ustra et al., 2012). Microbial activity can produce electrical signals (Atekwana et al., 2005) that can be detected with geophysics (Atekwana and Atekwana, 2010; Davis et al., 2006; Davis and Atekwana, 2006).

Contaminated sites have been investigated using frequency IP (Cassiani et al., 2009; Flores Orozco et al., 2012a) and time-domain IP (Johansson et al., 2017; Maurya et al., 2018; Ntarlagiannis et al., 2016). Frequency IP has been used for monitoring of uranium bioremediation (Flores Orozco et al., 2013) and the injection of zerovalent iron particles (Flores Orozco et al., 2015). The DCIP method can be used for monitoring (Kuras et al., 2016; Power et al., 2014) and has been successfully applied for monitoring contamination (Caterina et al., 2017; Park et al., 2016; Sparrenbom et al., 2017).

Recent advances in the DCIP method allow faster data acquisition (Olsson et al., 2015), advanced signal processing algorithms that can improve the signal quality (Olsson et al., 2016) and autonomous monitoring systems (Chambers et al., 2009) that can provide frequent reliable data (i.e. daily) to monitor

the changes in the subsurface. However, there are many challenges in finding efficient routines for effectively processing the resulting datasets and previous research on this topic focuses mainly on resistivity measurements (Chambers et al., 2009; Sjö Dahl et al., 2009). For frequency domain IP measurements reciprocals are often used to quantify the measurement error (Flores Orozco et al., 2012b) and this idea has been applied to monitoring data (Flores Orozco et al., 2019). There is a need for similar tools that can be applied to DCIP monitoring data to remove temporal outliers and provide more realistic representations of the changes in the subsurface.

In this study, we have analyzed the DCIP monitoring dataset from an on-going pilot remediation experiment from a former dry-cleaning facility in Alingsås, Sweden (Figure 1). The site is contaminated with chlorinated solvents, tetrachloroethylene (PCE) and the respective degradation products: trichloroethene (TCE), dichloroethane (DCE) and vinyl chloride (VC). The remediation started on November 2017 and the data until July 2019 will be analyzed and presented here.

## **Method description**

### Area of investigation

The area of investigation is an industrial-scale dry-cleaning facility (Alingsåstvätteriet) located in Alingsås, Sweden. Around the 1960s or 1970s, a single documented spill leaked into the ground approximately 200L of PCE; however other undocumented incidents might have occurred. The spread of PCE led to the formation of a secondary DNAPL source underneath the building. Over the years, the contaminant has migrated as a result of the groundwater flow and bedrock topography (Nivorlis et al., 2019), resulting in a formation of a larger DNAPL plume. Nowadays, PCE is not used and the facility is operating as a laundry and textile cleaning (water only) under the Administrative Region Västra Götaland, where approximately 40 tons of textiles are washed on a daily basis for hospitals and other health care institutions in the region.

The contaminants are mostly present in the fine-sediment layer (silty clay), which is dominant in the subsurface and extends from 2 to 7 m depth. A small amount is leaking through the thinner and coarser layer underneath and spreading downgradient. Based on soundings and well logs the crystalline bedrock can be found at 7 to 9 m depth, and based on previous investigations (Nivorlis et al., 2019) it is believed to be intact and act as an impermeable layer in our conceptual model. The geological conceptual model of the area from that work was based on the MIP soundings investigation and indicates that the highest

concentrations of the contaminants are found in the clay layer. A pilot in-situ remediation plan was designed using direct push injections of two different fluids, to evaluate their effectiveness for future use (Nivorlis et al., 2019). Figure 1 presents the locations of the direct push injections for Area A (purple) where a mixture of bacteria was injected and Area B (orange) where iron particles were injected.

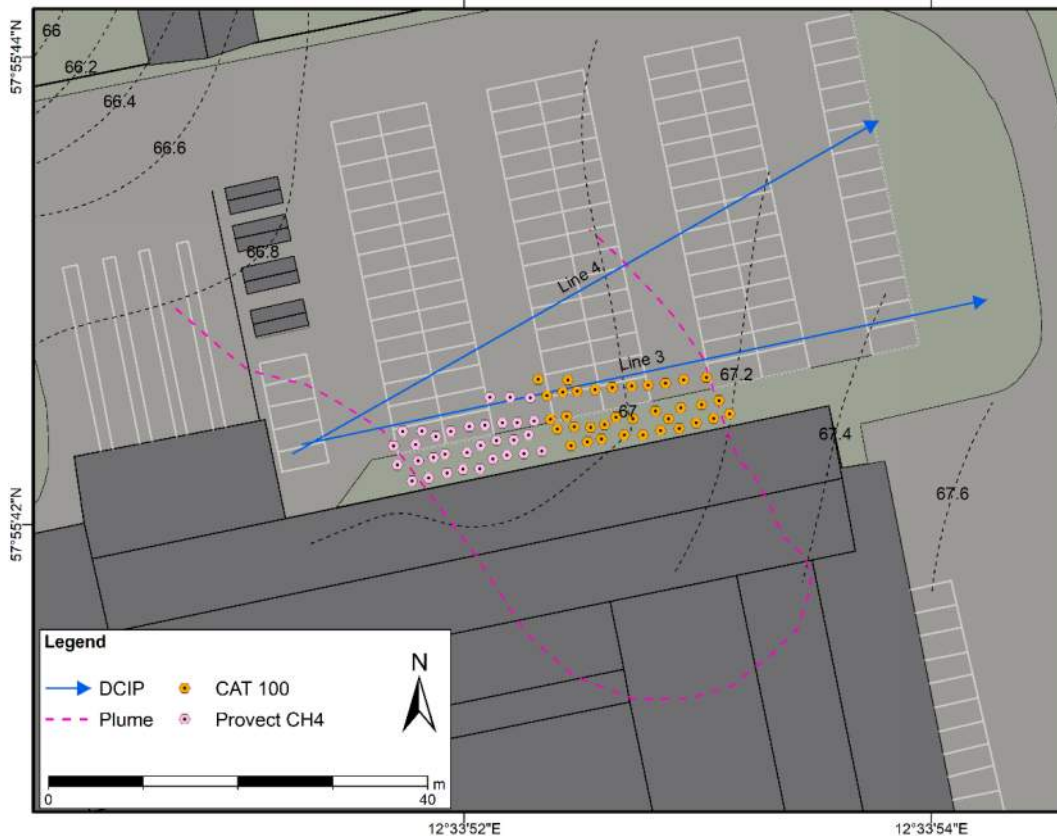


Figure 1. Alingsås field site. DCIP monitoring lines (solid blue) with the arrow that indicates the direction of local coordinates, interpreted DNAPL plume boundaries (pink dashed line) and the injection points of CAT100 (orange) and Provect CH4 (purple). The dashed black lines indicate the groundwater level measured at September 2017.

### Direct Current resistivity and time-domain Induced Polarization (DCIP)

The DCIP method is performed injecting direct current in the ground from two electrodes (A and B) and measuring the difference in potential between another pair of electrodes (M and N). The injected current creates a potential field that is governed by the electrical properties of the subsurface and more specifically by the electrical conductivity ( $\sigma$ ). The overall aim of a survey is to measure many combinations of current and potential electrode pairs, typically along a line for a 2D case, to be able to describe the

electrical field in order to infer the distribution of the electrical conductivity in the ground. The electrical resistivity can then be computed as it is simply the inverse of the electrical conductivity and can be related to different formations, porosity, groundwater level and contaminants.

The induced polarization method measures the ability of the ground to store electric energy while the current is injected (on-time) which is released, in form of current, when the current is turned off (off-time). The parameter that describes how much energy is stored in the ground is called chargeability, and it can also be measured in the on-time using a 100% duty cycle (Olsson et al., 2015). The chargeability is a physical parameter that can be affected by mineralization, heavy metals, contamination (Telford et al., 1991) and can be linked with hydraulic permeability (Maurya et al., 2018).

In the Alingsås site 4 profiles are measured daily, each with 64 electrodes at 1 m electrode spacing except at the end of the layouts where the electrode spacing is 2 m. The electrodes and the cables are buried into the ground approx. 30cm depth, (Figure 2) to minimize interference and provide a permanent installation of the system (Nivorlis et al., 2019). The measurements are taken using the multiple gradient array (Dahlin and Zhou, 2006) with a total of 1384 measurement. The s-factor is 9 in the majority of the data and few added with larger s, in addition to larger s-factors arising from the larger electrode separations at the layout ends. The a parameter has values 1, 2, 3, ... 7 electrodes between the measurement points, with some combinations with double electrode separation at the end of the spreads which gives a-values up to 14 . The s-factor is the distance of the current dipole, counted as multiples of a.

Four current pulses of 4 seconds are used, for a total of 16 seconds. Extra time for switching relays and setting up the current transmitter is required for each current injection. Four profiles (Figure 1) are measured daily to identify the changes in the subsurface that can be related to seasonal variations, and single events such as rainfalls and geochemical variations.

Unfortunately, the monitoring system installation was finished only 10 days before the remediation plan was scheduled to start. Ideally, a longer series of data would be preferred before changes start to happen in the subsurface due to remediation, but it was neither possible to postpone the remediation plan nor to get on the site earlier due to issues with the logistics. Even though a longer background monitoring period would have been beneficial in order to obtain information about the background variations and noise conditions, the current background period is deemed sufficient as baseline to describe the changes over time.

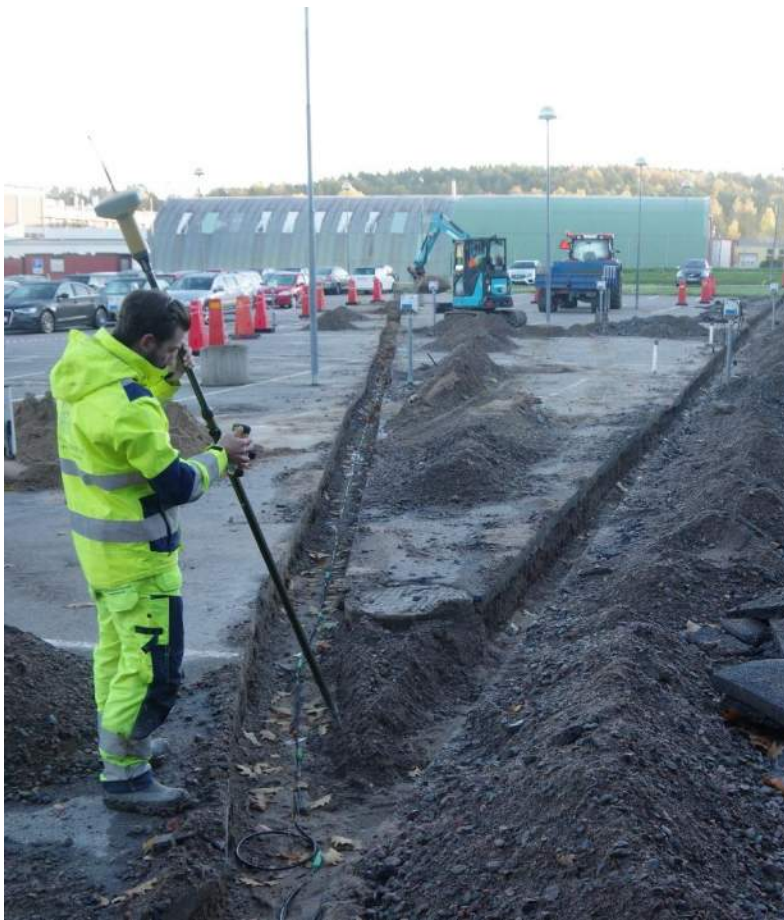


*Figure 2. Monitoring installation of the stainless-steel plate electrodes. The electrodes and the cables are buried 30 cm under the surface to ensure a permanent installation.*

### Automation

In a long-term monitoring experiment, it is imperative to fully automate the workflow of acquisition, processing and inverting the datasets. The routines developed for automating the workflow were calibrated on the initial time lapse steps and consist of five steps:

- Daily measurements
- Transferring of data from the local (field) PC to a remote server
- Processing to remove noise from the raw data

- Inversions
- Data visualization

First and foremost, an autonomous and automated data acquisition process is needed to provide resistivity and chargeability data. Secondly, the data handling component is responsible for transferring the data from the remote location, the contaminated site, to the available resources for further processing, archiving and storage of data. Next, a data processing scheme is needed for “de-noising” the raw data before they are pipelined through the inversion routines. Finally, routines for data visualization are needed in order to further analyze and interpret the inverted results.

### Long-term monitoring system

For data acquisition we use an ABEM Terrameter LS2 which is paired with external relay switches to allow several electrode spreads to be connected with the instrument in a sequence. The relay switches include an ABEM Electrode Selector ES10-64C, plus four two-way switch units with integrated transient protection for each individual electrode (designed and built at Lund University). The measurements are performed using the 100% duty-cycle instrument option (Olsson et al., 2015) where both resistivity and chargeability are measured during the on-time, which effectively reduces the amount of time by half and increases the signal to noise ratio. This measurement method is based on the processing of full waveform data developed by Olsson et al., (2016)

Software that communicates with the instrument and relay switches was developed, ensuring that all the different layouts are measured daily. The software, which is written in Python (**Long Term Monitoring System** or **LoTeMoSy**), runs on a compact industrial PC with Windows 10. Once the measurement sequence is complete, the data are transferred from the field PC to a server at Lund University.

### Digital signal processing

Geophysical data are generally contaminated by noise that needs to be identified and removed before the data are further processed and interpreted. The source of noise could be external power sources, natural currents or hardware problems, and it is important to identify and remove noisy measurements that could potentially corrupt the results. The changes in the subsurface due to seasonal variation or the effects from the remediation are expected to be smooth, apart from the injection of degradation

products, whereas rainfall or frozen ground could introduce more sharp changes in the daily measurements.

The apparent resistivity pseudosections presented in Figure 3 are generally a useful tool for qualitative inspection of the spatial distribution of the data, as values should not be much different from their neighboring values. It is evident that there are time steps (Figure 3, left column), where some data points are affected by dominant noise, showing extreme differences from their neighboring values.

The temporal distribution is a key factor that can be used when working with high frequency sampling data as it is possible to analyze each individual measurement over a period. If the noise is incoherent, the spatial inconsistency that can appear in a single profile will normally affect a limited number of measurements for few time steps, therefore it will not remain dominant for longer periods. The source of noise can be external, such as electromagnetic induction from buried facilities; or internal from the system, as for example coupling in electrode cables.

As shown in Figure 3 (left column), there are several data points that show extremely low apparent resistivities for 4 days (here exemplified by data from 16<sup>th</sup> and 18<sup>th</sup> of November), before the measurements became stable. The analysis of the time series of each individual data point (quadrupole) can be used to identify and eliminate points that show anomalous high frequency fluctuations over time.

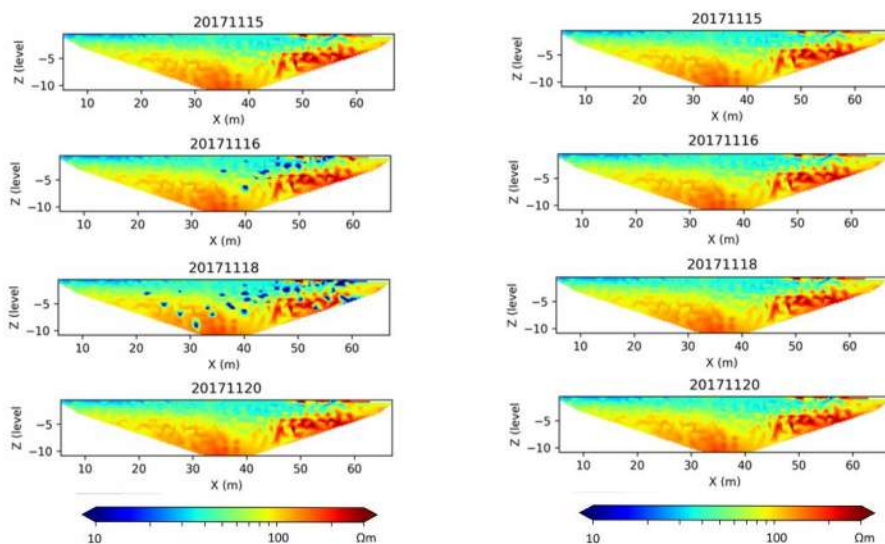


Figure 3. Examples of pseudosections for selected days: in the left column, pseudosection of raw data; in the right column, the pseudosections of the processed datasets. Dates are in YYYYMMDD format. We can identify spatial outliers that appear in the dates 16-19 November 2017 and that are removed by the processing framework.

Figure 4 illustrates an example of a time series of a single quadrupole that can be used to identify abrupt changes in the geophysical parameters. Extremely low values, which can also be identified in the pseudosections of Figure 3, are present in single time steps and they cannot be explained by natural processes that occur at lower frequencies. Some sharp transitions are more consistent (March 2018 and February 2019) and they are related to seasonal variations, specifically to frozen ground. For this reason, a low-pass Butterworth (LPB) filter was applied with a frequency response that is tuned during trial datasets with the aim to dampen sharp changes but to allow slower variations to remain unfiltered. To enhance the performance of the low-pass filter, a median filter is applied in a previous step to exclude extreme outliers that can create ringing in the results of the LPB filter.

The signal processing algorithm consists of two steps. First, a moving window median filter is applied with the aim of analyzing the signal quality of the time-series and removing extreme outliers. The filter is performed with a window length of 7 days. The second step is a low-pass Butterworth filter to further smooth the temporal series removing the higher frequency changes that may be related to noisy data points. The filter has a normalized threshold frequency fixed at 12% of the Nyquist frequency, order 2 and the frequency response of the filter is presented in Figure 5. The filters are included in the Scientific Python (SciPy) open-source library (Virtanen et al., 2020) which is available for the Python programming language.

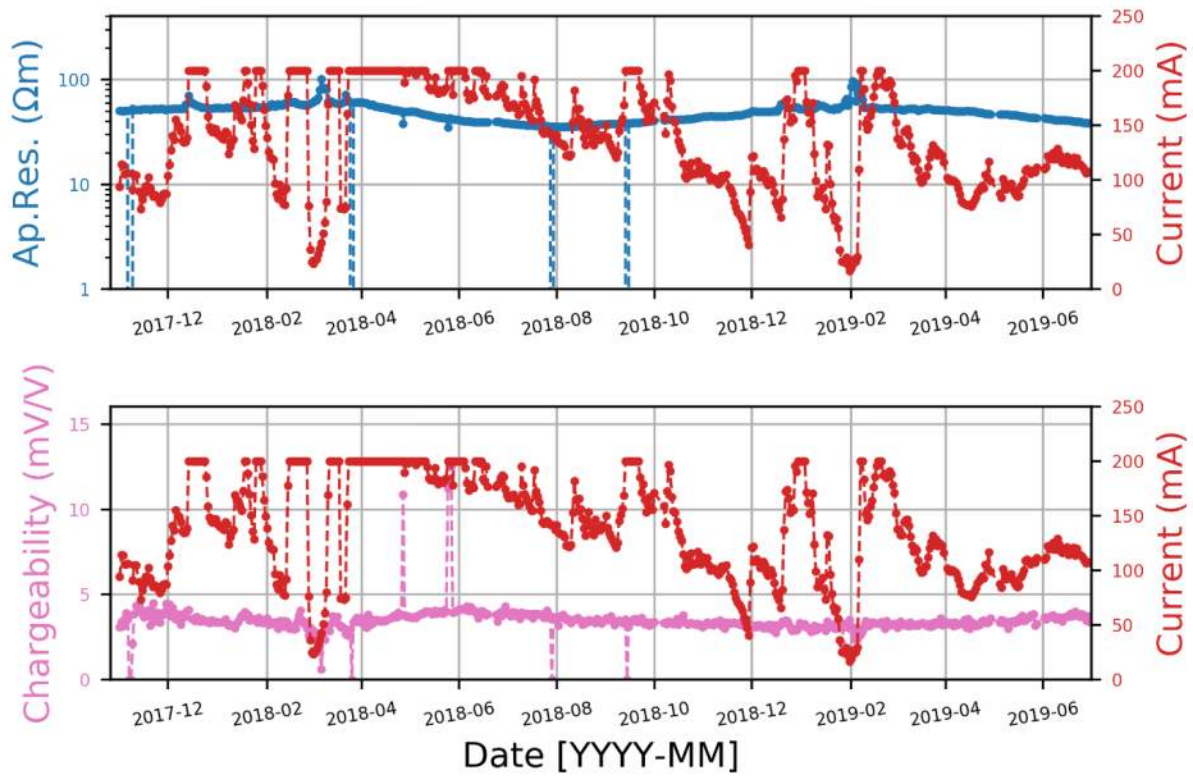


Figure 4. Example of the time series of raw data for a single quadrupole. The red lines indicate the current injection, the blue line the apparent resistivity and the purple line the apparent chargeability as measured by the instrument. The example refers to the data point involving electrodes distance 7-16-13-14 meters (A-B-M-N) of Line 3.

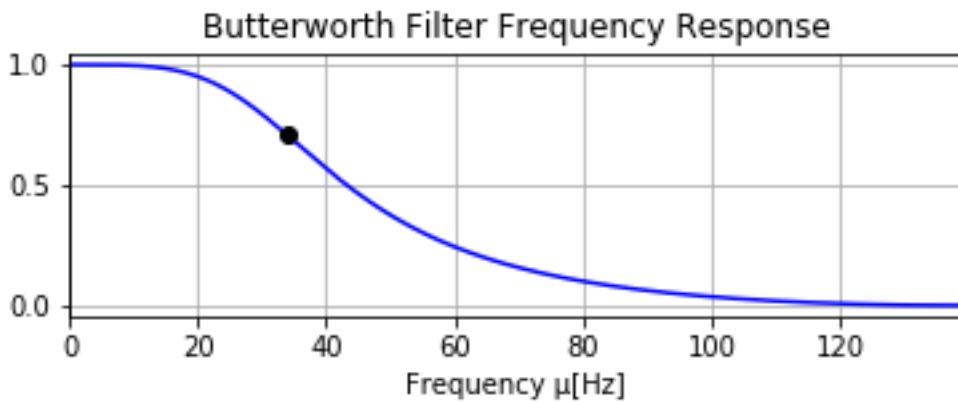


Figure 5. The frequency response of the low pass Butterworth filter. The frequency of the measurements was set at  $1/3600\text{Hz}$  and the frequency cutoff was set to  $34\mu\text{Hz}$ .

Figure 6 represents an example of the filter applied to a single quadrupole, the blue line shows the original data and the green line shows the filtered data. The same filter (median and LPB) was applied to every quadrupole to eliminate the outliers and replace them with a filtered value that matches past and future values, in order to avoid having missing data as an input to the inversion. The relative fluctuation in chargeability values appears stronger because the signal to noise ratio is much lower. The chargeability values are in general in a narrow range of few mV/V (from 1 to 10) for the entire dataset and time series.

Extremely sharp and inconsistent changes in the apparent resistivities cannot be explained by natural events, neither sudden (i.e. rainfall) nor slower (i.e. seasonal variations due to temperature effects). Furthermore, the effects due to the remediation are expected to be smooth, less dominant in amplitude and consistent in time, therefore it is clear that they are not related to sharp transitions.

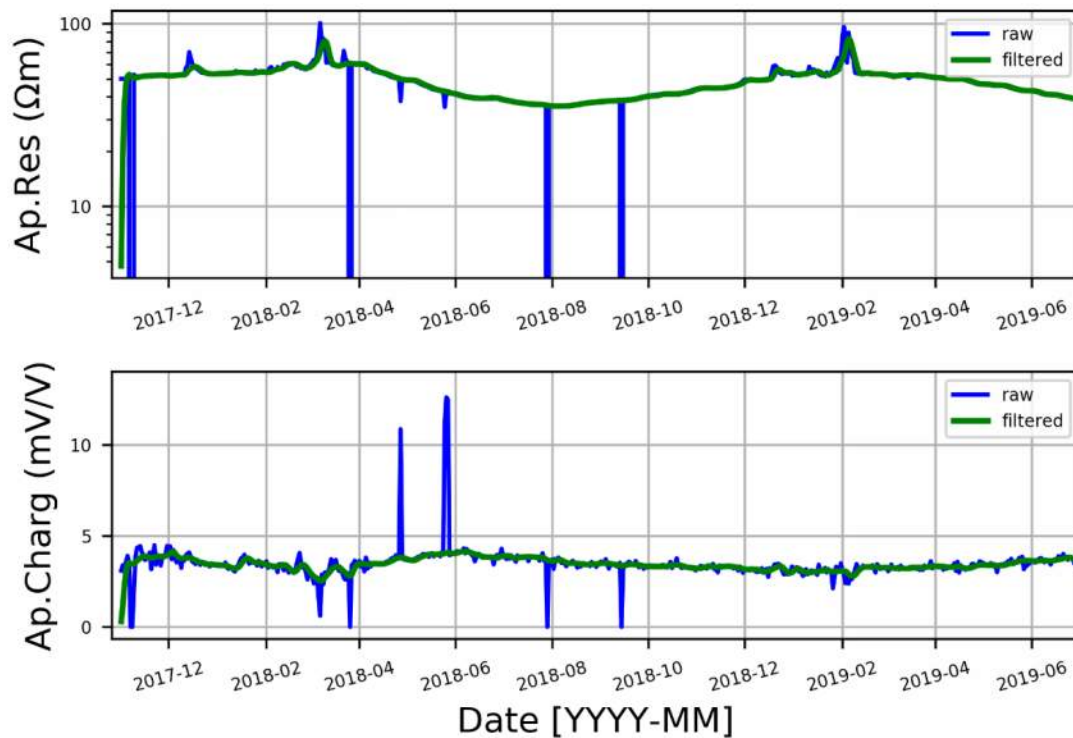


Figure 6. Example of filtering of raw data for quadrupole 34 of Line 3. The example refers to the data point involving electrodes distance 7-16-13-14 meters (A-B-M-N).

## Inversion

The inversion software Geotomo Res2DInv (v4.09) has been applied in the present work with a L1-norm smoothness constrain, both in space and time.

Inversion of large data sets can be computationally challenging, and therefore efficient routines for handling monitoring data need to be addressed. In the present work, it was decided to invert weekly averages to have an overview of the main changes that affect the geophysical parameters, adding further smoothing steps, as the principal interest is in the long term variations that can be linked to biogeochemical processes.

The weekly results aim to provide an overall understanding of how the subsurface is changing while keeping computation cost to the minimum. The datasets analyzed cover a period of 20 months, from November 2017 to June 2019.

## **Results and discussion**

### Identifying the baseline

A key aspect for inverting time-lapse data is the identification of a reference model (or baseline). The first 11 days of acquisition, before any remediation action took place, were inspected to assess a stable baseline dataset (Figure 7). After excluding two missing time steps (7<sup>th</sup> and 8<sup>th</sup> of November 2017), the remaining values of the time series are averaged for each single quadrupole to establish a robust baseline reference model.

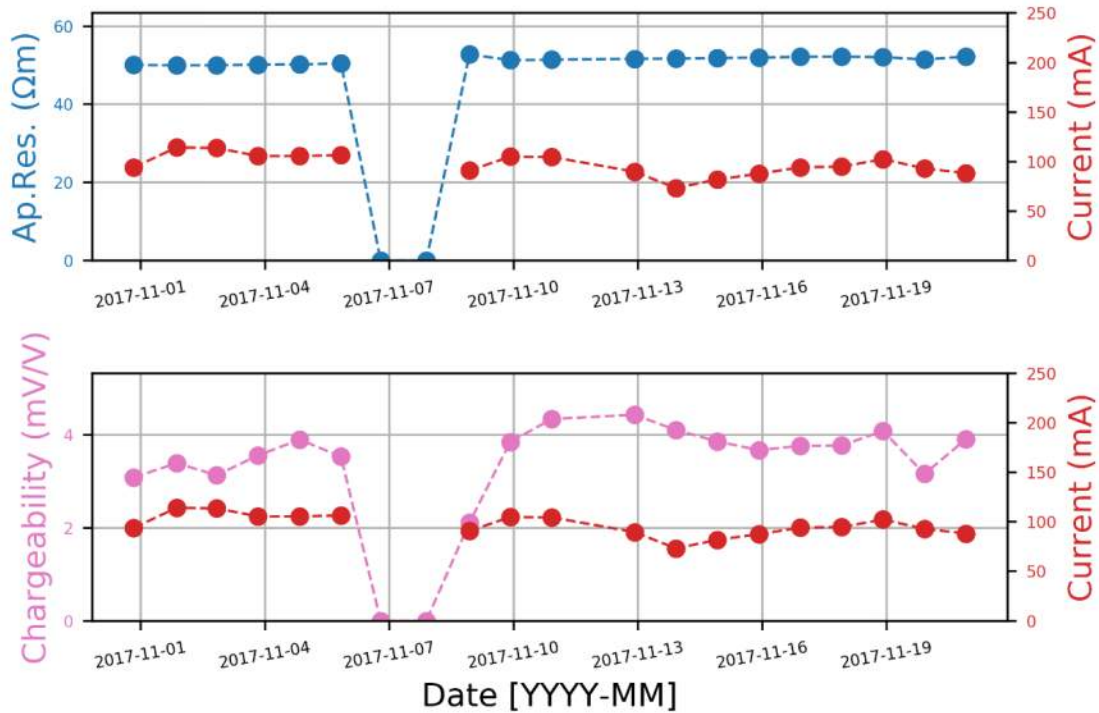


Figure 7. Example of electrical resistivity and integral chargeability time series data of a single quadrupole acquired before the remediation took place (started on 8th of October). The example refers to the data point involving electrodes distance 25-34-32-33 meters (A-B-M-N) of Line 3.

Then, weekly averages were extracted (Figure 8) for every week following the end of the baseline, which was inverted against the average reference model using the time-lapse constrained mentioned previously. Even if it is possible to fine-tune each individual inversion, the scope of the present work is to build a robust framework that can be applied with the same settings for long term monitoring projects. In many cases, data can be collected for years, therefore individual fine-tuning of daily, weekly or monthly data is practically impossible.

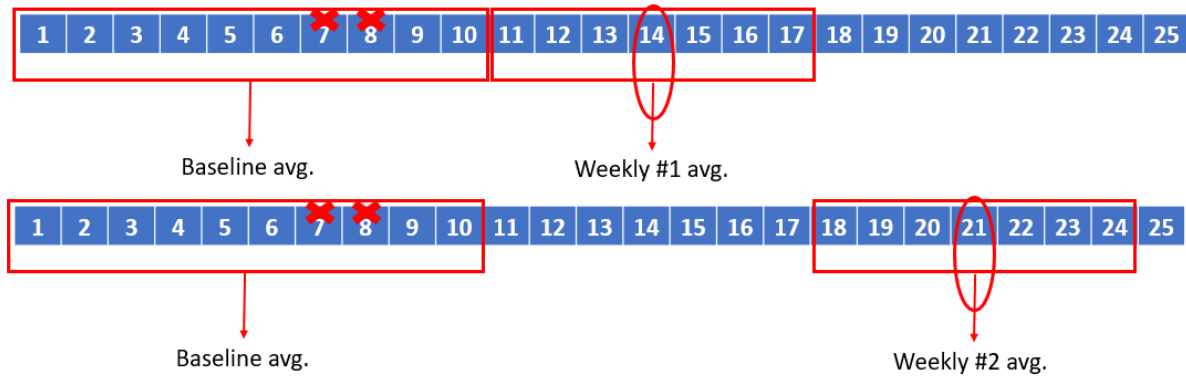


Figure 8. Time-lapse inversion of weekly averages against a constant average reference. The cells represent daily acquisitions. The 7<sup>th</sup> and 8<sup>th</sup> day were not included in the reference dataset (see Figure 7)

### Baseline results

The results of the inversions of the reference baseline datasets are presented in Figure 11 and Figure 12 for Line 4 and Line 3, respectively.

The resistivity distribution along Line 4 (Figure 9) clearly identifies the crystalline bedrock as a high resistivity bottom layer at around 7 m from topographic surface. A shallow high resistivity fill material, apparently thinner than 1 m, can also be identified. The resistivities of the sediments range from 10 to 40  $\Omega$ m. An area with an increased resistivity response is present between approx. 0 and 35 m along the profile at a depth of 2.5-5 m. This anomaly correlates with higher concentrations of the contaminants as pointed out by Nivorlis et al. (2019) (see also the position of plume boundaries in Figure 2). The chargeability response should not be affected by any infrastructure along Line 4 and there is a generally flat response with very low chargeability values (less than 4 mV/V).

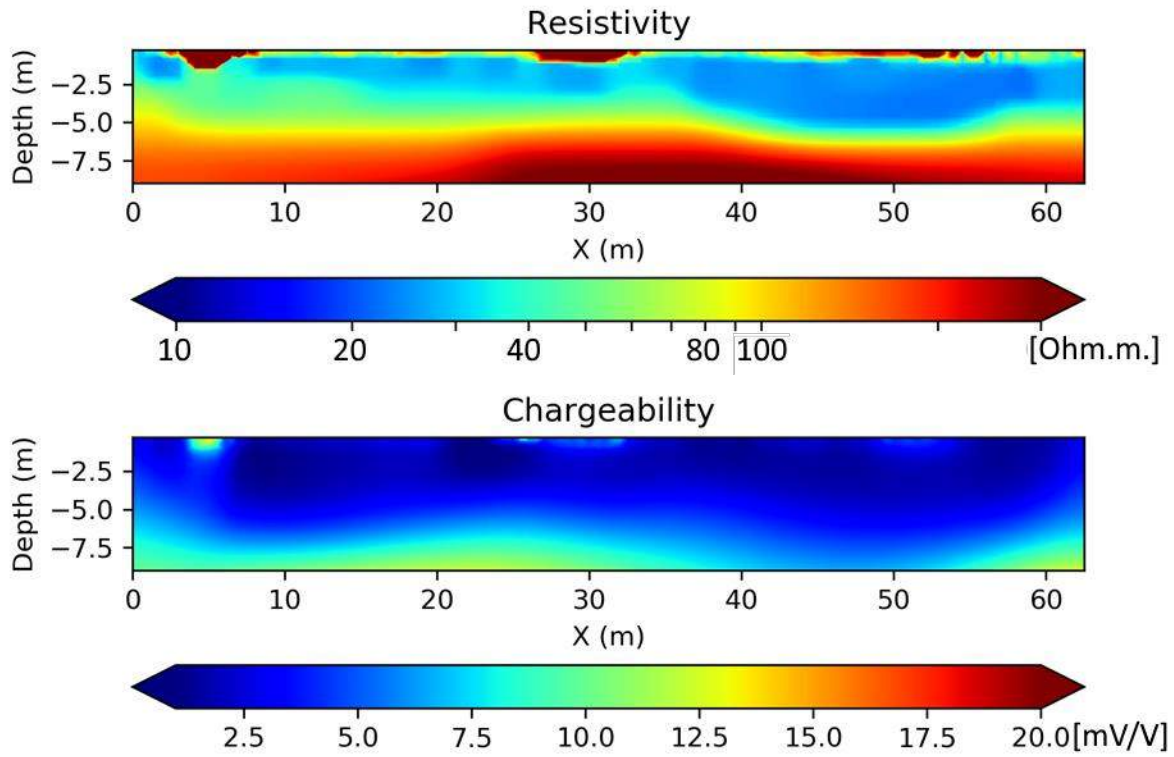


Figure 9. Inverted model for resistivity (top) and chargeability (bottom) of the baseline for line 4.

The resistivity distribution of Line3 (Figure 10) shows a shallower high resistivity bedrock at around 5 to 6 m from topographic surface. The transition between quaternary sediments and crystalline metamorphic bedrock is shallower than in Line 4, since the bedrock topography is dipping towards north (Nivorlis et al. 2019). The top fill material, with a maximum thickness of about 1 m, stands out with higher resistivity than the glaciofluvial sediments below. The sediments are defined by resistivity values between 20 to 40  $\Omega$ m. Along this profile, a higher concentration of contaminants (Nivorlis et al. 2019) correlates with an increase in resistivity between 0 and 30 m along the profile (Eastern part). The chargeability values are rather homogeneous in the subsurface with moderate values ( $< 10$  mV/V), except for a high chargeability response which is correlated with buried infrastructures.

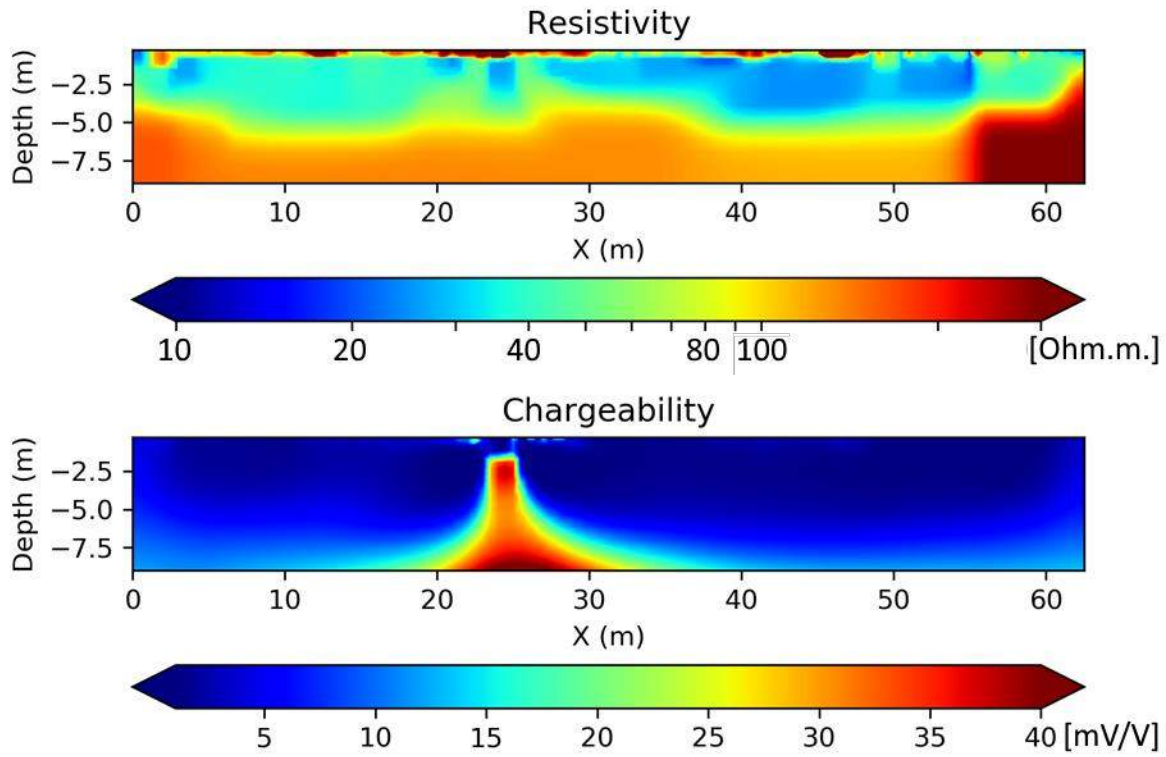


Figure 10. Inverted model of resistivity (top) and chargeability (bottom) of the baseline for Line3.

### Time-lapse results

The time-lapse results of weekly average data inverted against the baseline are showed in Figure 11 for Line 4 and Figure 12 for Line 3. Only three selected time-steps of the entire time-series are displayed and are presented as percentage variation of resistivity and absolute change in chargeability compared to the averaged baseline.

Analyzing the time-lapse results for Line 4 (Figure 11), mostly seasonal variations are observed, since the line is located several meters away from the area where the pilot remediation test is conducted (see Figure 2). The severe effect of frozen ground in the datasets around 2018-03-08 and 2019-02-27 appears as a strong increase in resistivity in the shallower depths, 2 m and 0.5 m, respectively. The upper soil was fully saturated (after a period of intense precipitation) during the installation of the monitoring system, which must have affected the baseline reference dataset. Further changes can be identified in the 3 m depth of

time-step 2018-10-21 that may probably relate to variations in the elevation of the groundwater table. The chargeability variations appear rather stable over the monitoring period, with small variations within in the range of  $\pm 2$  mV/V.

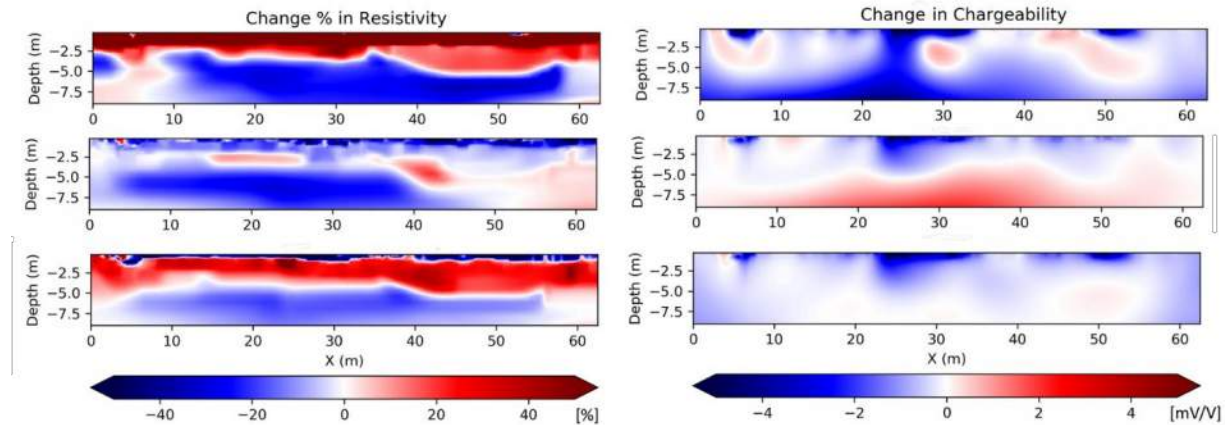


Figure 11. Examples of time-lapse inversions of Line4: from dates 2018-03-08 (top row), 2018-10-21 (middle row) and 2019-02-27 (bottom row). Percentage change in resistivity (left column) and absolute change in chargeability (right column) compared to baseline dataset.

The time-lapse results for Line 3 (Figure 12) are expected to be more complex due to the proximity of the remediation experiment and the infrastructure connected to the building. For this reason, the results from Line 4 (Figure 11) can be used to identify similar seasonal effects along Line 3. Analogous seasonal variations can be identified due to the frozen ground in the winter periods (dates 2018-03-08 and 2019-02-27).

When the frozen ground retreats, different responses are observed, both in Line 3 and Line 4, coming from the areas where the remediation products were injected. In Figure 12, a general decrease is identified in the resistivity in the central area of Line 3 (from 24 to 44 m along the profile) that is consistent for the entire analysed period and coincides with the portion of soil treated with zero-valent iron particles. In the western area (from 7 to 24 m along the profile), where the bacteria consortium was injected, the response shows a similar behaviour as the untreated part in the far right (eastern) side with a rather seasonal pattern. The chargeability is greatly affected by the high response of some probable buried

infrastructure at about 25 m along the profile. This anomaly is of an order of magnitude higher than the background levels, thereby masking the subtle changes in the background.

Line 4 (Figure 11) shows a smoother and more homogeneous pattern in the time-lapse inversions. Nevertheless, a different distribution of the changes in resistivity is identified in the portion of the profile about from 7 to 37 m (western portion) with a general decrease in resistivity.

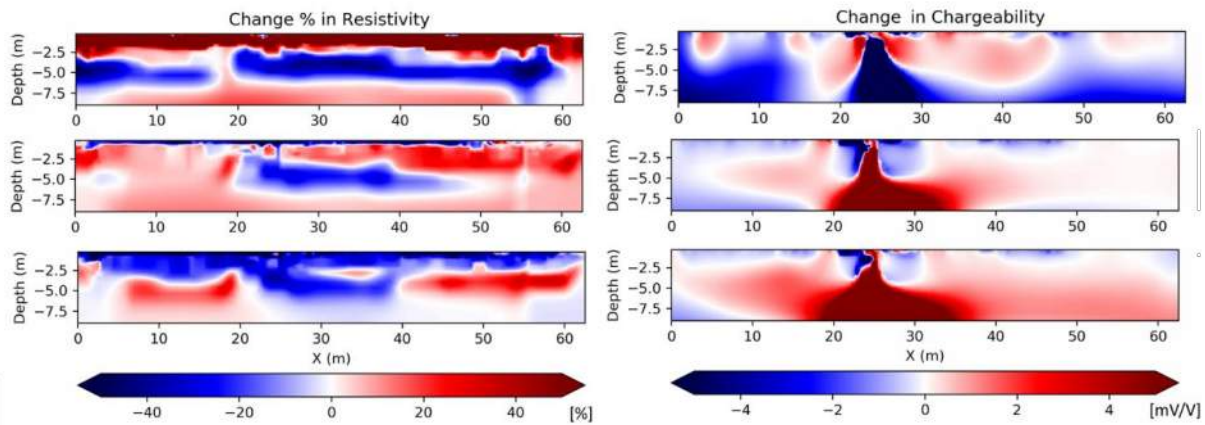


Figure 12. Examples of time-lapse inversions of Line3: from dates 2018-03-08 (top row), 2018-10-21 (middle row) and 2019-02-27 (bottom row). Percentage change in resistivity (left column) and absolute change in chargeability (right column) compared to baseline dataset.

Figure 13 compares the resistivity of the shallower soil of Line 3 and Line 4 with soil temperature. The time series of Line 3 and Line 4 are obtained by averaging the inverted resistivity for each available time step in a depth slice between the topographic surface and 1.5 m depth. The soil temperature data are collected via a temperature probe (107 Thermistor probe, Campbell Scientific) buried at 20cm depth in the central part of Line3 (27m along the profile), which samples every 10 minutes. The rapid increase of resistivity in March 2018 and February 2019 (Figure 13), which can be directly correlated with the observations in the raw-data (Figure 4), is evidently caused by frozen ground when the soil temperature drops below 0°C.

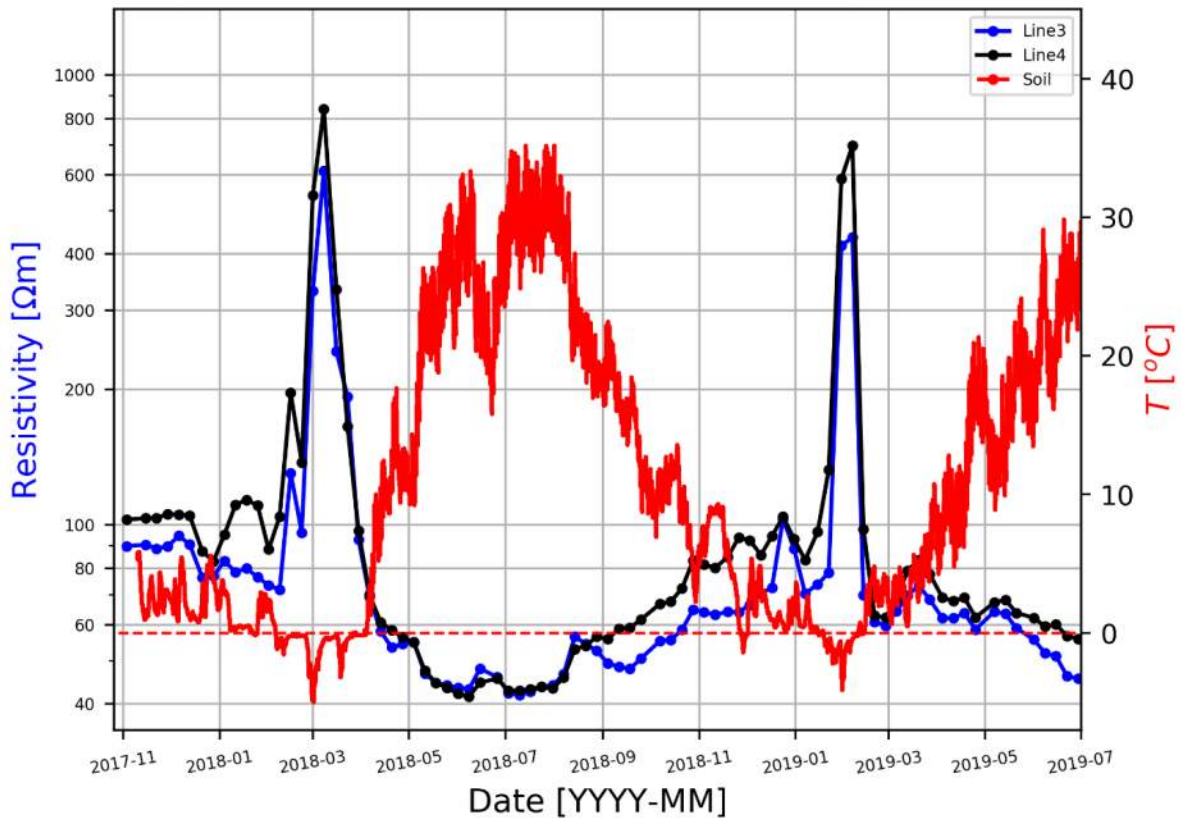


Figure 13. Averaged inverted resistivity values of the shallower soil ( $X$  m deep) for Line 3 (blue line) and Line 4 (black line) over the monitoring period. The red solid line represents the soil temperature, measured at the depth of 20cm, while the red dashed line highlights the level of  $0^{\circ}\text{C}$ .

Figure 14 and Figure 15 summarize the changes in resistivity (left plot) and chargeability (right plot) over the monitoring period, for Lines 4 and 3 respectively. The geophysical parameters (percentage change in resistivity and absolute change in chargeability) are obtained from the inverted results presented in Figure 11 and Figure 12, which are averaged over three areas of higher interest and present different patterns during time. The western area along Line 3 (marked as “a” in Figure 15) coincides with the portion of ground that were treated by injecting a fluid containing a bacteria consortium and nutrients. The central area of Line 3 (“b” in Figure 15) were treated by injecting a solution of zero-valent iron. The eastern area of Line 3 (“c” in Figure 15) represents the untreated and uncontaminated ground. Three areas with the same relative location along the profile are selected for Line 4 (Fig. 2).

Area “c” represents a volume of untreated and uncontaminated ground, both for Line 3 and Line 4 (Figure 15 and Figure 14 respectively). It is evident that the pattern of resistivity changes in those areas shows a high similarity, both in the shape of the curve over time and in the values of resistivity changes. Also the absolute changes in chargeability display the same behavior, even if the values are confined in a narrow range (between -1 and 1). These deviations from the baseline can be linked to seasonal variations. In particular, the temperature might play a dominant role, as both resistivity and chargeability increase during summer and decrease in winter.

Areas “a” and “b” along Line 3 (Figure 15) show completely different patterns over time. Central area “b” is represented by a consistent decrease in resistivity, while western area “a” has a pattern that reflects the untreated and uncontaminated ground (area “c”). The evident drop in resistivity of area “b” can be explained by the nature of the injected remediation product that is a solution containing coated particles of zero-valent iron. When the coating is dissolved, the iron particles start to oxidize and reduce the bulk resistance of the ground. The drop in the resistivity values is not associated with similar fluctuations in the chargeability values, even if they are not straightforward to interpret, since an anomaly connected to some buried infrastructure strongly influences this area. The fact that area “a” treated with a bioremediation product has a similar pattern than the uncontaminated area “c” could mean that the injection of the bacteria consortium was not successful, or that the degradation of the contaminant is not detectable by geoelectrical measurements.

The time series of inverted geophysical parameters along Line 4 in areas “a” and “b” (Figure 14) do not show the same pattern as along Line 3. Area “a prime” and area “b prime” are characterized by an almost identical curve, both for resistivity and chargeability changes. They differ from the uncontaminated area “c prime” and they present an overall reduction in resistivity. The curves resemble a blended pattern of areas “a” and “b” of Line 3 (Figure 12). This fact suggests a possible explanation for these different anomalies. Line 4 is not orthogonal to the groundwater flow (showed in Figure 2), so the fluids that intersect the geophysical profile could be a mixture of both remediation products that are well separated along Line 3, due to its proximity to the treated ground. It is clearly indicated that the geophysical response from the degradation of zero-valent iron particles is dominant, even if the degradation products are probably diluted as is suggested by relatively higher values in resistivity compared to area “b” in Line 3.

The shape of the curves that display the variations of inverted resistivity and inverted chargeability curves are consistent over the entire period of 20 months. This strengthens the claim that the applied methodology for processing and inverting the geophysical data is robust and has great potential in long-term monitoring systems, especially for enhancing the interpretation of slow geochemical processes.

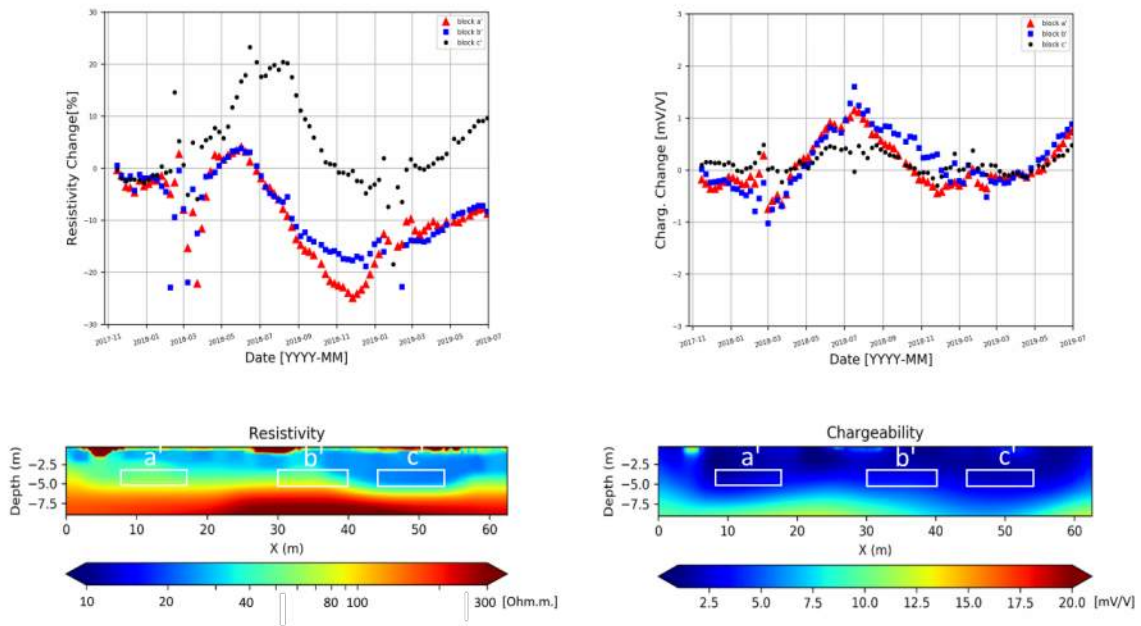


Figure 14. Analysis of the time dependent variations of resistivity (left) and chargeability (right) for Line 4. Resistivity is represented as percentage changes of inverted data respect to background, while chargeability is the absolute variation of inverted integral chargeability respect to background values. The values of the plots are calculated averaging inside the three areas (a, b, c) highlighted in the inverted results from the baseline (bottom).

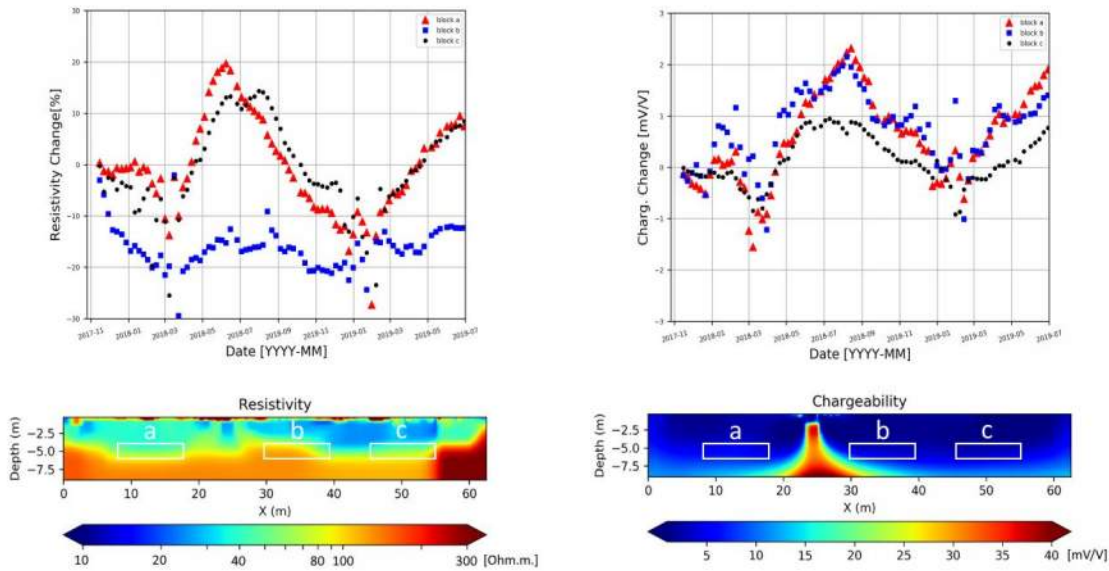


Figure 15. Analysis of the time dependent variations of resistivity (left) and chargeability (right) for Line 3. Resistivity is represented as percentage changes of inverted data respect to background, while chargeability is the absolute variation of inverted integral chargeability respect to background values. The values of the plots are calculated averaging inside the three areas (a, b, c) highlighted in the inverted results from the baseline (bottom).

## Conclusions

In the present work, the different components needed for long-term geophysical monitoring using the DCIP method with high temporal frequency sampling are described. The system is installed in Alingsås (Sweden), a site contaminated by chlorinated solvents, where a pilot in-situ remediation is on-going since November 2017.

Changes caused by strong seasonal variations due to frozen ground and smoother yearly variations due to changes in the air temperature are identified. Furthermore, it is seen that the areas where the two different remediation products were injected appear to have different behavior in the inverted time-series models. The area where a bacteria consortium was injected follows a similar trend as the untreated soil and the area where zero-valent iron particles were injected shows a steady decrease in the resistivity for the entire time period. The results from a geophysical profile that is some distance downstream from

the treated volume show that a decrease in the resistivity is probably caused by the degradation products of the iron particles that flow downgradient.

It is evident that the shapes of the inverted resistivity and chargeability time-series curves that are extracted for different areas of the profile, are consistent over the entire period of 20 months. This shows that the methodology used is very robust when applied to the Alingsås site, which suggests a strong potential for long-term monitoring at other sites. Furthermore, the daily measurements allow the capture the smoother seasonal variations between the summer and the winter period, which can be in the range of 25% change in resistivity and 4 mV/V change in chargeability. These seasonal changes can be falsely interpreted as natural changes if the measurements are repeated at widely spaced time intervals.

The different components of the system are automated separately and can be integrated together with some further optimization. That will make it possible to automatically acquire daily data that will be pipelined through the pre-processing algorithms, the inversion routines and the visualization scripts making real-time DCIP monitoring possible. The inverted results would be visualized, with a short delay due to data transferring and processing, and the system can be horizontally scaled to be applied in multiple sites.

## **Acknowledgments**

Funding is provided by the Swedish Research Council Formas – The Swedish Research Council for Environment, Agricultural Sciences and Spatial Planning (ref. 2016-20099), SBUF – The Development Fund of the Swedish Construction Industry (ref. 13336), ÅForsk (ref. 14-332), SGU – Swedish Geological Survey, Sven Tyréns Stiftelse, Västra Götalandsregionen and Lund University.

## **References**

- Abdulsamad, F., Revil, A., Soueid Ahmed, A., Coperey, A., Karaoulis, M., Nicaise, S., Peyras, L., 2019. Induced polarization tomography applied to the detection and the monitoring of leaks in embankments. *Engineering Geology* 254, 89–101. <https://doi.org/10.1016/j.enggeo.2019.04.001>
- Apgar, M.A., Langmuir, D., 1971. Ground-Water Pollution Potential of a Landfill Above the Water Table. *Groundwater* 9, 76–96. <https://doi.org/10.1111/j.1745-6584.1971.tb03582.x>

- Atekwana, E.A., Atekwana, E., Legall, F.D., Krishnamurthy, R.V., 2005. Biodegradation and mineral weathering controls on bulk electrical conductivity in a shallow hydrocarbon contaminated aquifer. *Journal of Contaminant Hydrology* 80, 149–167. <https://doi.org/10.1016/j.jconhyd.2005.06.009>
- Atekwana, E.A., Atekwana, E.A., 2010. Geophysical signatures of microbial activity at hydrocarbon contaminated sites: A review. *Surveys in Geophysics* 31, 247–283. <https://doi.org/10.1007/s10712-009-9089-8>
- Auken, E., Doetsch, J., Fiandaca, G., Christiansen, A.V., Gazoty, A., Cahill, A.G., Jakobsen, R., 2014. Imaging subsurface migration of dissolved CO<sub>2</sub> in a shallow aquifer using 3-D time-lapse electrical resistivity tomography. *Journal of Applied Geophysics* 101, 31–41. <https://doi.org/10.1016/j.jappgeo.2013.11.011>
- Bernstone, C., Dahlin, T., Ohlsson, T., Hogland, W., 2000. DC-resistivity mapping of internal landfill structures: Two pre-excitation surveys. *Environmental Geology* 39, 360–371. <https://doi.org/10.1007/s002540050015>
- Cabral, A., Demers, L., Ciubotariu, R., 2000. Potential contaminant migration at a contaminated soils landfill site in Quebec. Presented at the Geotechnical Special Publication, pp. 68–80.
- Cassiani, G., Kemna, A., Villa, A., Zimmermann, E., 2009. Spectral induced polarization for the characterization of free-phase hydrocarbon contamination of sediments with low clay content. *Near Surface Geophysics* 7, 547–562.
- Caterina, D., Flores Orozco, A., Nguyen, F., 2017. Long-term ERT monitoring of biogeochemical changes of an aged hydrocarbon contamination. *Journal of Contaminant Hydrology* 201, 19–29. <https://doi.org/10.1016/j.jconhyd.2017.04.003>
- Chambers, J.E., Kuras, O., Meldrum, P.I., Ogilvy, R.D., Hollands, J., 2006. Electrical resistivity tomography applied to geologic, hydrogeologic, and engineering investigations at a former waste-disposal site. *GEOPHYSICS* 71, B231–B239. <https://doi.org/10.1190/1.2360184>
- Chambers, J.E., Meldrum, P.I., Gunn, D.A., Wilkinson, P.B., Kuras, O., Weller, A.L., Ogilvy, R.D., 2009. Hydrogeophysical monitoring of landslide processes using automated time-lapse electrical resistivity tomography (ALERT). Presented at the Near Surface 2009 - 15th European Meeting of Environmental and Engineering Geophysics. <https://doi.org/10.3997/2214-4609.20147066>
- Chirindja, F.J., Dahlin, T., Juizo, D., 2017. Improving the groundwater-well siting approach in consolidated rock in Nampula Province, Mozambique. *Hydrogeology Journal* 25, 1423–1435. <https://doi.org/10.1007/s10040-017-1540-1>
- Dahlin, T., Zhou, B., 2006. Multiple-gradient array measurements for multichannel 2D resistivity imaging. *Near Surface Geophysics* 4, 113–123.
- Danielsen, B.E., Dahlin, T., 2009. Comparison of geoelectrical imaging and tunnel documentation at the Hallandsås Tunnel, Sweden. *Engineering Geology* 107, 118–129. <https://doi.org/10.1016/j.enggeo.2009.05.005>

- Davis, C.A., Atekwana, E., 2006. Potential application of biogeophysics to EOR and remediation investigations. SEG Technical Program Expanded Abstracts 25, 1471–1474. <https://doi.org/10.1190/1.2369798>
- Davis, C.A., Atekwana, E., Atekwana, E., Slater, L.D., Rossbach, S., Mormile, M.R., 2006. Microbial growth and biofilm formation in geologic media is detected with complex conductivity measurements. Geophysical Research Letters 33. <https://doi.org/10.1029/2006GL027312>
- Fernandez, P.M., Bloem, E., Binley, A., Philippe, R.S.B.A., French, H.K., 2019. Monitoring redox sensitive conditions at the groundwater interface using electrical resistivity and self-potential. Journal of Contaminant Hydrology 226. <https://doi.org/10.1016/j.jconhyd.2019.103517>
- Fetter, C.W., 2001. Applied Hydrogeology, 4th ed. Prentice Hall.
- Flores Orozco, A., Kemna, A., Binley, A., Cassiani, G., 2019. Analysis of time-lapse data error in complex conductivity imaging to alleviate anthropogenic noise for site characterization. Geophysics 84, B181–B193. <https://doi.org/10.1190/GEO2017-0755.1>
- Flores Orozco, A., Kemna, A., Oberdörster, C., Zschornack, L., Leven, C., Dietrich, P., Weiss, H., 2012a. Delineation of subsurface hydrocarbon contamination at a former hydrogenation plant using spectral induced polarization imaging. Journal of Contaminant Hydrology 136–137, 131–144. <https://doi.org/10.1016/j.jconhyd.2012.06.001>
- Flores Orozco, A., Kemna, A., Zimmermann, E., 2012b. Data error quantification in spectral induced polarization imaging. Geophysics 77, E227–E237. <https://doi.org/10.1190/geo2010-0194.1>
- Flores Orozco, A., Velimirovic, M., Tosco, T., Kemna, A., Sapion, H., Klaas, N., Sethi, R., Bastiaens, L., 2015. Monitoring the injection of microscale zerovalent iron particles for groundwater remediation by means of complex electrical conductivity imaging. Environmental Science and Technology 49, 5593–5600. <https://doi.org/10.1021/acs.est.5b00208>
- Flores Orozco, A., Williams, K.H., Kemna, A., 2013. Time-lapse spectral induced polarization imaging of stimulated uranium bioremediation. Near Surface Geophysics 11, 531–544. <https://doi.org/10.3997/1873-0604.2013020>
- Forquet, N., French, H.K., 2012. Application of 2D surface ERT to on-site wastewater treatment survey. Journal of Applied Geophysics 80, 144–150. <https://doi.org/10.1016/j.jappgeo.2012.02.002>
- Garrido, T., Fraile, J., Niñerola, J.M., Figueras, M., Ginebreda, A., Olivella, L., 2000. Survey of ground water pesticide pollution in rural areas of Catalonia (Spain). International Journal of Environmental Analytical Chemistry 78, 51–65. <https://doi.org/10.1080/03067310008032692>
- Gazoty, A., Fiandaca, G., Pedersen, J., Auken, E., Christiansen, A.V., 2012. Mapping of landfills using time-domain spectral induced polarization data: the Eskelund case study. Near Surface Geophysics 10, 575–586. <https://doi.org/10.3997/1873-0604.2012046>
- Hopkins, G.J., Popalisky, J.R., 1970. Influence of an industrial waste landfill operation on a public water supply. Journal of the Water Pollution Control Federation 42, 431–436.

- Johansson, S., Sparrenbom, C., Fiandaca, G., Lindskog, A., Olsson, P.-I., Dahlin, T., Rosqvist, H., 2017. Investigations of a Cretaceous limestone with spectral induced polarization and scanning electron microscopy. *Geophysical Journal International* 208, 954–972. <https://doi.org/10.1093/gji/ggw432>
- Kelly, W.E., 1966. Ground-water pollutions near a landfill. *J. ENVIRON. ENGG. DIV.-PROC., ASCE* 102, 1189–1199.
- Kolpin, D.W., Barbash, J.E., Gilliom, R.J., 2000. Pesticides in ground water of the United States, 1992-1996. *Ground Water* 38, 858–863. <https://doi.org/10.1111/j.1745-6584.2000.tb00684.x>
- Kuras, O., Wilkinson, P.B., Meldrum, P.I., Oxby, L.S., Uhlemann, S., Chambers, J.E., Binley, A., Graham, J., Smith, N.T., Atherton, N., 2016. Geoelectrical monitoring of simulated subsurface leakage to support high-hazard nuclear decommissioning at the Sellafield Site, UK. *Science of The Total Environment* 566–567, 350–359. <https://doi.org/10.1016/j.scitotenv.2016.04.212>
- Leroux, V., Dahlin, T., 2006. Time-lapse resistivity investigations for imaging saltwater transport in glaciofluvial deposits. *Environmental Geology* 49, 347–358. <https://doi.org/10.1007/s00254-005-0070-7>
- Liapis, K.S., Miliadis, G.E., Tsiropoulos, N.G., 2000. Confirmation of pesticides in water samples by mass spectrometry. *Bulletin of Environmental Contamination and Toxicology* 65, 811–817. <https://doi.org/10.1007/s0012800194>
- Loke, M.H., Chambers, J.E., Rucker, D.F., Kuras, O., Wilkinson, P.B., 2013. Recent developments in the direct-current geoelectrical imaging method. *Journal of Applied Geophysics* 95, 135–156. <https://doi.org/10.1016/j.jappgeo.2013.02.017>
- Maurya, P.K., Balbarini, N., Møller, I., Rønne, V., Christiansen, A.V., Bjerg, P.L., Auken, E., Fiandaca, G., 2018. Subsurface imaging of water electrical conductivity, hydraulic permeability and lithology at contaminated sites by induced polarization. *Geophysical Journal International* 213, 770–785. <https://doi.org/10.1093/gji/ggy018>
- Nivorlis, A., Dahlin, T., Rossi, M., Höglund, N., Sparrenbom, C., 2019. Multidisciplinary characterization of chlorinated solvents contamination and in-situ remediation with the use of the direct current resistivity and time-domain induced polarization tomography. *Geosciences (Switzerland)* 9. <https://doi.org/10.3390/geosciences9120487>
- Ntarlagiannis, D., Robinson, J., Soupios, P., Slater, L., 2016. Field-scale electrical geophysics over an olive oil mill waste deposition site: Evaluating the information content of resistivity versus induced polarization (IP) images for delineating the spatial extent of organic contamination. *Journal of Applied Geophysics* 135, 418–426. <https://doi.org/10.1016/j.jappgeo.2016.01.017>
- Olsson, P.-I., Dahlin, T., Fiandaca, G., Auken, E., 2015. Measuring time-domain spectral induced polarization in the on-time: Decreasing acquisition time and increasing signal-to-noise ratio. *Journal of Applied Geophysics* 123, 316–321. <https://doi.org/10.1016/j.jappgeo.2015.08.009>
- Olsson, P.-I., Fiandaca, G., Larsen, J.J., Dahlin, T., Auken, E., 2016. Doubling the spectrum of time-domain induced polarization by harmonic de-noising, drift correction, spike removal, tapered gating and

- data uncertainty estimation. *Geophysical Journal International* 207, 774–784. <https://doi.org/10.1093/gji/ggw260>
- Park, S., Yi, M.-J., Kim, J.-H., Shin, S.W., 2016. Electrical resistivity imaging (ERI) monitoring for groundwater contamination in an uncontrolled landfill, South Korea. *Journal of Applied Geophysics, New trends in Induced Polarization* 135, 1–7. <https://doi.org/10.1016/j.jappgeo.2016.07.004>
- Power, C., Gerhard, J.I., Karaoulis, M., Tsourlos, P., Giannopoulos, A., 2014. Evaluating four-dimensional time-lapse electrical resistivity tomography for monitoring DNAPL source zone remediation. *Journal of Contaminant Hydrology* 162–163, 27–46. <https://doi.org/10.1016/j.jconhyd.2014.04.004>
- Power, C., Tsourlos, P., Ramasamy, M., Nivorlis, A., Mkandawire, M., 2018. Combined DC resistivity and induced polarization (DC-IP) for mapping the internal composition of a mine waste rock pile in Nova Scotia, Canada. *Journal of Applied Geophysics* 150, 40–51. <https://doi.org/10.1016/j.jappgeo.2018.01.009>
- Röling, W.F.M., Van Breukelen, B.M., Braster, M., Goeltom, M.T., Groen, J., Van Verseveld, H.W., 2000. Analysis of microbial communities in a landfill leachate polluted aquifer using a new method for anaerobic physiological profiling and 16S rDNA based fingerprinting. *Microbial Ecology* 40, 177–188. <https://doi.org/10.1007/s002480000033>
- Rossi, M., Dahlin, T., Olsson, P.-I., Günther, T., 2018. Data acquisition, processing and filtering for reliable 3D resistivity and time-domain induced polarisation tomography in an urban area: Field example of Vinsta, Stockholm. *Near Surface Geophysics* 16, 220–229. <https://doi.org/10.3997/1873-0604.2018014>
- SEPA, 2014. Nationell Plan för Fördelning av Statliga Bidrag för Efterbehandling; Report 6617. Swedish Environmental Protection Agency: Stockholm, Sweden Volume 30.
- Sjödahl, P., Dahlin, T., Johansson, S., 2009. Embankment dam seepage evaluation from resistivity monitoring data. *Near Surface Geophysics* 7, 463–474.
- Sparrenbom, C.J., Åkesson, S., Johansson, S., Hagerberg, D., Dahlin, T., 2017. Investigation of chlorinated solvent pollution with resistivity and induced polarization. *Science of The Total Environment* 575, 767–778. <https://doi.org/10.1016/j.scitotenv.2016.09.117>
- Telford, W.M., Geldart, L.P., Sheriff, R.E., 1991. *Applied Geophysics*, (2nd edition). ed. Cambridge University Press.
- Ustra, A.T., Elis, V.R., Mondelli, G., Zuquette, L.V., Giacheti, H.L., 2012. Case study: A 3D resistivity and induced polarization imaging from downstream a waste disposal site in Brazil. *Environmental Earth Sciences* 66, 763–772. <https://doi.org/10.1007/s12665-011-1284-5>
- Virtanen, P., Gommers, R., Oliphant, T.E., Haberland, M., Reddy, T., Cournapeau, D., Burovski, E., Peterson, P., Weckesser, W., Bright, J., van der Walt, S.J., Brett, M., Wilson, J., Millman, K.J., Mayorov, N., Nelson, A.R.J., Jones, E., Kern, R., Larson, E., Carey, C.J., Polat, İ., Feng, Y., Moore, E.W., VanderPlas, J., Laxalde, D., Perktold, J., Cimrman, R., Henriksen, I., Quintero, E.A., Harris, C.R., Archibald, A.M.,

Ribeiro, A.H., Pedregosa, F., van Mulbregt, P., 2020. SciPy 1.0: fundamental algorithms for scientific computing in Python. *Nature Methods* 17, 261–272. <https://doi.org/10.1038/s41592-019-0686-2>

Zago, M.M., Fries, M., Ramires, J.E.F., 2020. Groundwater infiltration in a gold mine—A geoelectrical investigation model as an aid to dewatering process determination. *Journal of Applied Geophysics* 172. <https://doi.org/10.1016/j.jappgeo.2019.103909>